TÉCNICO LISBOA

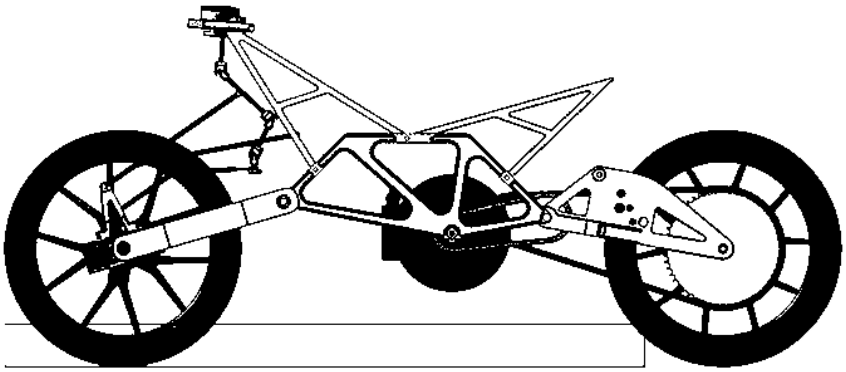

Front and Rear Swing Arm Design of an Electric Racing Motorcycle

João Diogo da Cal Ramos

Thesis to obtain the Master of Science Degree in

Mechanical Engineering

Supervisor: Prof. Luís Alberto Gonçalves de Sousa

Examination Committee

Chairperson: Prof. João Orlando Marques Gameiro Folgado
Supervisor: Prof. Luís Alberto Gonçalves de Sousa
Member of the Committee: João Manuel Pereira Dias

November 2016

Dedicado aos meus pais

Acknowledgments

The author would like to express his most sincere gratitude to his supervisor, Prof. Luis Sousa. This was not the shortest of rides, but his knowledge, patience and friendship were always there when needed. It was an honour and a privileged to work with him.

To all TLMoto team members. It was a pleasure to learn and work so much with great future engineers on this passionate topic.

To my family. My father and my mother. This is as much my success as it is yours.

To all my professors, family and friends, thank you.

Resumo

A indústria motociclista lida atualmente com os novos desafios impostos pelo design de veículos elétricos. As soluções mais vanguardistas são por vezes testadas primeiro no mundo da competição. Este estudo pretende examinar o design inicial e consequente processo iterativo de melhoramento dos braço oscilante traseiro e frontal, de acordo com as regras impostas pela competição MotoStudent. Todas as partes desenhadas foram concebidas para serem fabricadas na liga de alumínio 7075-T6 e maquinadas em CNC. O Método Clássico de Cossalter é de medição da rigidez de braços oscilantes foi complementado com um novo estudo de condições sob carga vertical extrema (3580 N no perpendiculares ao eixo da roda). FEA foi usada no processo de simulação iterativo de diferentes modelos sob condições de carga vertical, torsional e laterais. Os modelos finais do braço oscilante traseiro e frontal respeitam o coeficiente de segurança $n_{proj} = 1.82$ e os intervalos de rigidez de Cossalter ($K_{lateral}$ = 0.8-1.6 kN/mm and $K_{torsional}$ = 1-2 kNm/°). O peso final atingido em ambos foi, 4,86 kg and 2,84 kg, respetivamente. No entanto, a complexidade final de ambas as partes devido a pormenores internos e numerosas soldaduras torna a maquinação por CNC inviável. Um novo Sistema de direção frontal foi proposto para a consequente utilização do braço oscilante frontal.

Palavras-chave: Design estrutural, mota, braço oscilante, veículos elétricos, FEA, CAD, CNC

Abstract

Motorcycle manufacturers worldwide grapple with the new design challenges posed by electric motorcycles. The competition world is where the most cutting edge design solutions are firstly tested. The present study examined the initial design and consequent iterative process of improvement of both rear and frontal swing arms for an electric motorcycle according to the rules of the MotoSudent competition. All parts were designed to be fabricated in aluminium alloy 7075-T6 and CNC machining. The classic Cossalter approach for stiffness measurement of swing arms was complemented with new studies in extreme vertical loading (3580 N perpendicular to the wheel axle). FEA was used through the iterative process of simulating different swing arm models under vertical, torsional and lateral loads. Final models for rear and front swing arms comply with derived safety coefficient factor of $n_{proj} = 1.82$ and Cossalter's stiffens intervals ($K_{lateral}$ = 0.8-1.6 kN/mm and $K_{torsional}$ = 1-2 kNm/°). Final weight of achieved for rear and front swing arm, 4,86 kg and 2,84 kg, respectively. However, final complexity of parts proved to have to many welds and internal details for CNC machining to be a viable option. As an outcome of the new design proposals for the frontal swing arm, a new steering system was conceived.

Keywords: Structural design, motorcycle, swing arm, electric vehicles, FEA, CAD, CNC

Contents

Acknowledgments v

Resumo vii

Abstract ix

1. Introduction 1

1.1 Motivation and Context 1

1.2 The Competition 2

1.3 Aims and Objectives 3

1.4 The Modern Competition Electric Motorcycle 4

1.4.1 Electric motor 5

1.4.2 Battery Pack 6

1.4.3 Frame 8

1.4.4 Swing arm 11

2 Theoretical Overview 17

2.1 Structural Criteria Selection 17

2.2 Simplified Motion of a Motorcycle 20

2.2.1 Centre of Gravity 20

2.2.2 Motorcycle Loads and Limit Situations 22

2.3 Squat and Dive 26

2.3.1 Rear Suspension Balance 27

2.3.2 Squat Ratio and Squat Angle 29

3 Swing Arm Design and testing 31

3.1 Finite Element Analysis Observations 31

3.2 Material Selection 38

3.3 Initial Geometry of the Rear Swing Arm 40

3.4 Test Procedures 43

3.5 Rear Swing Arm First Iteration (HM1) 45

3.6 Model HMF 49

3.7 Model LM1 52

3.8 Model LMF 55

3.9 Final Rear Swing Arm Model 58

3.9 Frontal Swing arm design 60

3.11 Model FSS2 63

4 Manufacturing 68

4.1 Designing to Manufacture 68

4.2 Interior Corners 70

4.3 Weld location and sizing 72

5 Conclusions and future developments 76

5.1 Conclusions 76

5.2 Future Developments 78

References 79

Annex 1 81

Annex 2 82

Annex 3 83

Annex 4 85

Annex 5 91

List of Tables

Table 1 Material characteristics relative to material, loads and stress analysis for n_{sx} 18
Table 2 Fail impact for n_{sy} 18
Table 3 Main differences in behaviour due to Centre of Gravity shift 21
Table 4 General specs of an Aprilia RS250 22
Table 5 Dynamic changes due to shift in CG 24
Table 6 Initial assumed approximate hg 25
Table 7 Variation in R – rear suspension 30
Table 8 Variation in R - front suspension 30
Table 9 Percentage variation of Maximum Stress in relation to previous mesh dimension 33
Table 10 Percentage variation of Minimum Stress in relation to previous mesh dimension 34
Table 11 Simulation time per mesh size in seconds 34
Table 12 Percentage variation of Minimum Safety Factor 35
Table 13 Percentage variation of Maximum Safety Factor 35
Table 14 Comparison between Aluminium 7075-T6 and Steel AISI 4340 39
Table 15 General Properties of an Aluminium 7075-T6 39
Table 16 Comparison between HE and LE 42
Table 17 Lateral Loading Results (HM1) 47
Table 18 Vertical Results (HM1) 47
Table 19 Torsional Results (HM1) 48
Table 20 Lateral Results (HMF) 50
Table 21 Vertical Results (HMF) 50
Table 22 Torsional Results (HMF) 50
Table 23 Results Comparison (Models HM1 and HMF) 50
Table 24 Lateral Results (LM1) 54
Table 25 Torsional Results (LM1) 54
Table 26 Vertical Results (LM1) 54
Table 27 Lateral Results (LMF) 55
Table 28 Torsional Results (LMF) 56
Table 29 Vertical Results (LMF) 56
Table 30 Results Comparison (LM1 and LMF) 56
Table 31 Lateral Results (LMF) 59

Table 32 Torsional Results (LMF) 59
Table 33 Vertical Results (LMF) 59
Table 34 Lateral Results (FSS1) 61
Table 35 Torsional Results (FSS1) 62
Table 36 Vertical Results (FSS1) 62
Table 37 Lateral Results (FSS2) 65
Table 38 Torsional Results (FSS2) 65
Table 39 Vertical Results (FSS2) 65
Table 40 Results Comparison (FSS1 and FSS2). 65
Table 41 Raw material blocks and plates VS final machined part weight (Rear Swing arm) 69
Table 42 Raw material blocks and plates VS final machined part weight (Front Swing arm) 70
Table 43 Increase in weight VS increase in interior corner radius 72
Table 44 SolidWorks general weld sizing prediction under vertical loading of 1790 N 74
Table 45 Chain Standards and Motor size 97

List of Figures

Figure 1: Graphic description of horizontal and vertical static tests 3
Figure 2: Moto3.e the EM prototype constructed by MEF Technologies (2013) 3
Figure 3 Converted BMW S1000RR constructed at MIT 4
Figure 4 (a) BMW S1000RR initial structure; (b) Critical structural assembly without powertrain parts; (c) Motorcycle with electric powertrain. [21] 5
Figure 5 Heizmann PMS 150 Air-Cooled CAD model 6
Figure 6 Cost per Unit Energy [$/kWh] related to Cost per Unit Power [$/kW] [10] 7
Figure 7 Efficiency related to lifetime at 80% DoD – Cycles [10] 7
Figure 8 Power Density [W/kg] related to Energy Density [Wh/kg] [10] 8
Figure 9 Motorcycle types 8
Figure 10 Mission R (Mission Motors Company) uses a truss frame (yellow strut) 9
Figure 11 R1 Yamaha Twin-Spar frame example [11] 10
Figure 12 The BMW boxer frame with engine as central structural member. 10
Figure 13 (left) Original Moto Guzzi pivoted rea spring. Long springs are actuated by a triangulated fork; (right) 3Fasi, presented in 2014, by Energyca Ego, has a conventional superbike swing arm. 11
Figure 14 Schemes of rear suspension with swing arms [14] 12
Figure 15 Schemes of rear suspension with swing arm and four-bar linkage. [14] 13
Figure 16 Schemes of rear suspensions with four-bar and six-bar linkage. [14] 13
Figure 17 Lateral deflection in telescopic fork systems. 14
Figure 18 Hard braking leads to extreme compression of the fork. 15
Figure 19 Schemes of front suspension with pushed and pulled wishbones. 15
Figure 20 Schemes of four-bar linkage suspension 15
Figure 21 Schemes of four-bar linkage front suspension with prismatic pairs. 16
Figure 22 (left) BMW H2R with telelever system; (right) Vyrus 986 M2 with a frontal swing arm system (both different takes on four-linkage applications) 16
Figure 23 Cossalter's Approach for torsional and lateral swing arm testing 17
Figure 24 Motorcycle weight distribution 23
Figure 25 Balance of forces and moment on rear wheel and swing arm 28
Figure 26 Squat - Load transfer lines 29
Figure 27 Dual chain rear example ..... **Error! Bookmark not defined.**

Figure 28 Rear Suspension Rocker 33
Figure 29 Swing arm link a) Geometry; b) Non adaptative mesh (Elem. size =5mm); c) Adaptative mesh (Element size (5;1)[mm]) 33
Figure 30 Corner mesh deformation (Von Mises local Stress) 37
Figure 31 General behaviour of metal alloys 39
Figure 32 Single chain rear example 41
Figure 33 Dual chain rear example 41
Figure 34 HE - high motor assembly Figure 35 D2 - low motor assembly . 42
Figure 36 Cantilever Beam example (base is fixed to rigid wall) 43
Figure 37 Swing arm fixtures, considering a fully recoiled rear suspension 43
Figure 38 a) Cossalter's vertical test; b) Extreme conditions vertical test 44
Figure 39 Cossalter's lateral test 44
Figure 40 Cossalter's torsional test 44
Figure 41 Perspective view of HE 45
Figure 42 Main Dimensions and geometry limits of HE 46
Figure 43 Main dimensions and geometry of HM1 47
Figure 44 Von Mises Stress propagation in Model 1.0 .....**Error! Bookmark not defined.**
Figure 45 Von Mises Stress propagation in HM1 48
Figure 46 Design improvements on Model 1.1 49
Figure 47 Local Stress concentration (rear suspension mount) 51
Figure 48 Deformed shape of HMF (Deformation scale 21.5) 52
Figure 49 Perspective view of LM 53
Figure 50 Main dimensions and geometry limits of LM 53
Figure 51 Main dimensions and geometry of LM1 53
Figure 52 Design improvements on LMF 55
Figure 53 Von Mises Stress propagation in LMF 57
Figure 54 Deformed shape of LMF (Deformation scale 21.5 57
Figure 55 Final rear swing arm model 58
Figure 56 Von Mises Stress propagation in Final Model 59
Figure 57 Deformed shape of Final Model (Deformation scale 21.5) 60
Figure 58 Main dimensions and geometry of FSS1 61
Figure 59 Proposed front wheel external steering system 63
Figure 60 Main dimensions and geometry of steering system 63
Figure 61 Main dimensions and geometry of FSS2 64
Figure 62 Von Mises Stress propagation in FSS2 with single side suspension 66

Figure 63 Von Mises Stress propagation in Final FDS2 with dual suspension 66
Figure 64 Deformed shape of FSS2 with single side suspension (Deformation scale 21.5) 67
Figure 65 Deformed shape of FDS2 with dual suspension (Deformation scale 21.5)..... 67
Figure 66 Rear (left) and Front (right) swing arms with respective composing parts 69
Figure 67 Interior corners and deep pockets machining 70
Figure 68 Rear Swing Arm interior pockets..... 71
Figure 69 Edged weld formulation (SolidWorks 2014) 73
Figure 70 Edge weld main dimensions..... 73
Figure 71 Simplification of half of frontal swing arm..... 74
Figure 72 Von Mises Stress propagation in simplified model..... 75
Figure 72: Final design of the battery and motor structural frame. 82
Figure 73: Two DC electric motors connected by a steel shaft with a 16T sprocket 82
Figure 74 (a) battery module assembly; (b) frame fabricated using waterjet..... 82
Figure 75 Example of Altrax PWM Controller 24-48V 300A 85
Figure 76 General Cd distribution for different vehicles..... 92
Figure 78 Chain Standard dimensioning 97

List of Graphs

Graph 1 Maximum Stress Variation - Non Adaptative/Adaptative Mesh 34
Graph 2 Minimum Stress Variation - Non Adaptative/Adaptative Mesh 34
Graph 3 Variation of Minimum Safety Factor - Non Adaptative/Adaptative Mesh 35
Graph 4 Variation of Maximum Safety Factor - Non Adaptative/Adaptative Mesh 36
Graph 5 General Varations depending on number of nodes per 3D Elements 36
Graph 6 Stress concentration on tight corner under uniaxial traction [23] 37
Graph 7 Local Stress Variation 38
Graph 8 Machining cost distribution 71
Graph 9 Resistance Power 94
Graph 10 Driving and Resistance Forces 95
Graph 11 Relation of Rotation Speeds between Rear wheel and Motor 95

Nomenclature

Mg	Total Weight
$Mmoto$	Motorcycle weight
$Mrider$	Rider (human) weight
n_{proj}	Project safety factor
σ_{yy}	Yield Strength (y direction)
υ	Poisson's Coefficient
$K_{lateral}$	Lateral stiffness
$K_{torsional}$	Torsional stiffness
$K_{vertical}$	Vertical stiffness
W_b	Wheel base
CG	Centre of gravity (motorcycle + rider)
a	Distance between front wheel and CG
b	Distance between rear wheel and CG
h_g	Height of CG
a_{lf}	Acceleration to lift front
a_{sr}	Acceleration to spin rear
r_{lr}	Retardation to lift rear
r_{sf}	Retardation to slide front
L	Swing Arm length
N_{tr}	Moment generated by the load transfer
S	Moment generated by the driving force
T	Moment generated by the chain force
M_v	Additional elastic moment generated by the suspension
ϕ	Swing arm inclination angle with horizontal axis, x
$\Re$	Squat ratio
S	Thrust Force
R_r	Rear wheel radius
τ	Load transfer angle
σ	Squat line angle
ρ	Fluid Density (air)
C_D	Drag Coefficient

A	Frontal Area
V	Forward speed
f_w	Rolling force
μ	Friction coefficient between tires and road

Glossary

CAD	Computer Assisted Design
CAE	Computer Assisted Engineering
CM	Centre of Mass
DoD	Depth of Discharge
EV	Electric Vehicle
EM	Electric Motorcycle
LCA	Life Cycle Assessment
FEA	Finite Element Analysis

1. Introduction

In this chapter is presented a brief explanation on what motivated the author to follow studies on the swing arm design for an electric racing motorcycle. Also, an overview regarding the MotoStudent competition and how this fits into the discussed theme.

1.1 Motivation and Context

The first series production motorcycle dates back to 1894, when Hildebrand and Wolf Müller [1] became the first builders of machines that were called for the first time motorcycles. However, only a decade was needed for the first official motorcycle competitions to be nationally held [2]. The motorcycle vehicle concept has been kept till the present day:

- Two or three wheels vehicle
- Propulsion through a combustion, or electric motor

Nevertheless, the design and engineering challenges involved in the construction of such machines greatly varies depending on a constantly expanding list of demands:

- Long distance travel
- Commuting
- Cruising
- Sports racing on and off-road
- Fashion
- Low carbon emissions
- Safety

Nowadays, motorcycle industry faces evermore strict International Policies [3]. Oil prices have been suffering major fluctuations along the past decade, however, an overall rise in its price has been noticeable [20]. Consequently, oils sub products suffer from the same fate, being gasoline the main power source for motorcycle engines worldwide. Additionally, some of the world's largest automobile and motorcycle manufacturers have been progressively focusing efforts in improving batteries technology and durability [7]. Allied to an increasing environmental awareness, all this factors are operating a shift in the motorcycle international market. Some of the advantages offered by electric powered vehicles may be consulted on Annex 1.

This list of demands gives way to large list of complex studies conducted through industrials and academicals alike. It is clear however that commercial and race vehicles belong to two very different worlds. Often cutting edge solutions only reach consumers after exhaustive testing on the race tracks. In this field however, only recently Universities worldwide started establishing close relations with International Motorcycle Foundations such as MEF, in order to create, for the first time, a motorcycling student focused competition called MotoStudent. This year, for the first time, MotoStudent 2016 Edition will provide the opportunity for university teams to compete with electrical motorcycle prototypes.

1.2 The Competition

MotoStudent is an event promoted by Moto Engineer Foundation (MEF) directed exclusively to University Students Worldwide. Teams design and build a race motorcycle that will compete at Motor Land, Aragón (Spain), one of the tracks from the internationally known MotoGP. The first MotoStudent competition held by the organization dates back to 2010.

All participating motorcycles are evaluated by a board of members from MotoGP teams and invited specialist engineers. Dynamic and static performance, design, production applicability and theoretical knowledge applied during model concept are the most important parameters under evaluation. The organization parts this process in two stages, MS1 and MS2.

MS1 – Project presentation and industrial production plan

The MS1 stage students are confronted with the difficulties of a project industrialization. Each team presents its motorcycle, innovation, manufacturing processes and any other justification required by the jury regarding the construction of the prototype.

MS2 – Safety tests and race

The MS2 stage is based on a number of tests where the dynamic behaviour of all motorcycles is assessed. These tests consist on the horizontal and vertical static load of the prototype (Figure 1: Graphic description of horizontal and vertical static tests), while chassis deformation is recorded.

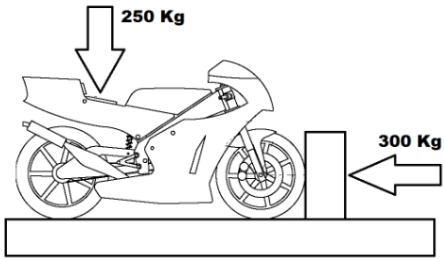

Figure 1: Graphic description of horizontal and vertical static tests

After the static tests, all motorcycles go through a dynamic test, where designated pilots rides each motorcycle through a series of tight low speed corners and obstacles. A pass on this test is achieved if the test pilot deems the motorcycle as safe to ride, after measuring a satisfactory dynamic behaviour. Prototypes that pass both dynamic and static assessments, may participate on the final race, *Figure 2*: Moto3.e the EM prototype constructed by MEF Technologies (2013.

Figure 2: Moto3.e the EM prototype constructed by MEF Technologies (2013)

1.3 Aims and Objectives

Aim

The main goal is to design light and rigid aluminium structures known as swing arms to be manufactured at IST, or other local facilities, on a CNC machine.

Objectives

Design both frontal and rear swing arms that can perform correctly under the dynamically demanding situations posed by racing on a circuit.

All structures developed are intended to be built and assembled at IST, except for welding processes.

The handling of the motorcycle is strongly influenced by the geometry of the swing arms, so a successful design needs to comply with the minimum requirements set by MotoStudent organization and also excel amongst motorcycles of the same characteristics.

1.4 The Modern Competition Electric Motorcycle

EM Competitions are proliferating worldwide and interest from masses is rising. One example is the annual Isle of Man TT, the oldest international motorcycle competition to be held till the present date [8]. Since 2010, a contest called the TT Zero features an electric motorcycles category. The importance of such competitions cannot be neglect regarding the evolution of technology involved. In the particular case of TT Zero. One of the Zero TT prototype race motorcycles will be used to briefly describe the modern racing motorcycle. A team from the Massachusetts Institute of Technology (MIT) converted a 2010 BMW S1000RR into an EM [21], Figure 3.

Masses			
Rolling Chassis	*Battery Modules*	*Motors*	*Other*
77kg	106kg	25kg	23kg
Mass Distribution w/out Rider			
Front Wheel	*Rear Wheel*	*Total Mass*	
122kg	109kg	231kg	
Mass Distribution w/ 80kg Rider			
157kg	154kg	311kg	
Battery Specifications			
Paral./series	*Voltage*	*Capacity*	
6/30	99V	11.9 kWh	
Motor Specifications (2 motors combined)			
Cont. Power	*Cont. Current*	*Model Number*	
32 kW	400A	D135RAG	
Motor Controller Specifications			
Voltage	*Cont. Current*	*Model Number*	
18-136V	540A	KDH12121E	
Drivetrain Specifications			
Sprocket Ratio	*Chain Size*	*O-Rings*	
53/16T	428	No	

Figure 3 Converted BMW S1000RR constructed at MIT

Although the initial base motorcycle was not an EM, using commercial motorcycle structures as a base for an electrical prototype is not uncommon in competition EM for the following reasons:

- Mechanical design already tested and approved according to engineering standards.
- Reduced monetary investment related to critical structural parts. In commercial products, many of these parts are designed using very conservative structural safety factors of approximately 3.0, while race prototypes might use around 1.1. This means that critical parts still allow for some reengineering and functional flexibility.
- In the case of twin spar chassis (Chapter 2.3.1), as the one presented on Figure 4, the motorcycle main structural integrity is not dependent on the motor. So, overall stiffness

of the system is maintain, even if all original power train parts are replaced by a completely different assembly.

- Project time and labour can be reduced since less parts require manufacturing.

It can be stated that modern race EMs are usually an assembly between structural parts (swing arms, main frame, sub frame, rear and front suspensions) already fairly known, with an electric power train system. Figure 4 briefly shows how this concept can be applied (the green truss present in the different pictures represents the linking frame points preserved for a proper load triangulation).

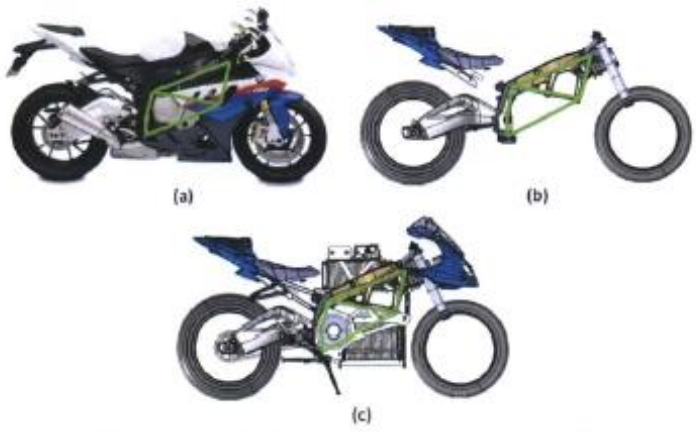

Figure 4 (a) BMW S1000RR initial structure; (b) Critical structural assembly without powertrain parts; (c) Motorcycle with electric powertrain. [21]

This motorcycle raced during Zero TT 2013 with positive results. For more information regarding the structure of the powertrain used on this project (Annex 2). It can be concluded that both combustion and electric motorcycles can share critical parts, such as frames, swing arms, sub-frames and suspension and direction systems.

1.4.1 Electric motor

The electric motor is a central part of any EV. Although electric motors can be separated in two main groups, DC and AC, there is an immense variety regarding subtypes, shapes and sizes. For more information on main types of motors and parameters of interest, Annex 3. MotoStudent dictates that all participating teams must use the same electric motor model [9], Figure 5.

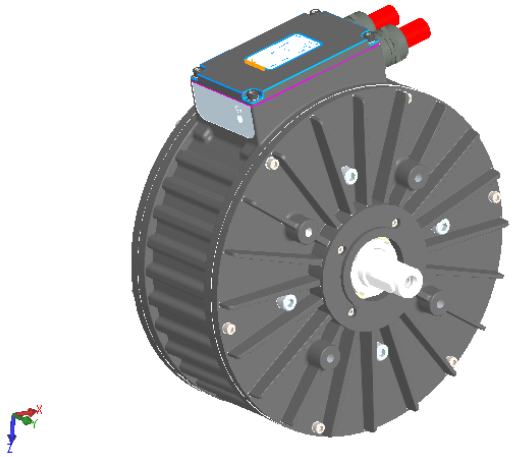

Figure 5 Heizmann PMS 150 Air-Cooled CAD model

Main dimensions and how the motor affects the swing arm design will be discussed further ahead in this document. Also, for more information on motor controller, Annex 4.

1.4.2 Battery Pack

The choice of an electric motor is critical, however, the choice of what batteries type to use and how to displace all cells throughout the prototype is possibly the most important design decision with direct implications on space, weight and cost. The goal while constructing a battery pack for a competition EM is to attain the maximum energy storage possible in limited space, giving the vehicle the required range during high power demands.

While battery technology advancement is still and ongoing process, given the previous goal, the obvious choice for a main battery cell in a competition EM will usually relay on advanced high power density batteries. Nevertheless, options are vast and the following analogies should be taken into account.

- Capital Cost per Unit Energy [$/kWh] related to Capital Cost per Unit Power [$/kW], Figure 6
- Efficiency related to lifetime at 80% Depth of Discharge (DoD) – Cycles, Figure 7
- Power Density [W/kg] related to Energy Density [Wh/kg], Figure 8

Again, the shown information could be further studied and much more complex analogies presented. Though, from Figure 7 to 9, some battery families are clearly better candidates for an EV than others. For a start, high power capacitors, while extremely efficient through a long range of life cycles, are also the most expensive to buy and operate in normal conditions. Others, as the lead acid, Ni-Cd and Ni-MH are already known and reliable technologies, though a low power and energy density exclude them as competitive batteries for the discussed application.

Li-ion batteries and similar exemplars are the most common choice for competitions Ems. This type of battery shows the best overall set of values through the presented categories and given its mass production during the last decade, consumer prices are lower than the ones observed for high power capacitors.

It is clear now that electric motor and battery pack are two decisive volumes of any EM final design. Taking again the example of MIT's converted BWM S1000RR, the combined weight of motors and batteries is 133 kg, which is approximately 57.1% of total vehicles mass.

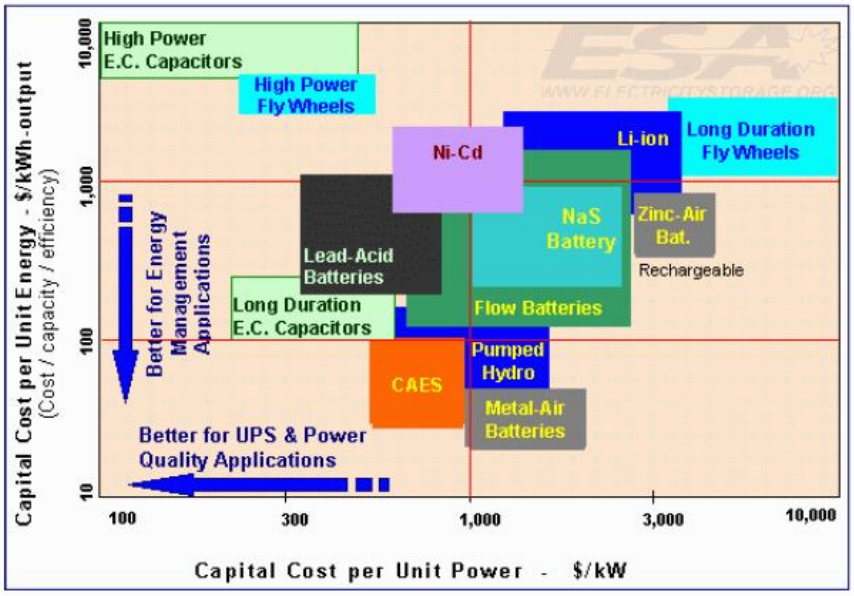

Figure 6 Cost per Unit Energy [$/kWh] related to Cost per Unit Power [$/kW] [10]

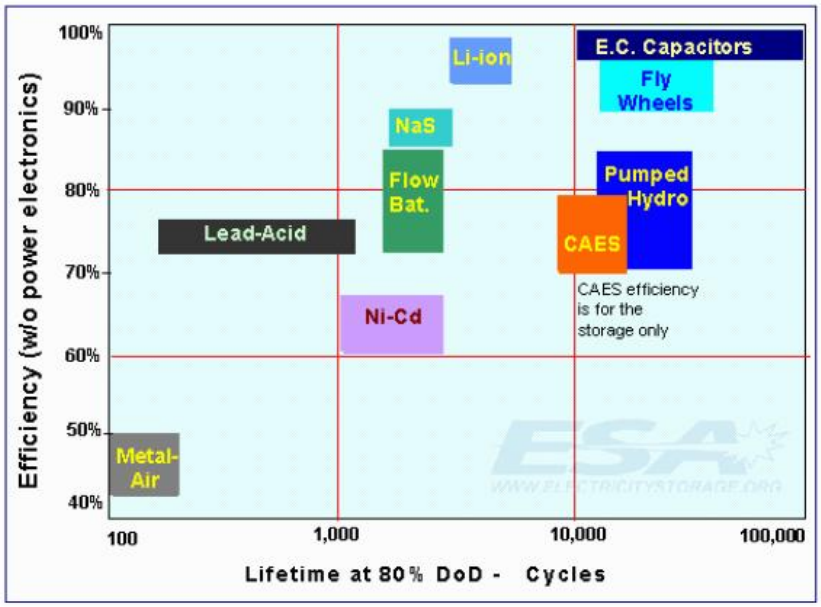

Figure 7 Efficiency related to lifetime at 80% DoD – Cycles [10]

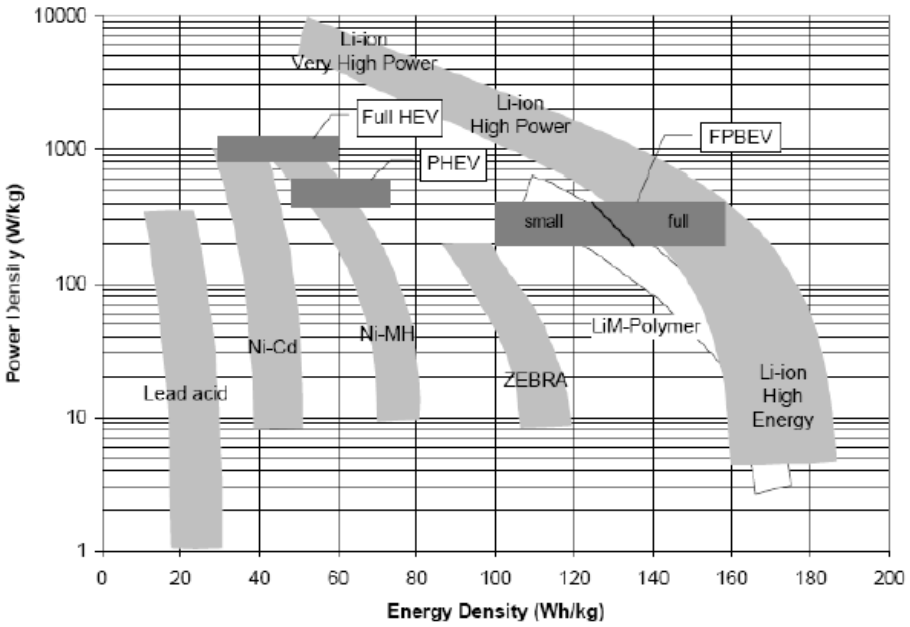

Figure 8 Power Density [W/kg] related to Energy Density [Wh/kg] [10]

1.4.3 Frame

The optimum frame design depends on the size and shapes of the engine and the intended purpose of the machine [11]. Much like cars, motorcycles can be parted in to several different groups, depending on function.

Figure 9 demonstrates the 7 main groups of motorcycles. Within the scope of this thesis the superbike model represents the type of lines sought on a competition motorcycle. Also, modern superbikes use very specific types of frames, which shortens the list of frames that can be used in race EMs. As stated previously, critical structures as the frame, although adapted to EM design constraints, tend to be kept within classical lines, previously used on combustion motorcycles. Three types of frames may be highlighted.

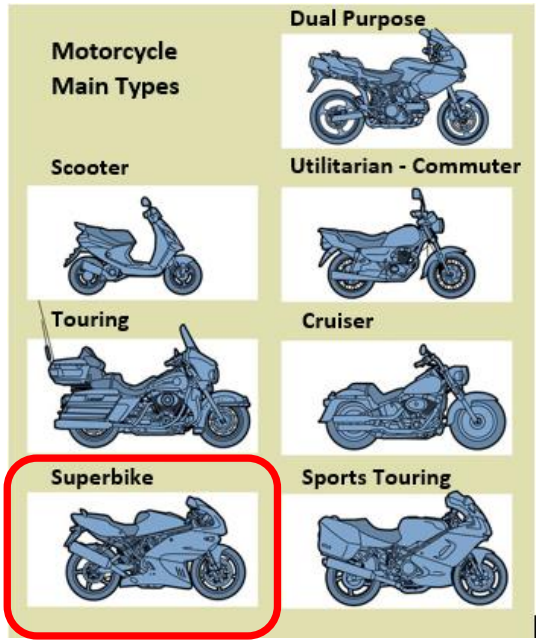

Figure 9 Motorcycle types

Triangulated/truss frames

Characterized by a high structural efficiency, these are not the most common frames, Figure 10. The appointed reasons are:

- Complex automatized facilities are required to mass produce these frames, due to intricate welds and shapes. Even nowadays truss frames are more common in low production motorcycles, many times welded by manual processes.
- Because of shape and size most popular combustion engine types would require a wide and complicated truss structures.

A common problem that may occur with long truss tubes of small diameter is engine-excited resonance. Severe vibration in the tubes caused by unbalanced engine inertia forces at a critical frequency. The solution to this is increasing the tubes natural frequency, by increasing their diameter or shortening them. However, in EM this problem should not happen due to almost less vibrations generated by the motor. [11]

Figure 10 Mission R (Mission Motors Company) uses a truss frame (yellow strut)

Twin-Spar

The most common for top ranged sports motorcycles, Figure 11. Typically made in aluminium alloys, it consists of two beams set at each side of the engine/gearbox/transmission units, joining the head stock to the swing arm pivot mountings.

The common disadvantage pointed to this design is the need for increasing width and thickness of the beams in order to achieve similar stiffness values to truss steel chassis. From a structural stiffness/weight point of view, even in aluminium, this construction method does not result in very high ratios.

Though, the industrial process required to assemble this frames are vastly used and easy to apply in mass production motorbikes:

- Extruded tube, often with internal ribbing
- Fabricated original aluminium plate (CNC)
- Castings

Figure 11 R1 Yamaha Twin-Spar frame example [11]

Structural engine

In the case of large engines, or large engine housing structures this is one structurally efficient way to build a frame, Figure 12. The principle is to use the integral stiffness offered by the engine and gear box units to provide the main support between the steering head and rear-suspension pivot. However, this is not a design option for MotoStudent prototypes – the electric motor external armature was not designed to have a structural stiffness comparable to motorcycle frames.

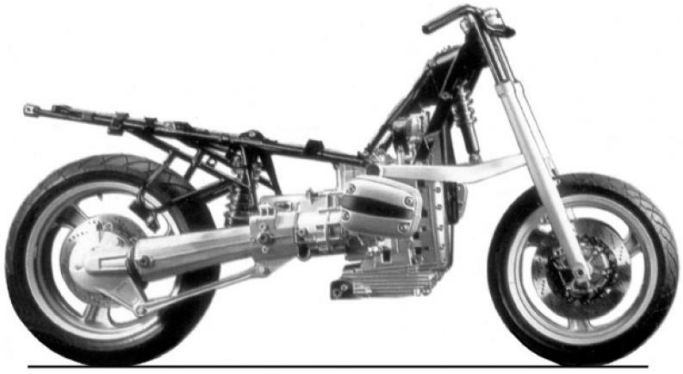

Figure 12 The BMW boxer frame with engine as central structural member.

1.4.4 Swing arm

The common term applied to a trailing pivoted arm or fork is swing arm. For long this structure has been established for rear suspension mounting and linking between frame and rear wheel. Although this concept remains unchanged, there was a certain amount of structural redesigning through the years.

Rear Swing arm

To find the first ancestor of the modern rear swing arm, it is necessary to analyse 1928 Vinent-H. R. D patent, later on (mi-1930s), applied by Moto Guzzi, Figure 13. This was the first weight-efficient strut to triangulate the fork and connect the apex to the spring medium. Current superbikes still apply the same notion.

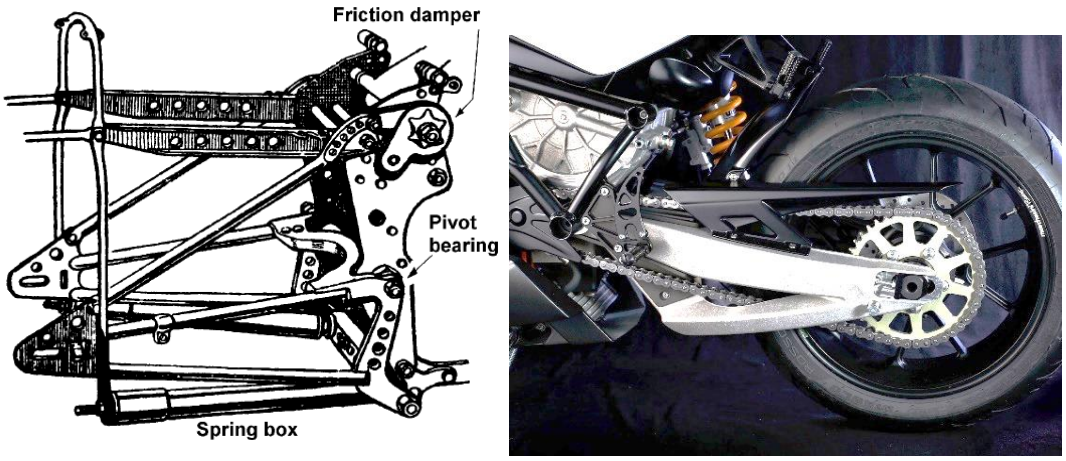

Figure 13 (left) Original Moto Guzzi pivoted rea spring. Long springs are actuated by a triangulated fork; (right) 3Fasi, presented in 2014, by Energyca Ego, has a conventional superbike swing arm.

Conventional swing arms are very similar across manufacturers. Structural changes are many times more a matter of marketing/fashion than necessarily structural performance. The same however cannot be said about the rear suspension assembly, between swing arms and frames, being here where very difference options are noticeable.

The classical rear suspension is a system composed of two trailing arms with two spring-damper units, one each side, inclined at a certain angle with respect to the swing arm, Figure 14.

The main advantages of the traditional rear suspension are:

- Simplicity of construction.
- Shock absorbers easily dissipate produced heat.
- Large amplitude of motion of spring-damper units which is nearly equal to the vertical amplitude of the wheel motion and which therefore causes high compression and extension velocities of shock absorbers.

- Low reaction forces transmitted to the chassis.

The main disadvantages:

- Limitation of vertical oscillation amplitude of the wheel.
- Force-displacement relation not very progressive.
- Possibility that the two spring-damper units generate different forces, with consequent malfunctioning of the suspension, due to generation of torsional moments that stress the swing arm.

One variation of the dual-strut suspension is the cantilever mono-shock system (more common in race applications) characterized by only one spring-damper unit. It has the following advantages over the twin shock arm:

- Ease of adjustment, since there is only one shock absorber.
- Reduced unsprang mass.
- Higher torsional and bending stiffness.
- High vertical wheel travel amplitude.

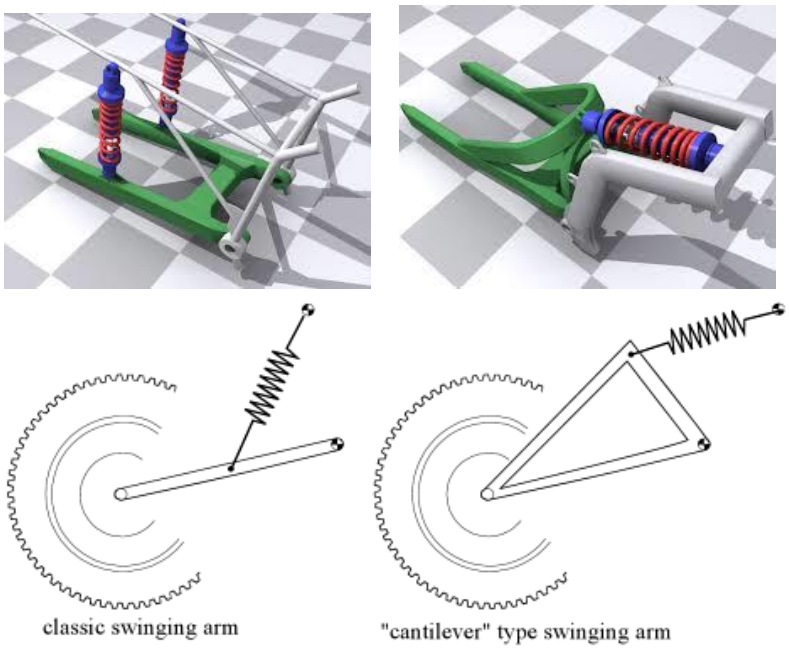

Figure 14 Schemes of rear suspension with swing arms [14]

The main disadvantage is that this suspension assembly does not permit a progressive force-displacement behaviour and the positioning of the spring-shock absorber unit above or behind the motor can cause heat dissipation problems.

More recent design advancements (mid 1980s) started introducing to both classic and cantilever systems a linkage mechanism in the rear suspension, making it easier to obtain the desired

stiffness curves. These designs are generally based on the four bar linkage. These are distinguished only by different attachment point of spring-damper unit, which can be exemplified by Figure 15.

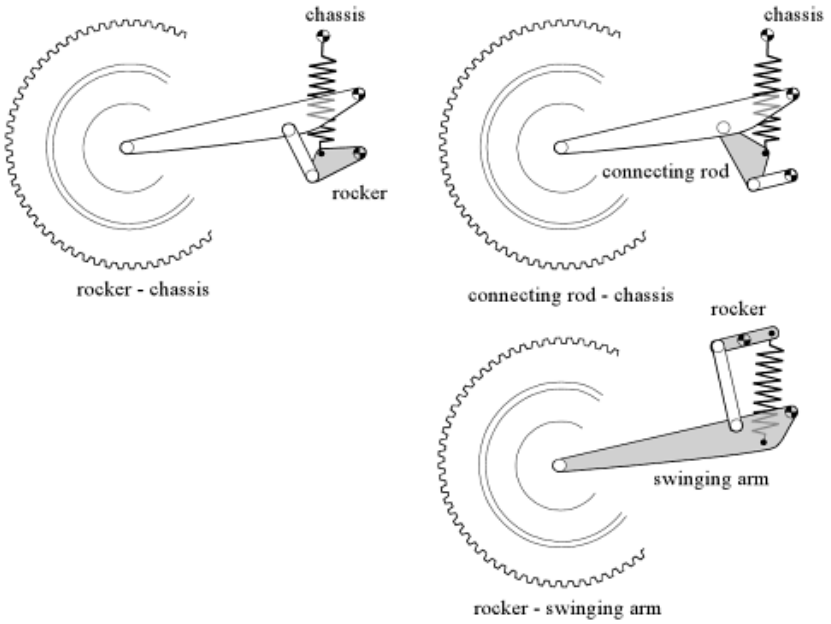

Figure 15 Schemes of rear suspension with swing arm and four-bar linkage. [14]

Other types of suspension systems based on six-bar linkage has also been tried by Morbidelli. This can potentially generate curves with more unique progression of suspension stiffness. However, this is a rare mechanism, since the highly complex construction does not justify the few gains in stiffness control, Figure 16.

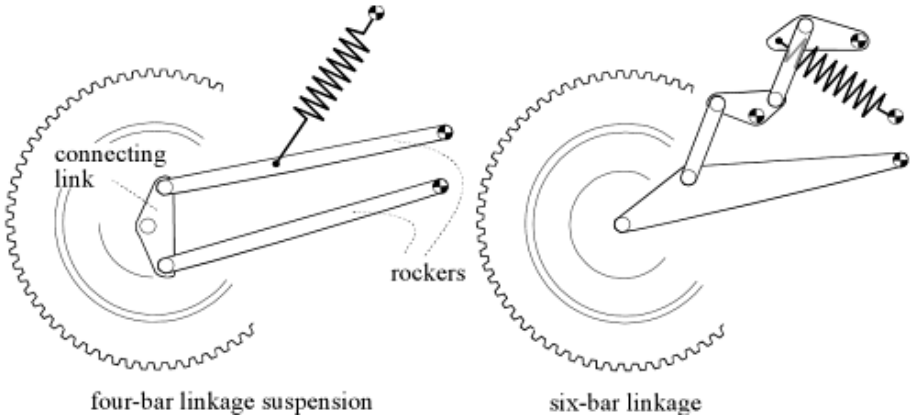

Figure 16 Schemes of rear suspensions with four-bar and six-bar linkage. [14]

Front Swing arm

Telescopic forks are practically universal among scooters and motorcycles. From a manufacturer point of view, the main reasons for this widespread steering solutions are:

- Telescopic forks have experienced as extensive period of study and development, which cannot be compared to any of the alternative designs.
- Most parts that compose a telescopic fork are prone to mass production, which directly leads to many times a reduced price of production.

However, the main reason is aesthetic. Marketing and R&D departments of manufacturers admit that telescopic forks have a clean and simple appearance that the fashion-conscious motorcyclist finds attractive. Thus, the risk of trying alternatives on competitive markets is high.

Nowadays there is a changing trend regarding the use of alternative options. Modern motorcycles are getting more powerful and motorcyclists and safety standards commissions alike demand for an ever more precise dynamical behaviour under extreme loads. Due to its long tubular construction, the telescopic fork presents a number of obvious structural disadvantages considering this evolving demands:

- Lateral flex – bumps can cause lateral displacement and the long lever arm causes high bending movements in the fork legs and steering head, Figure 171.
- Leverage – a great quantity of leverage can occur on the steering head. This results in very large forces that have to be resisted by a strong hence heavy frame.
- Nosedive – under braking, telescopic forks deform due to mass transfer, Figure 182.
- Stiction – due to stiction of the sliders, telescopic forks tend to have a poor response to small depressions/bumps.

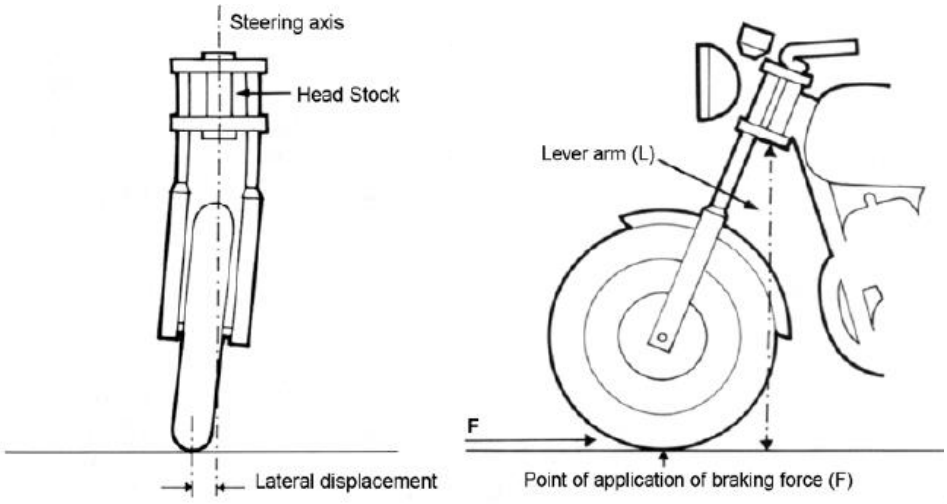

Figure 17 Lateral deflection in telescopic fork systems.

Figure 18 Hard braking leads to extreme compression of the fork.

To overcome this inherent defects of the telescopic fork, different suspension systems have been suggested, Figure 19 to Figure 21:

- Push arm.
- Trailing arm.
- Four-bar linkage.

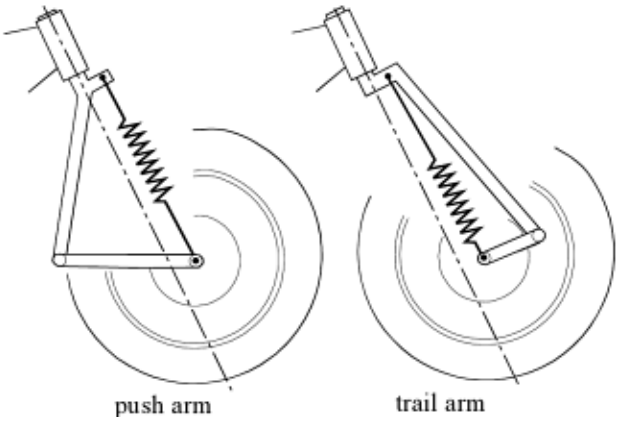

Figure 19 Schemes of front suspension with pushed and pulled wishbones.

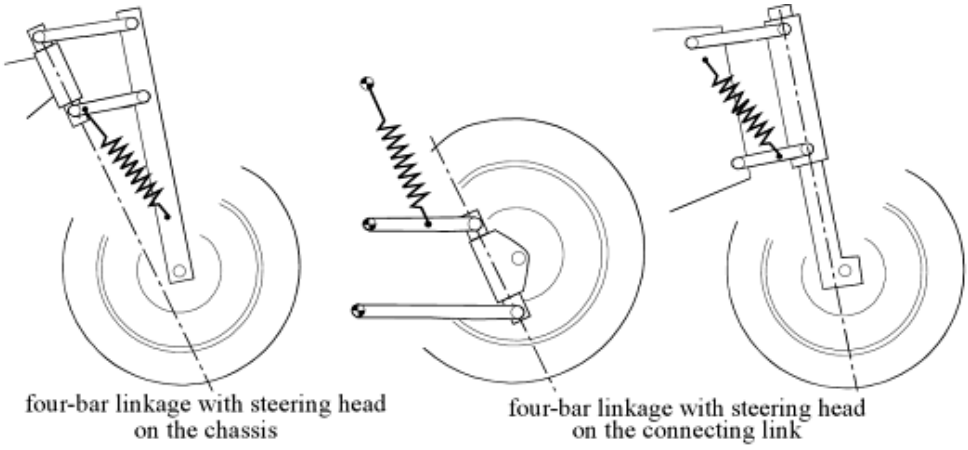

Figure 20 Schemes of four-bar linkage suspension.

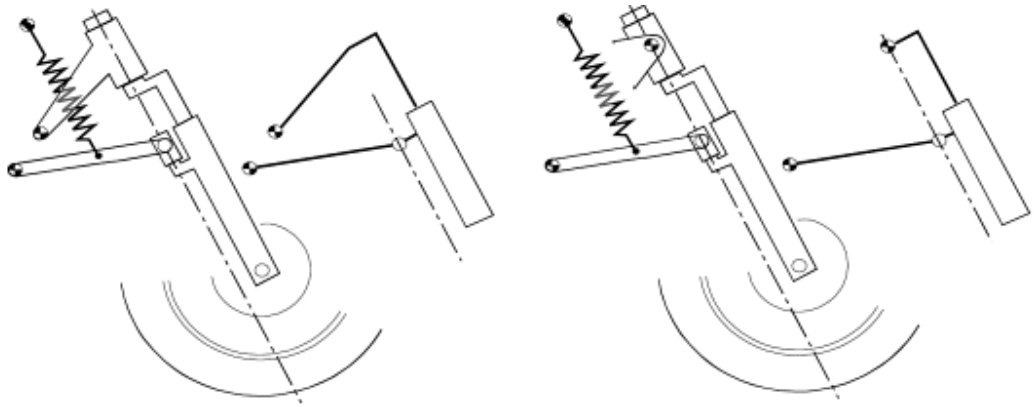

Figure 21 Schemes of four-bar linkage front suspension with prismatic pairs.

All these systems have specific advantages and disadvantages. Though, when compared to the telescopic fork, the following improvements can be appointed (Figure 22):

- Higher structural stiffness.
- Low levels of strut bending when braking, due to shorter parts. Therefore, sliding tubes have less tendency to jam.
- Weight advantage and responsive performance (In some examples, steering is completely detached from suspension loads).
- These systems allow for certain geometry designs that only allow minimal dive upon sudden braking (improved rider feedback).

Figure 22 (left) BMW H2R with telelever system; (right) Vyrus 986 M2 with a frontal swing arm system (both different takes on four-linkage applications)

2 Theoretical Overview

2.1 Structural Criteria Selection

Swing arms, as all critic structural parts on a motorcycle, are not designed for failure situations. Since, structural stiffness is of high priority, this means that under normal use conditions deformations are minimal.

Cossalter suggests the following values:

- Swing arm lateral stiffness $K_{lateral}$ = 0.8-1.6 kN/mm.
- Swing arm torsional stiffness $K_{torsional}$ = 1-2 kNm/°.

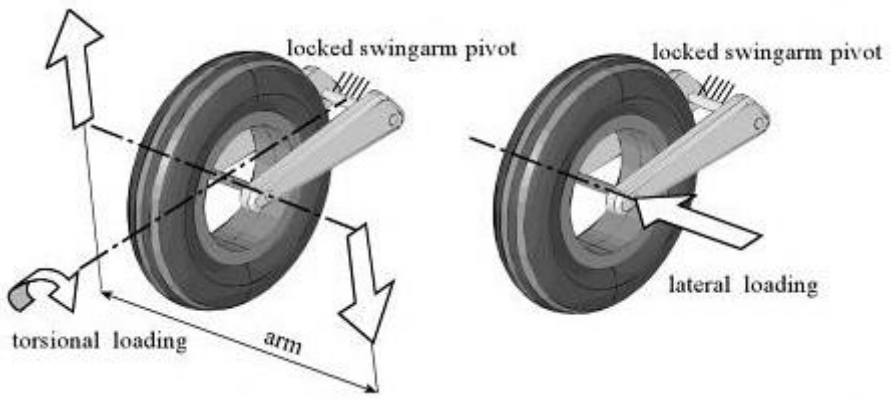

Figure 23 Cossalter's Approach for torsional and lateral swing arm testing

For design purposes, the range of stiffness values proposed by Cossalter [22] will be used.

Another very important criteria that has to be defined in any mechanical project is the coefficient of safety. Although, the function for which the swing arm is being designed is well known, uncertainty of conditions during its use is a concern. This level of uncertainty ultimately defines the safety coefficient and is directly related to following factors:

- Material quality
- Manufacturing process
- Accuracy of initial modelling

These uncertainties can have a direct impact on the vehicle, driver and general public, should they provoke an unexpected geometry change, or stiffness alteration on the strut (structural failure). Pugsley Method (Schmidt et al. (2013)) is a standard procedure followed to correctly define a safety coefficient, whose values are obtained from

Table 1 and

Table 2.

$$n_{proj} = n_{sx} \times n_{sy} \quad (3.1)$$

Table 1 Material characteristics relative to material, loads and stress analysis for n_{sx}

			B		
A	**C**	**Vg**	**g**	**f**	**P**
vg	**vg**	1.1	1.3	1.5	1.7
	g	1.2	1.45	1.7	1.95
	f	1.3	1.6	1.9	2.2
	p	1.4	1.75	2.1	2.45
g	**vg**	1.3	1.55	1.8	2.05
	g	1.45	1.75	2.05	2.35
	f	1.6	1.95	2.3	2.65
	p	1.75	2.15	2.55	2.95
f	**vg**	1.5	1.8	2.1	2.4
	g	1.7	2.05	2.4	2.75
	f	1.9	2.3	2.7	3.1
	p	2.1	2.55	3	3.45
p	**vg**	1.7	2.15	2.4	2.75
	g	1.95	2.35	2.75	3.15
	f	2.2	2.65	3.1	3.55
	P	2.45	2.95	3.45	3.95

vg – very good; g – good; f – satisfactory; p – poor

A – quality of materials, manufacturing, maintenance and inspection

B – control over applied load

C – stress analysis precision, experimental data or testing of similar parts

Table 2 Fail impact for n_{sy}

		D		
		Ns	s	vs
D	ns	1	1.2	1.4
	s	1	1.3	1.5
	vs	1.2	1.4	1.6

vs – very severe; s – severe; ns – not severe

D – level of danger to people

E – economic impact

Taking into consideration all factors A, B, C and D present on the tables, the following assumptions are proposed:

- Given this is a concept motorcycle and therefore loads are theoretically estimated and not measured based on real prototypes, the first assumption would be to give a poor trust level to A. Also, this is a competition project, so, weight loss is a priority, which enters in direct conflict with majored safety structural factors. This motorcycle is designed for the extreme situation of a race, but even in that situation, most effective usage will occur during close to stationary behaviour (studies on extreme situations are presented further ahead on this document). Also, it is safe to assume that an electric based power unit will produce less vibrations, than a combustion one, lowering down structural fatigue due to high frequency loads. Therefore, it was decided that a medium score should be used, B = g.
- If only critical structural components are analysed, it is possible to conclude that the chosen alloy properties and quality are well known. The manufacturing process will be shared between CNC machining (done in IST) and welding (by a sponsor). After a first participation of TLMoto on MotoStudent 2013/2014, team members and sponsors have gained experience on the structural challenges such motorcycles undergo. The current cooperation and knowledge share between all parts led to a final A = vg.
- The critical structural mechanical parts in this project, as in any modern similar project, independently of scale, is highly supported on FEA studies. This is a numerical method of reference in the study of stress, strain, safety factor and displacement. Thus C = vg.
- Economic impact depends most times more on the size and external image of the project, than necessarily on the building process. TLMoto is a team of students and not a professional company, therefore the aim of this project will never be profit. Nevertheless, image towards sponsors and partners is important, since most income comes inevitably from them. The team is fairly new and this is a new project, so income is limited, which means that failure on critical expensive parts could dictate a severe impact on the overall project strategy, therefore, E = vs.
- Active and passive safety associated to motorcycles is by nature inferior, for example, to cars. There are currently several innovative devices and solutions in both topics to make vehicles ever more safe to operate (ABS, stability and traction control, airbags, close distance alarms, driver behavioural active analysis, etc.). Yet, given the economic resources, structural and dynamic main concerns of this project, only high performance braking is considered an indirect safety priority. The motorcycle will however always be

ridden by a professional pilot, which, given the real average speeds of these races, dramatically decreases the chance of a catastrophic accident. Therefore, D = s.

Finally, the project safety value can be weighted.

Parameters	**A**	**B**	**C**	**D**	**E**
Score	vg	g	vg	s	Vs

Which result in the following final score:

$$\begin{cases} n_{sx} = 1.3 \\ n_{sy} = 1.4 \end{cases}$$

$$n_{proj} = 1.82$$

2.2 Simplified Motion of a Motorcycle

Many assumptions and studies could be conduct regarding the normal motion of a motorcycle. At any given time, numerous nonlinear forces and vibrations can be generated or imposed to the system motorcycle + driver. The swing arms being critical load transfer parts, would likely be affected by most of those external and internal solicitations. However, considering such a complex and real model would be extremely time consuming and liable to error.

However, as already stated, competition in the motorcycle world already has a long story. This means that in the absence of studies, there is still plenty of useful information achieved by experience of motorcycle designing teams.

The 3D motion of a motorcycle can be parted into two different main types: rectilinear and cornering motion. In this chapter, only the rectilinear motion is further suited, for the reasons already appointed. Cornering behaviour will be assumed as satisfactory if the following rules are followed.

2.2.1 Centre of Gravity

One of the most important design features of any motorcycle is the manner in which weight is distributed throughout the machine. According to John Bradley [13], there are four basic requirements when it comes to CG placing:

- All components have to fit physically acceptable locations
- The rider has to fit comfortably on the motorcycle in a position that minimises aerodynamic drag.
- The centre of gravity must be in a suitable position. If it is not, the motorcycle will experience artificially low limits on its acceleration and braking as well as various handling problems.
- The swinging arm geometry must be acceptable. It must allow a sensible chain run without excessive changes in the centre distance and it must not induce excessive pro-squat or anti-squat tendencies.

The centre of gravity of an object is defined as the point at which the entire weight of the object may be assumed to act. With any object, this is always an idealisation, since the weight of the motorcycle is distributed throughout the space that it occupies. However, from a design and dynamics point of view, it can be an accurate representation of reality.

It is understood that the battery pack will affect the final CG more than any other sub assembly on the prototype. Having this in mind, a market study on batteries and pre-design of an entire battery box was conducted. Main final geometry and details can be consulted on Annex.

There are several methods to calculate the CG, however, one can neglect all physical methods [13], since the motorcycle prototype does not exist yet. The pursue for a suitable CG in initial stages of a design can be considered purely theoretical, however, nonetheless critical. When a car is considered, advantages of a low CG are clear – the lower the CG is, the better handling and grip a race track car will have. In a motorcycle this conception is not so clear, Table 3:

Table 3 Main differences in behaviour due to Centre of Gravity shift

Forward Centre of gravity	The motorcycle tends to over-steer (in curves the rear wheel slips laterally to a greater extent)
Rear centre of gravity	The motorcycle tends to under-steer (in curves the front wheel slips laterally to a greater extent)
High centre of gravity	The front wheel tends to lift in acceleration. The rear wheel may lift in braking.
Low centre of gravity	The rear wheel tends to slip in acceleration. The front wheel tends to slip in breaking.

Again, the best practice is to search for a good real example that suits the needs of this project. For 2013 MotoStudent Edition, TLM01 was designed taking into consideration most technical aspects of Aprilia RS250. This machine, in production from 1994 to 2004, with minimal upgrades was inspired on the Aprilia GP250, Table 4. This design decision leads to a more forward and high CG.

Table 4 General specs of an Aprilia RS250

Aprilia RS 250 and rider main static technical features	
Dry Weight	130 kg
Wet Weight (with only necessary fuel for race)	140 kg approx.
Wheel Base	1350 mm
Weight Distribution (Percentage of Weight on front wheel) = %ant	55% approx. (55% front – 45% rear)
Rider weight (average 16 year old male)	60.8 kg
hg (height of system CG - Motorcycle + Rider)	600-650 mm

2.2.2 Motorcycle Loads and Limit Situations

When in motion, a motorcycle can be subjected to a number of loads/forces. As any other dynamic machine, these can be divided in statics and dynamics. Although static and dynamic loading have different structural effects, it is accepted that static loading should define the initial steps of a structural project.

Now, the importance of assuming a real world example becomes apparent. Taking into consideration structural dimensions from Aprilia RS250 and applying a momentum balance equation to the structure, it is possible to calculate the normal static loading of the motorcycle with a rider on top. For calculation purposes, front and rear forces on wheels are referred to as Ff and Ft, respectively, Figure 24.

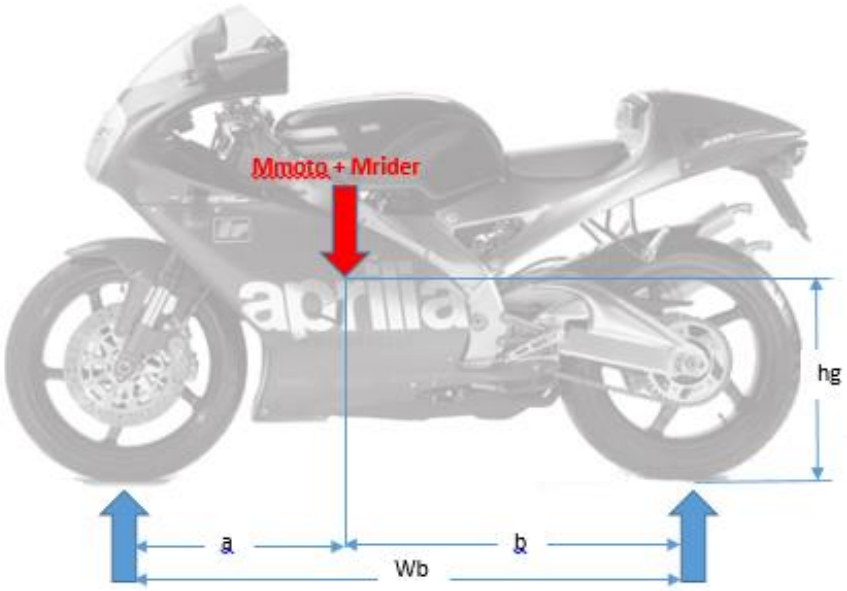

Figure 24 Motorcycle weight distribution

a Distance between front wheel and CG

b Distance between rear wheel and CG

F_f Front wheel force

F_t Rear wheel force

Mg Total Weight

$$Mg = (Mmoto + Mrider)g = (140kg + 60{,}8kg) * 9{,}8\frac{m}{s^2} \tag{3.2}$$

$$a = (1 - \%ant) \qquad F_f = \%ant * Mg$$

$$b = \%ant \qquad F_t = (1 - \%ant)Mg$$

$$\begin{cases} Mg = 1967{,}84\ N \\ a = 607{,}5\ mm \\ b = 742{,}5\ mm \\ F_f = 1082{,}31\ N \\ F_t = 885{,}53\ N \end{cases}$$

These first values can be only considered an estimation, since there was no access to a similar vehicle. However, values for vertical force on the wheels should not differ much, since that would only happen due to different measures of oil and fuel (Wet weight). Also, some considerations taken on Annex 2 regarding battery box and overall weight, help corroborating this assumption.

The definition of approximate weight distribution through both wheels is important, since, according to John Bradley [13], a, b and hg can be used for calculation of four critical limiting situations:

- Front wheel lifting due to forward acceleration
- Rear wheel spin due to forward acceleration
- Rear wheel lifting due to retardation
- Front wheel slide due to retardation

Before calculating the four limiting situations it is worth to understand hg. This measure is not constant and it would be a mistake to consider a single value for it. That happens because the rider changes position during extreme braking and forward acceleration situations, changing the position of hg. A designer can ultimately define the ideal wet weight hg for a motorcycle, but in the competition world, that will always depend on the personal preference of a pilot. So, regarding initial structural, hg should be considered an interval of possible values. Conclusions should be drawn from how much is hg indeed interfering with the four limiting situations, Table 5.

Acceleration to lift front $$a_{lf} = \frac{g(W_b - a)}{h_g} \quad (3.3)$$

Acceleration to spin rear $$a_{sr} = \frac{\mu g a}{(W_b - \mu h_g)} \quad (3.4)$$

Retardation to lift rear $$r_{lr} = \frac{ga}{h_g} \quad (3.5)$$

Retardation to slide front $$r_{sf} = \frac{\mu g(W_b - a)}{(W_b - \mu h_g)} \quad (3.6)$$

Table 5 Dynamic changes due to shift in CG

	hg = 600mm	hg = 650mm	hg = 700mm
1.	$a_{lf} = 12{,}13\frac{m}{s^2}$	$a_{lf} = 11{,}19\frac{m}{s^2}$	$a_{lf} = 10{,}40\frac{m}{s^2}$
2.	$a_{sr} = 13{,}58\frac{m}{s^2}$	$a_{sr} = 15{,}33\frac{m}{s^2}$	$a_{sr} = 17{,}59\frac{m}{s^2}$
3.	$r_{lr} = 9{,}92\frac{m}{s^2}$	$r_{lr} = 9{,}16\frac{m}{s^2}$	$r_{lr} = 8{,}51\frac{m}{s^2}$
4.	$r_{sf} = 16{,}60\frac{m}{s^2}$	$r_{sf} = 18{,}73\frac{m}{s^2}$	$r_{sf} = 21{,}50\frac{m}{s^2}$

Before taking any initial conclusions on CG height, it is plausible to discuss first the assumed weight distribution and tyre friction coefficient.

A weight distribution of 45%/55% and 55%/45% front to rear laden covers most tarmac racing motorcycles. The figures with a greater rear end bias are found on early classic racers, because previously it was commonly understood, that handling could be slightly sacrifice to account for

lower powered motors and inferior rear tyre frictions. Nowadays, 55%/45% is a more common distribution, since higher loads on the front tyre will improve handling, given that high performance braking systems and tyres are used. Also, modern motors are by norm overpowered for most situations on the track, while modern tyres can achieve friction coefficients of 1,3, which eventually decreases the necessity of higher loads on the rear tyre.

The manufacturer states that an Aprilia RS 250 should be able to reach 100 km/h (27,78 m/s) in approximately 3,9 seconds. This means that for this model, forward accelerations up to 7,12 m/s^2 are possible. As for retardation limits, it is commonly assumed, according to John Bradley [13], that 1 g is a safe limit, since rider and motorcycle can both suffer from fatigue under such circumstances, undermining the possibility to brake and corner effectively.

It is noticeable that rear and front spinning are the less likely situations with minimum acceleration values well above 7,12 m/s^2 and 9,8 m/s^2, respectively. Given the current geometry it seems that the most likely extreme event is rear lifting under braking. As stated above, 9,81 m/s^2 should be the limit acceleration value under retardation. So, rearranging Equation (3.6) as limiting condition, we have , see Table 6:

r_{lr}	Retardation to lift rear
a	Distance between front wheel and CG
g	Gravity acceleration
h_g	Height of CG

$$r_{lr} = \frac{ga}{h_g} \leftrightarrow h_g = \frac{ga}{r_{lr}} \leftrightarrow h_g = a \tag{3.7}$$

$$r_{lr} = g$$

Table 6 Initial assumed approximate hg

	hg = 607.5mm
1.	$a_{lf} = 11{,}98 \frac{m}{s^2}$
2.	$a_{sr} = 13{,}81 \frac{m}{s^2}$
3.	$r_{lr} = 9{,}81 \frac{m}{s^2}$
4.	$r_{sf} = 16{,}88 \frac{m}{s^2}$

In conclusion, a precise CG is both a requisite and a consequence of critical design decisions, should as geometry of swing arms, frame and battery pack.

2.3 Squat and Dive

Initial swing arm design must take into consideration load transfer in transient situations. Previously, a CG was calculated for the system motorcycle + rider. Although this concept is useful for static calculations of nominal and extreme situations, it is known that a motorcycle will experience conditions of acceleration, or retardation, during most of its riding time. Load transfer is an effect of that continuous variable behaviour. To simplify, every time we apply brakes or open the throttle in any road wheeled vehicle, it is possible to feel the tyre load lightening at one end whereas increasing at the other. Motorcycles experience this effect to a much greater extent than most vehicles due to their relatively high CG in relation to their short wheels.

Suspension systems and different structural parts (swing arm, chassis, sub-frame, etc.) must cope with load transfer coming from mainly four sources:

- Inertial forces, or forces necessary to accelerate and brake
- Aerodynamic forces – the tendency for drag force to lift the front and load the rear
- Road inclination – when going downhill, more weight is supported by the front and vice-versa.
- Torque reaction from accelerating the crankshaft and clutch, etc.

The main four sources of weight transfer are usually well known, however, being this an initial stage of the project and given the final application of this motorcycle, some reflexion is necessary over the priority of tackling each source. Motor power, wheelbase, motorcycle and rider weight and overall theoretical CG were all discussed before and are critical variables capable of interfering with structural geometry during acceleration and braking.

On the other hand, drag is the most prominent component of motion resisting forces and, ultimately, drag is what limits the motorcycle top speed. However, fairing characteristics are still unknown and given the expected top speed of approximately 140 km/h, this will be neglected for now. It is possible, if necessary, in a later stage of the project to counteract the front lifting force with different preload settings on rear and front suspensions.

Road inclination could be also a critical aspect if this motorcycle was being designed for uphill, downhill circuits, or even off-road. However, the final objective is for this motorcycle to participate at MotorLand Aragón Circuit, with a maximum inclination of 7.2% and a difference in height of only 50m, over a track length of 5345m. Consequently, like aerodynamic forces, designing a motorcycle for steep inclinations is not a priority, therefore, suspensions can be adjusted at a later stage depending on track and conditions.

Torque reaction from accelerating the crankshaft and clutch is a concern only across frame engines, which is not case. Also, electric motors are a small source of out of balance masses and vibrations when compared to combustion engines, which eventually defines this source of load transfer as almost negligible.

Now that acceleration and braking moments are taken as critical for geometry design, the next step is to understand how much squat and dive behaviour should be expected from the motorcycle. Squat and dive refer to the pitch and height changes of the sprung part of the motorcycle. Dive is a forward pitching motion caused usually by braking, while squat denotes the reward rotation normally due to acceleration and aerodynamic forces.

Another term that should be understood is motorcycle trim. This term implies the geometry configuration changes that a motorcycle acquires under different loading conditions. Both transient and steady motions affect the system rider + motorcycle. However, given that the current design is to be applied on a track, transient extreme conditions are of critical importance. Squat and dive, under high acceleration and braking are the two major symptoms of load transfer that ultimately affect the motorcycle trim.

As it will be explained, motorcycle trim depends on the stiffness characteristics of the front and rear suspensions, on the forces operating on the motorcycle, and on the inclination angle of the chain and the swing arm.

2.3.1 Rear Suspension Balance

Assuming a forward motion, the forces applied on the rear swing arm system may be represented by the following, Figure 25:

- Thrust force S;
- Vertical dynamic load Nr;
- Chain force T;
- Elastic torque M.

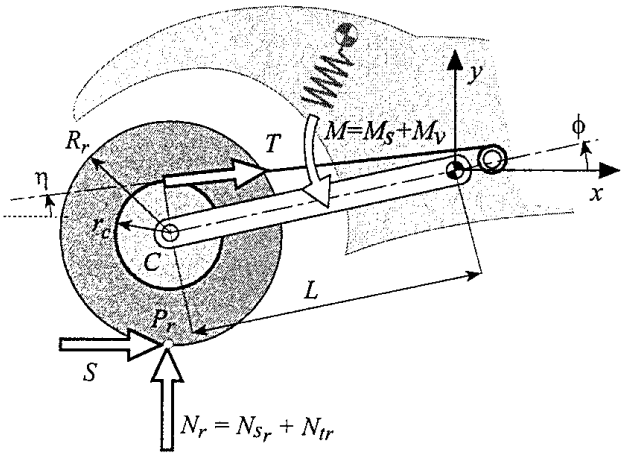

Figure 25 Balance of forces and moment on rear wheel and swing arm

The following balance of moments on the swing arm pivot may be derived:

$$M_v = N_{tr}Lcos\phi - S(R_r + Lsin\phi) + T[r_c - Lsin(\phi - \eta)] \quad (3.8)$$

M_s and N_{sr}, the static elastic moment applied by the suspension spring and the moment generated by the static vertical load Nsr directly balance each other. Thus they are out of presented balance.

The four different moments acting on the swing arm are:

- N_{tr}, the moment generated by the load transfer that compresses the suspension;
- S, the moment generated by the driving force that tends to extend the suspension;
  T, the moment generated by the chain force that compresses the suspension;
- M_v, the additional elastic moment generated by the suspension that can be positive or negative.

It is possible to simplify the driving force by assuming it constant and related to the chain force.

$$S = \frac{T * r_c}{R_r} \quad (3.9)$$

Getting back to (3.8), assuming there is a thrust force, the trim of the rear suspension (arm position with respect to the frame), depends on the values of the three above-mentioned components. Stating the driving force as a function of the chain force, the equilibrium equation, with respect to the swing arm pivot, can be rearranged as:

$$M_v = N_{tr}Lcos\phi - TL\left[\frac{r_c}{R_r}\sin\phi + sin(\phi - \eta)\right] \quad (3.10)$$

It is comprehensible that M_v is part of the elastic moment, necessary to balance the moments generated by load transfer, chain force and driving force.

Some initial conclusions can be drawn from this equation.

- In a scenario that load transfer is larger than chain force and driving force, the suspension is more compressed, when compared to the deflection caused by static load only (M_v > 0).
- On the other hand, if chain force and driving force components are prominent over the load transfer component, the suspension is extended (M_v < 0).

2.3.2 Squat Ratio and Squat Angle

Now that the balance of moments on the rear swing arm system is understood, it is possible to calculate squat and dive properties of the whole structure. To do that however, it is necessary to assume the coupling forces generated at the front wheel, Figure 26.

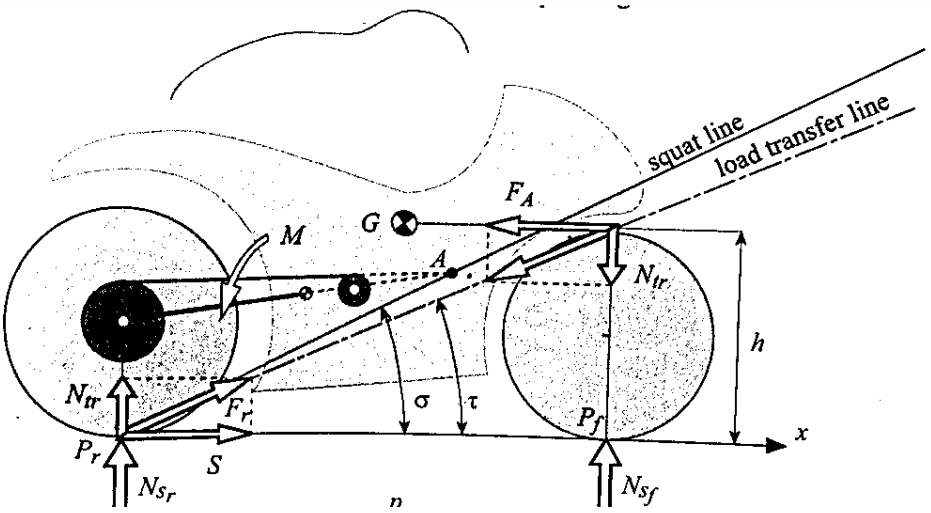

Figure 26 Squat - Load transfer lines

Certain additional geometrical terms need to be considered. Take intersection point A, between the axis of the upper chain branch and the straight line passing through the centre of the wheel and through the swing arm pivot. A straight line between the rear wheel Pr and point A can be drawn, this line is called squat line. Its inclination to the horizontal plane is called the squat angle.

Squat properties can derived through the calculation of the squat ratio. This is the ratio between load transfer and the moment generated by the sum of the chain force and the driving force.

$$\Re = \frac{N_{tr} L cos\phi}{S[R_r + Lsin(\phi)]} \tag{3.12}$$

It is possible to further simplify the expression of squat Ratio by expressing load transfer as a function of the driving force. The ratio becomes then function of the load transfer and squat angle tangents, Table 7.

$$\Re = \frac{\tan \tau}{\tan \sigma} \tag{3.13}$$

Three different scenarios are identifiable:

Table 7 Variation in R – rear suspension

R = 1	While on thrust, there no additional moments operating on the swing arm – suspension spring is no longer stressed in reference to the static condition scenario.
R > 1	The moment generated by Fr causes spring compression.
R < 1	The moment generated by Fr causes spring extension.

Table 8 Variation in R - front suspension

R = 1	Although no noticeable extension on the rear spring. The front spring will extend proportionally to the load transfer only.
R > 1	The moment generated by Fr causes rear spring compression. So, front spring will extend proportionally to load transfer and rear compression.
R < 1	The moment generated by Fr causes rear spring extension. So, front spring will extend proportionally to load transfer, while being compressed by rear spring extension.

In general, angle σ is greater than load transfer τ, therefore the ratio $\Re$ is less than one. This means that the suspension is always extended under thrust. It is now clear that the swing arm length will greatly affect squat and dive behaviour.

3 Swing Arm Design and testing

All major components that dictate the initial design of motorcycle swing arms were analysed to different depths. Other geometry and dynamic aspects could also be taken into consideration before starting swing arms design, cornering behaviour, chassis design, pilot position and control unit components. However, that would deviate from the main aim of this document, to design and provide a study on the initial aspects of swing arm design on a competition electric motorcycle.

3.1 Finite Element Analysis Observations

In this chapter, some considerations will be taken relatively to Finite Element Analysis. Computational FEA is commonly applied tool in modern mechanical design. As a numerical method, it makes use of partial differential equations to find approximate solutions, when the correct, or closest possible, boundaries are applied. Since only approximate solutions are possible, numerical error analysis is another concern. In this case, mechanical parts are design to only operate on an elastic regime (elastic properties of composing materials), so, being an elastic behaviour problem, it can be represented by the following equations:

$$\frac{\delta\sigma_{xx}}{\delta x}+\frac{\delta\sigma_{xy}}{\delta y}+\frac{\delta\sigma_{xz}}{\delta z}+f_x=\rho\frac{\delta^2u_x}{\delta t^2} \tag{5.1}$$

$$\frac{\delta\sigma_{xy}}{\delta x}+\frac{\delta\sigma_{yy}}{\delta y}+\frac{\delta\sigma_{yz}}{\delta z}+f_y=\rho\frac{\delta^2u_y}{\delta t^2} \tag{5.2}$$

$$\frac{\delta\sigma_{xz}}{\delta x}+\frac{\delta\sigma_{yz}}{\delta y}+\frac{\delta\sigma_{zz}}{\delta z}+f_z=\rho\frac{\delta^2u_z}{\delta t^2} \tag{5.3}$$

σ_{ij} is the stress component, f_i the volumetric force, ρ the specific mass and u_i the displacement field.

Using the three dimensional general boundary conditions (applied loads along a specific boundary within the analysis domain) equations:

$$\sigma_{xx}n_x+\sigma_{xy}n_y+\sigma_{xz}n_z=\hat{t}_x \tag{5.4}$$

$$\sigma_{yx}n_x+\sigma_{yy}n_y+\sigma_{yz}n_z=\hat{t}_y \tag{5.5}$$

$$\sigma_{zx}n_x+\sigma_{zy}n_y+\sigma_{zz}n_z=\hat{t}_z \tag{5.6}$$

And essential boundary conditions (prescribed displacements (and its derivatives)).

The constitutive relation for isotropic materials is given by:

$$\begin{bmatrix}\sigma_{xx}\\ \sigma_{yy}\\ \sigma_{zz}\\ \sigma_{xy}\\ \sigma_{xz}\\ \sigma_{yz}\end{bmatrix} = \frac{E}{(2\upsilon-1)(1+\upsilon)}\begin{bmatrix}\upsilon-1 & -\upsilon & -\upsilon & 0 & 0 & 0\\ -\upsilon & \upsilon-1 & -\upsilon & 0 & 0 & 0\\ -\upsilon & -\upsilon & \upsilon-1 & 0 & 0 & 0\\ 0 & 0 & 0 & \frac{2\upsilon-1}{2} & 0 & 0\\ 0 & 0 & 0 & 0 & \frac{2\upsilon-1}{2} & 0\\ 0 & 0 & 0 & 0 & 0 & \frac{2\upsilon-1}{2}\end{bmatrix}\begin{bmatrix}\frac{\delta\sigma_x}{\delta x}\\ \frac{\delta\sigma_y}{\delta y}\\ \frac{\delta\sigma_z}{\delta z}\\ \frac{\delta u_x}{\delta y}+\frac{\delta u_y}{\delta x}\\ \frac{\delta u_x}{\delta z}+\frac{\delta u_z}{\delta x}\\ \frac{\delta u_y}{\delta z}+\frac{\delta u_z}{\delta y}\end{bmatrix}$$

(5.7)

Since, FEA is so extensively applied to CAD, there are well established methods to decrease the numerical error associated to this process. It is known that depending on type of finite element used, shape and dimension (mesh) will directly affect precision and consequently, final error of results. To define the most appropriate mesh, the method followed on this document consists of iterative testing of the same mechanical piece with several different meshing sizes and properties, starting from larger to smaller sizes – Convergence Method. Results are then compared between iterations till convergence of factors such as limit Stress and limit Safety factors is achieved. The software used in this work is SolidWorks version 2014.

When generating a mesh, SolidWorks 2014 uses two specific methods:

- **Standard Mesh** – finite elements are generated according to dimensions specified by user.
- **Adaptive or curvature based Mesh** – finite elements are generated mostly according to user specified dimensions, however, in areas of increased geometrical complexity, as tight corner and fillets, the software will adapt elements size to achieve increased stability of calculation.

Ultimately, adaptive mesh elements will provide an improved approximation to model geometric details, while avoiding near zero Jacobians during numerical integration of reference elements to global elements and aftermost global stiffness matrix composition.

SolidWorks also provides a three main types of elements with 4, 16 nodes (also known as Gaussian points). In previous versions of SolidWorks the options were 4 and 10 nodes, however the last was drop in preference to a 16 nodes element. Higher grade elements, or parabolic

(more than 4 nodes) should provide a more accurate mapping of curved geometries, with a penalty of increased computational time.

A standard rocker part (Figure 27), or linkage (Section 1.4.4), was choose to test mesh properties, Figure 28. Two hinge type constraints are applied on the likely connections between rocker and liking rod (1) and rocker and rear suspension (2). A vertical load of 1000 N is applied on (3) to simulate the action of a swing arm. It is understood that this structure is much simpler than a swing arm, however, it should simulate the same mesh issues on a smaller geometrical scale.

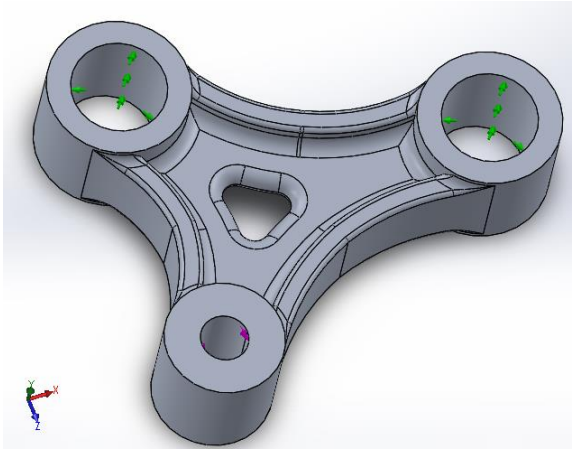

Figure 27 Rear Suspension Rocker

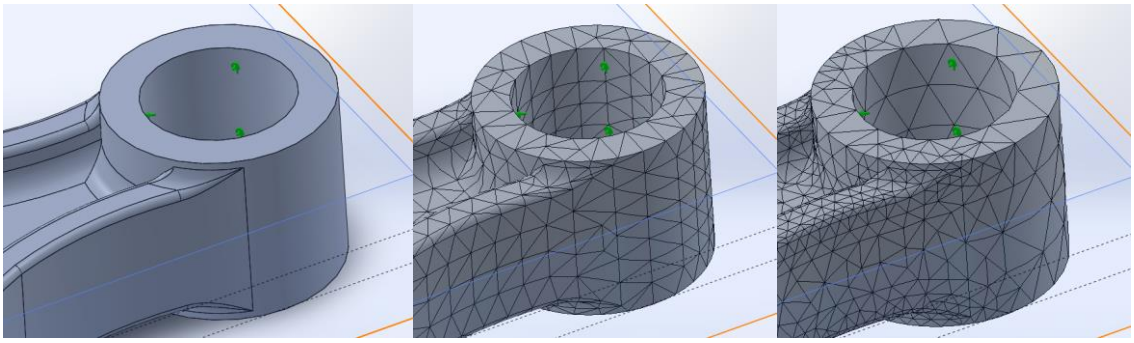

Figure 28 Swing arm link a) Geometry; b) Non adaptative mesh (Elem. size =5mm); c) Adaptative mesh (Element size (5;1)[mm])

Results for Maximum and Minimum stress according to Finite Element dimension and type are presented in Table 9 to Table 11.

Table 9 Percentage variation of Maximum Stress in relation to previous mesh dimension

Mesh variation (mm)	**5 – 3,75**	**3,75 – 2,5**	**2,5 – 1,75**	**1,75 - 1**
Standard Mesh	-9,67%	7,06%	-5,37%	-1,58%
Curvature based Mesh	6,29%	1,56%	-0,27%	13,66%

Table 10 Percentage variation of Minimum Stress in relation to previous mesh dimension

Mesh variation (mm)	**5 – 3,75**	**3,75 – 2,5**	**2,5 – 1,75**	**1,75 - 1**
Standard Mesh	-95,28%	36,88%	21,68%	8,28%
Curvature based Mesh	-99,10%	-25,50%	-237,46	6,31%

Table 11 Simulation time per mesh size in seconds

Mesh variation (mm)	**5**	**3,75**	**2,5**	**1,75**	**1**
Standard Mesh (s)	3	4	8	10	20
Curvature based Mesh (s)	3	5	11	22	36

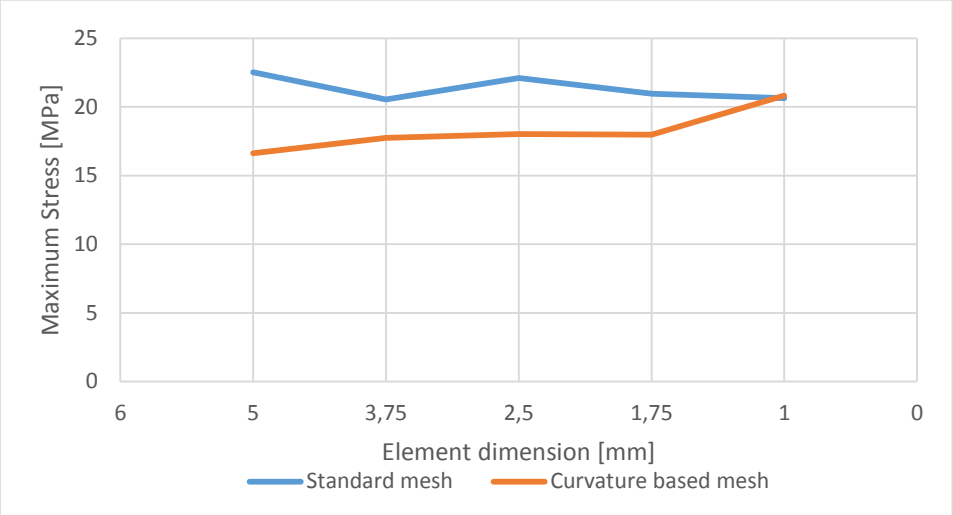

Graph 1 Maximum Stress Variation - Non Adaptative/Adaptative Mesh

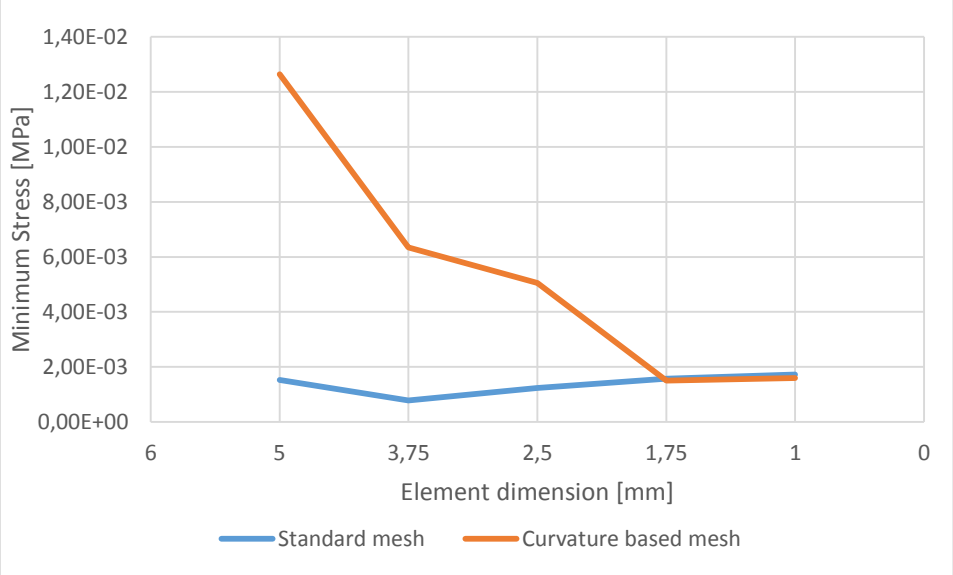

Graph 2 Minimum Stress Variation - Non Adaptative/Adaptative Mesh

After observing graphs 4 and 5 it is noticeable that smaller dimension elements tend to converge to the same Stress values. Surprisingly, adaptive mesh shows less stable results with larger elements, when compared to standard mesh. The computational cost was however noticeable, with a difference approximately 80% more time regarding elements of 1 mm. Given this initial results, it is possible to conclude that standard mesh can be a plausible choice for this type of static loading. It is understood that mesh refinement can be done locally in the case of more complex geometries, so it can be an advantage to keep a simpler type of mesh for the time being and manually alter size locally only when required.

Results for Maximum and Minimum Safety factors according to Finite Element dimension and type are presented in Table 12 and Table **13**.

Table 12 Percentage variation of Minimum Safety Factor

Mesh variation (mm)	**5 – 3,75**	**3,75 – 2,5**	**2,5 – 1,75**	**1,75 - 1**
Standard Mesh	8,81%	-7,55%	5,11%	1,50%
Curvature based Mesh	-6,71%	-1,57%	0,26%	-15,68%

Table 13 Percentage variation of **Maximum** Safety Factor

Mesh variation (mm)	5 – 3,75	3,75 – 2,5	2,5 – 1,75	1,75 – 1
Standard Mesh	48,78%	-58,38%	-27,73%	-9,01%
Curvature based Mesh	49,76%	20,32%	30,89%	54,22%

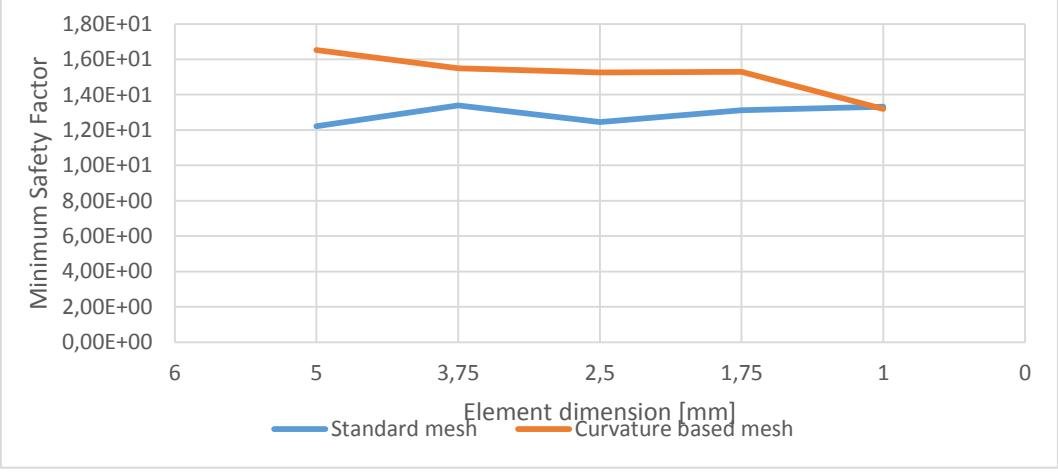

Graph 3 Variation of Minimum Safety Factor - Non Adaptative/Adaptative Mesh

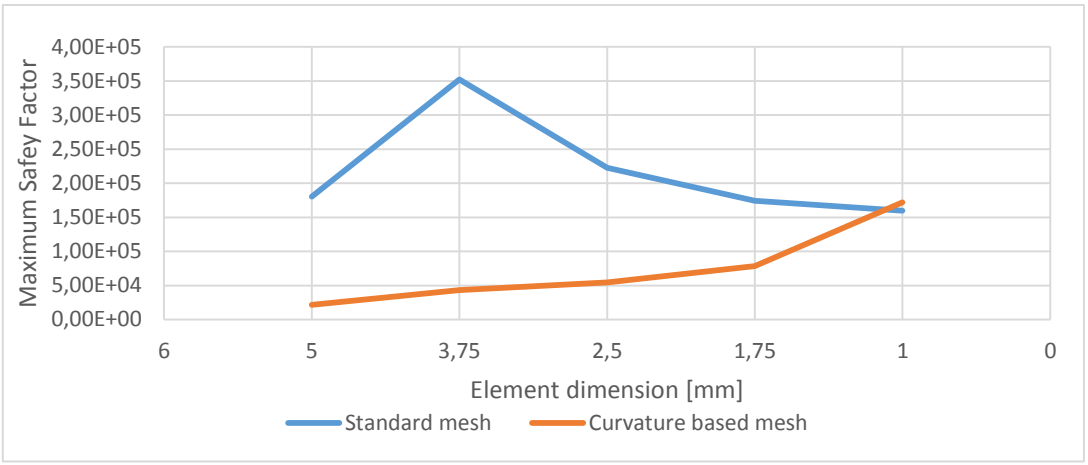

Graph 4 Variation of Maximum Safety Factor - Non Adaptative/Adaptative Mesh

Knowing the correct value for the minimum Safety Factor is critical in most mechanical parts. However, in this case it is possible to use it as a convergence analysis tool. Results become similar with finer element sizes, however both mesh types present a stable behaviour throughout range. The next mesh property to be tested is the number of nodes per 3D element.

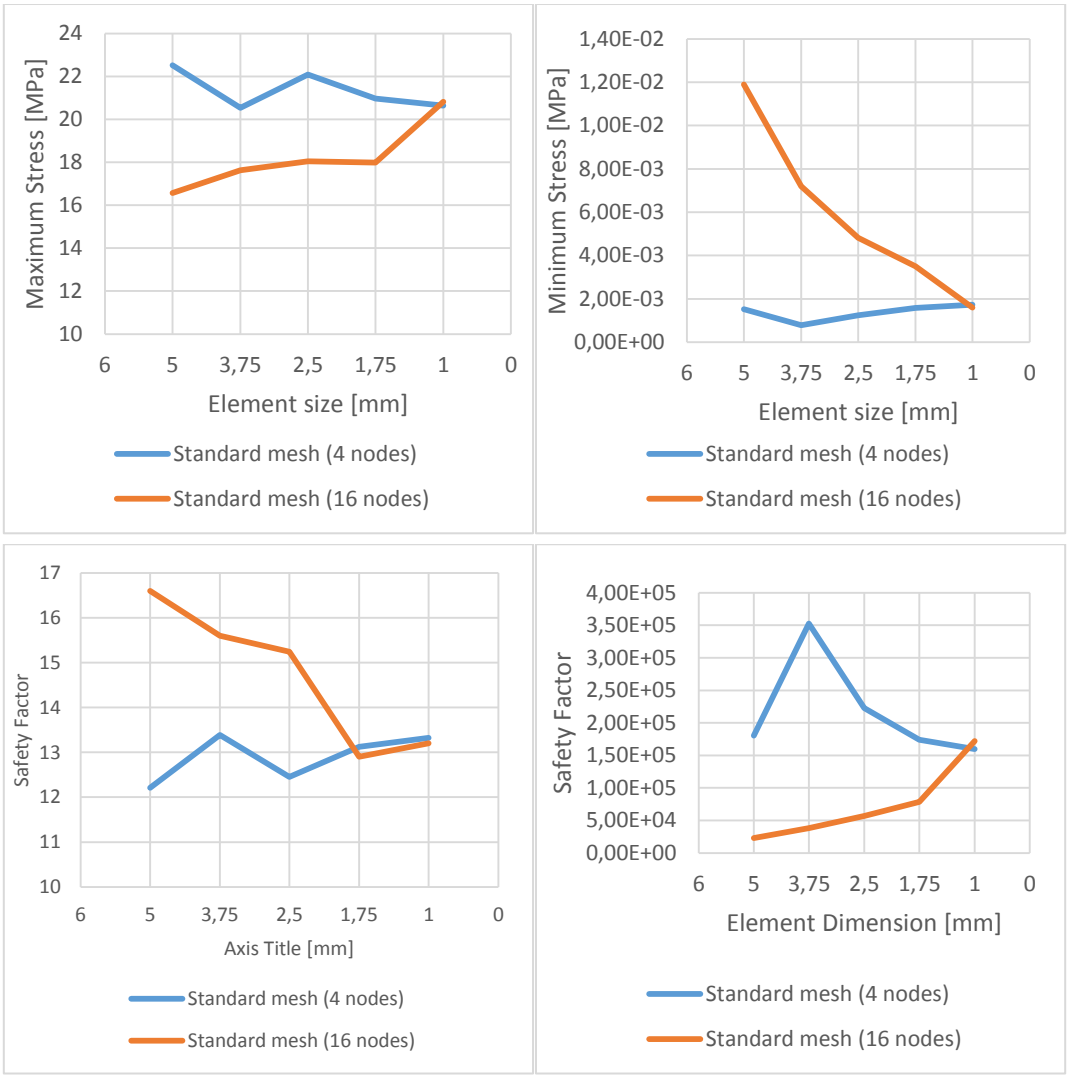

Graph 5 General Varations depending on number of nodes per 3D Elements

Once again, the 4 nodes approach proved to be in average more stable than the higher grade 16 nodes.

The next aspect to keep in mind regarding the use of fine mesh is areas of stress concentration. When locally altering elements size to better approximate a geometrical trait, it should be kept in mind that local maximum stresses may increase. To understand this behaviour the following rule determined by Hosford [23] may be applied where a stress factor K is related to local geometry detail parameters r/h.

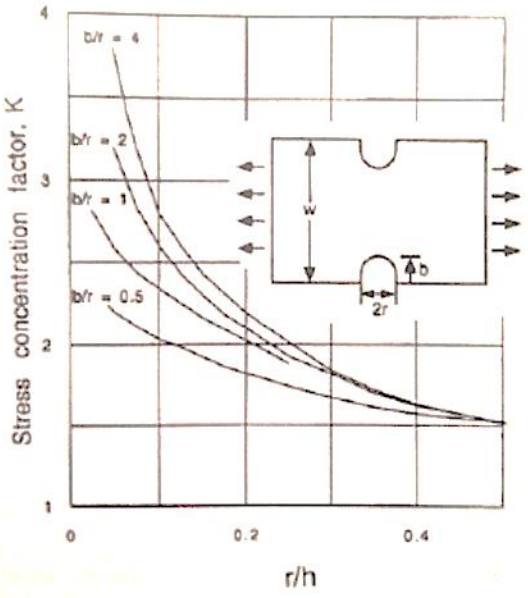

Graph 6 Stress concentration on tight corner under uniaxial traction [23]

The same simulation was processed, but this time on a model without fillets, originating several "live corners", known to be high concentration stress spots, Figure 29.

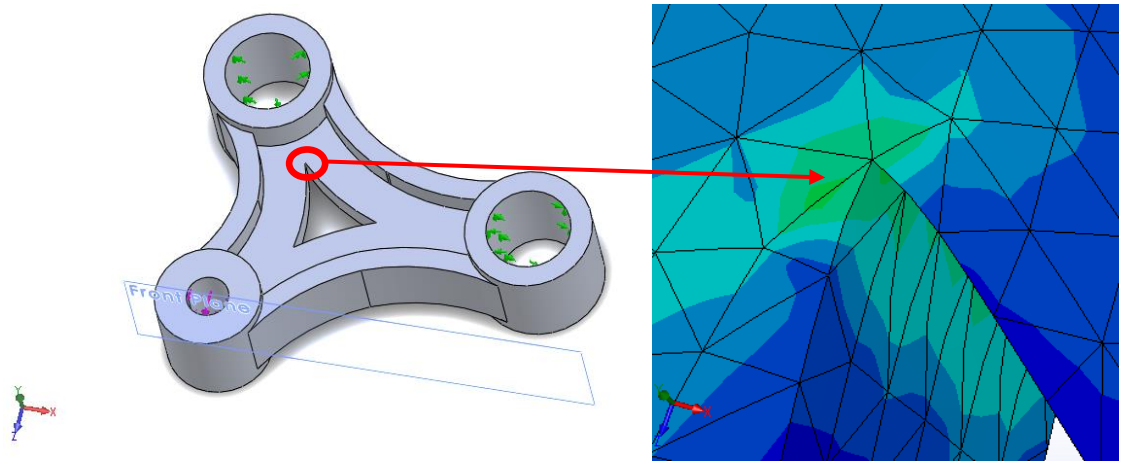

Figure 29 Corner mesh deformation (Von Mises local Stress)

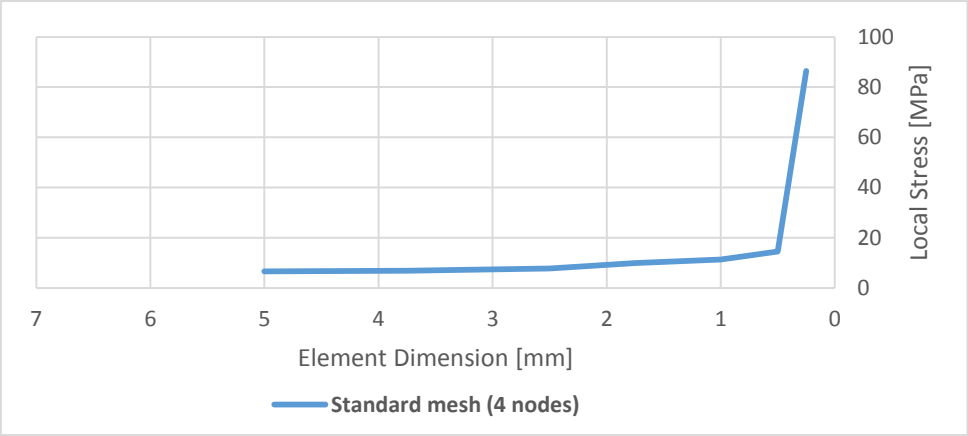

Graph 7 Local Stress Variation

3.2 Material Selection

The use of metal alloys for critical structural parts has been a common practice in motorcycle building since their first examples. In recent years, aluminium alloys have been taking the place of the previously used steel carbon alloys. This design option is mostly motivated by possibility of light weight structural designs that aluminium struts provide, when compared to steel examples, **Error! Reference source not found.**. Also, the following vantages are common etween both metal types:

- Available and relatively affordable market.
- Great knowledge and vast prove application examples.
- Cost efficient production and fabrication in most cases.
- Easy mass production.
- Almost boundless geometrical and dimensional design freedom.
- Finishing treatments quality.
- High stiffness.
- Homogenous and isotropic behaviour.

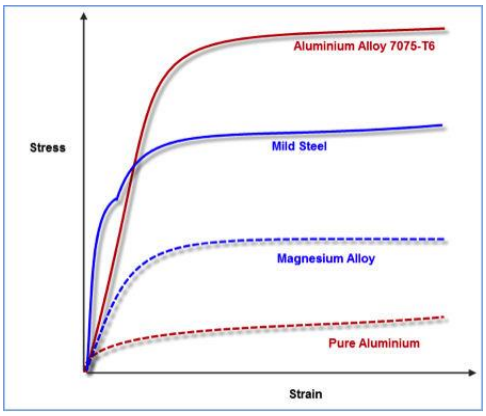

Figure 30 General behaviour of metal alloys

Several steel and aluminium alloy types were considered for this project. Two examples are presented and compared in Table 14**Error! Reference source not found.**.

Table 14 Comparison between Aluminium 7075-T6 and Steel AISI 4340

Aluminium 7075-T6	**Steel AISI 4340**
$\frac{\sigma_{yy}}{\rho} = \frac{505000000\mathrm{N/m^2}}{2700\mathrm{kg/m^3}} = 187037.0\frac{\mathrm{N.m}}{\mathrm{kg}}$	$\frac{\sigma_{yy}}{\rho} = \frac{710000000\mathrm{N/m^2}}{7850\mathrm{kg/m^3}} = 90445.9\frac{\mathrm{N.m}}{\mathrm{kg}}$
Price: 7.5€/kg	**Price: 1.88€/kg**

The ratio between mechanical resistance and mass density of these options show a clear superiority of the aluminium alloy (2.06 times higher). On the contrary, price is approximately 4 times higher, which is a common setback when designing parts for race motorcycles. Nonetheless, a good dynamical behaviour is of high priority in such projects, thus the final weight of the structure must be kept as low as possible. For this reason, 7075-T6 (mechanical properties on **Error! Reference source not found.**) is the chosen material for all parts shown in his document, unless pointed otherwise.

Property	Values
Elastic Modulus [N/mm^2]	72000
Poisson's Ratio	0.33
Shear Modulus [N/mm^2]	26900
Mass Density [kg/m^3]	810
Tensile Strength [N/mm^2]	570
Yield Strength [N/mm^2]	505

Table 15 General Properties of an Aluminium 7075-T6

3.3 Initial Geometry of the Rear Swing Arm

Battery and motor are two major structural and power parts of the concept, however, to complete the powertrain it is necessary to analyse how this power should be transmitted from the motor to the rear wheel. It was discussed before, that there are two common ways to this task in motorcycles – through a chain, or system of chains or through a driving shaft.

A dual system of chains was the option of choice for this project for the following reasons:

- Shaft systems are known to be reliable and require low maintenance. However, these prove to be complex to manufacture and bulky in most cases due to the increased dimensions of the swing arm (the shaft system needs to fit inside the arm structure). This system is rarely seen in high end track motorcycles.
- A single chain system is the most common solution for track motorcycles. However, this does not mean that it is the perfect solution.

Single Chain System	
Advantages	**Disadvantages**
Simple and reliable	Erosion is severely higher when compared to shaft, or belt transmission.
Easy and quick maintenance, or replacement	Chatter effect due to squat and dive, or when rear wheel is spinning
Light weight	It can be a consequence of the previous, but nonetheless a different effect. Stress on motor parts and interference with rear suspension action.
Economical when compared to shaft systems	
Able to resist high tensile loads.	

Chatter, or slack effect of chains however is well known and, in most cases, manufacturers accept these as a given fault. Again, these effects only become evident

in extreme scenarios, rare during daily use. Nonetheless, it is important to keep in mind that this motorcycle will be exposed to extreme track conditions. The dual chain system is a partial solution to this issue.

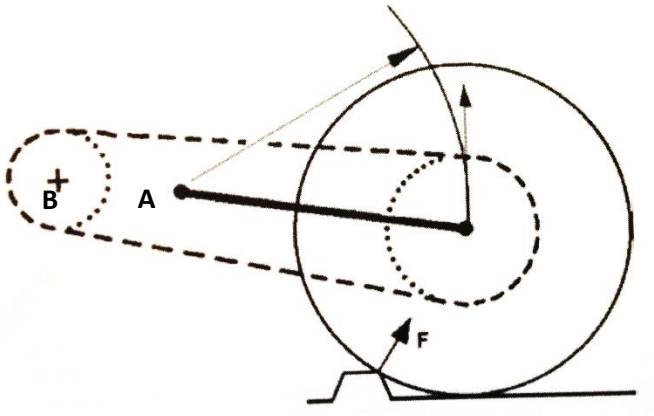

Figure 31 Single chain rear example

Figure 32 shows the classic representation of swing arm and chain. Point A represents the swing arm pivot point, while point B represents the motor sprocket. Taking the example of a bump in the road, it becomes clear that both parts will rotate according to their specific pivot point. Since the centre of rotation is not shared, the radius of rotation is different. Now, obviously, the swing arm is an extremely stiff structure, which means that the chain will be the one giving in. This would not be a problem in itself, if it would not give origin to oscillation in chain drive force. Rapid oscillation in chain load will indirectly impact a rear suspension system incapable of absorbing properly these high frequency loads.

A possible solution to this is using a second chain, creating a second pivot point concentric with the swing arm one, Figure 33.

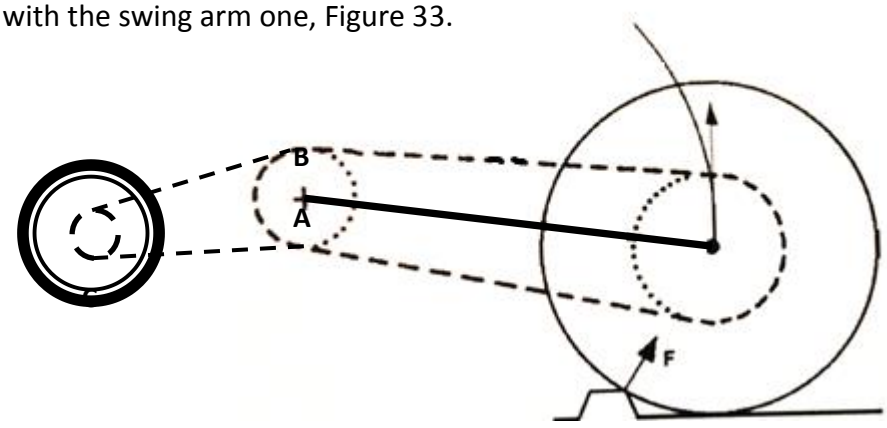

Figure 32 Dual chain rear example

Motorcycle design in general favours compact and light solutions. In the case of electrical motorcycle design, this philosophy becomes more critical, since energy is not so efficiently, in terms of weight and volume, as in combustion engine motorcycles. Because of this, space and structural flexibility to accommodate the battery package is a priority. Two scenarios were considered, Figure 33 and Table 16:

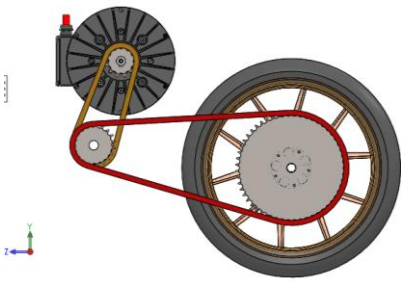

Figure 33 HE - high motor assembly

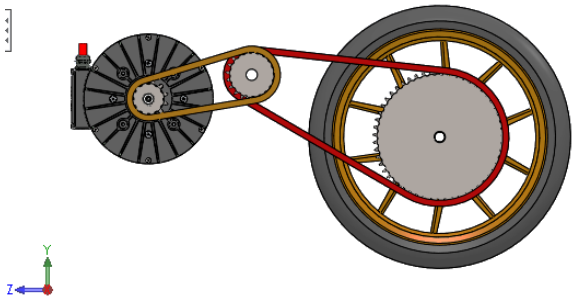

Figure 34 D2 - low motor assembly

Table 16 Comparison between HE and LE

HE	**D2**
<u>Advantages</u> - More compact - Centralised battery pack and control units - Motor assembled too close to rear wheel may increase risk of rear slippage.	**<u>Advantages</u>** - Increased freedom of suspension adjustment. - Swing arm structure more symmetrical as possible.
<u>Disadvantages</u> - Decreased suspension adjustment capability and decentralised action. - Swing arm structure and loads are highly asymmetric.	**<u>Disadvantages</u>** - A lower motor may force battery pack to be assembled too high in the chassis. - Less space efficient.

This two examples will be analysed by designing a swing arm that fits each situation. The structural performance of each swing arm will be evaluated according to the following criteria:

- Maximum Stress
- K stiffness factors for vertical, lateral and torsional behaviour.
- Safety Factor

- Manufacturing process
- Final Weight

3.4 Test Procedures

The FEA procedures for swing arm study are based on the Cossalter's analogy of K stiffness factors [22]. According his works, the swing arm pivot must be locked, while the rear end of the swing arm is loaded. This procedure is arguable, because although it provides a simple system that could be compared to the fixed cantilever beam, Figure 35 [16], it may not provide real world values to characterize the swing arm under normal use. This happens due to fixed fixtures being structurally too restricting. Is simple to understand that a swing arm is actually fix to a hinge fixture to the chassis and not fixed, otherwise rear suspensions would be useless.

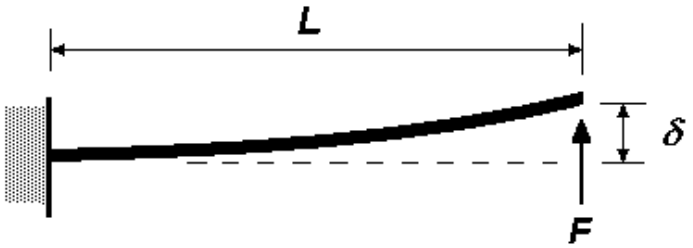

Figure 35 Cantilever Beam example (base is fixed to rigid wall)

The proposed solution to this issue is to use Cossalter's approach for comparison with the already known values for K factor stiffness, but once optimised models are achieved, produce a simulation with hinged pivot fixtures and a suspension vertical support, for a better understanding of the swing arm final behaviour, Figure 36.

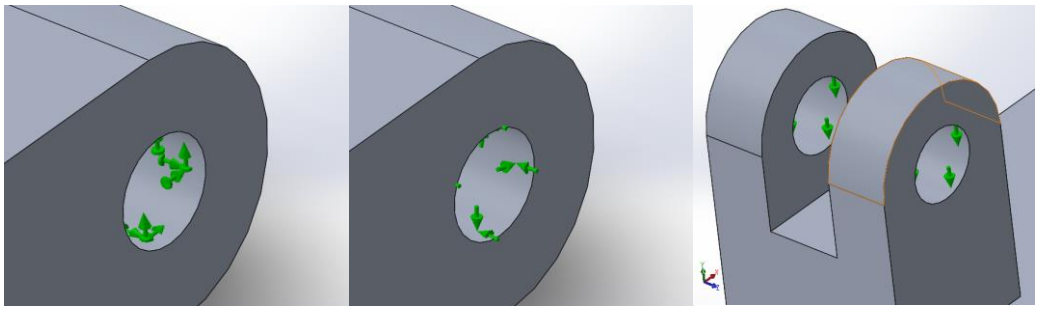

Figure 36 Swing arm fixtures, considering a fully recoiled rear suspension

Vertical Test

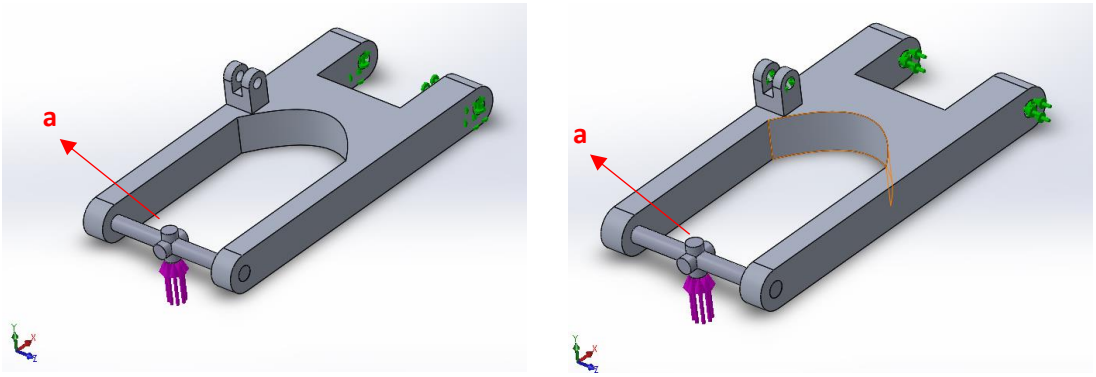

Figure 37 a) Cossalter's vertical test; b) Extreme conditions vertical test

Vertical stiffness ($K_{vertical}$) is calculated by measuring the displacement of point **a** (top of rigid rear axle) and applying the following formula, Figure 37:

$$K_{vertical}[\frac{kN}{mm}] = \frac{Vertical\ load\ [kN]}{Vertical\ displacement\ [mm]} \quad (6.1)$$

Lateral Test

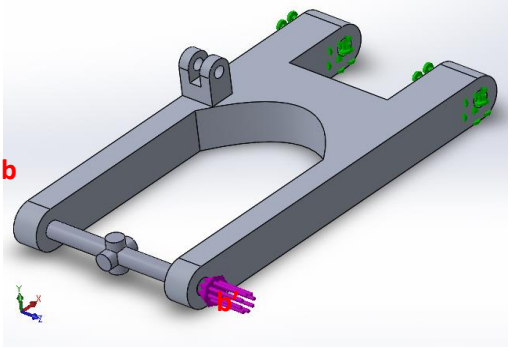

Figure 38 Cossalter's lateral test

Torsional Test

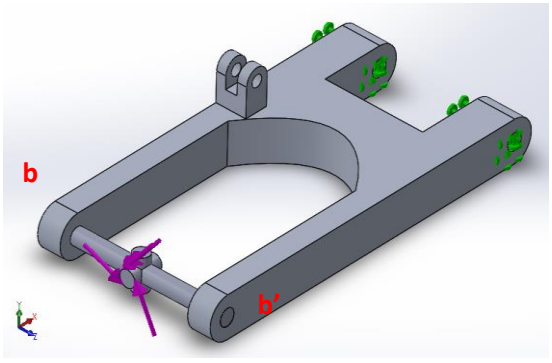

Figure 39 Cossalter's torsional test

Lateral stiffness ($K_{lateral}$) is calculated by measuring the displacement of points **b** and **b'** (right and left ends of rigid axle, respectively) and applying the following formula, Figure 38:

$$\boldsymbol{K}_{lateral}[\frac{kN}{mm}] = \frac{Lateral\ load\ [kN]}{Lateral\ displacement\ [mm]} \quad (6.2)$$

Torsional stiffness ($K_{torsional}$) is calculated by measuring the angle generated between points **b** and **b'** over the interior spam between arms (230 mm), Figure 39:

$$Angular\ displacment\ [°] = \left(\frac{180°}{\pi}\right) \text{asin}\left(\frac{\Delta b + \Delta b'}{230}\right) \tag{6.3}$$

$$\boldsymbol{K}_{lateral}\left[\frac{kN}{mm}\right] = \frac{Torsional\ load\ [kNm]}{Angular\ displacement\ [°]} \tag{6.4}$$

HM1 is further explained on Section *6.3*, however it serves for the purpose demonstrating different types of fixture throughout all different types of loading situations. In all situations a rigid axle is used to apply the necessary loads. The axle is bonded to the swing arm, representing the wheel cube, spacers and rear wheel axle. This will give the swing arm additional stiffness, since the axle is considered non deformable. This option also agrees with Cossalter's approach [22] and is the closest representation of a real situation. If the wheel system and connect parts is properly assembled, it should not allow for any local displacement, otherwise rear instability through vibrations affect handling and safety properties of the whole motorcycle.

3.5 Rear Swing Arm First Iteration (HM1)

The first scenario to be analysed is HM (High Motor assembly), Figure 40. Before presenting an initial swing arm model it is necessary to take a more detailed look into the particular challenges of this choice.

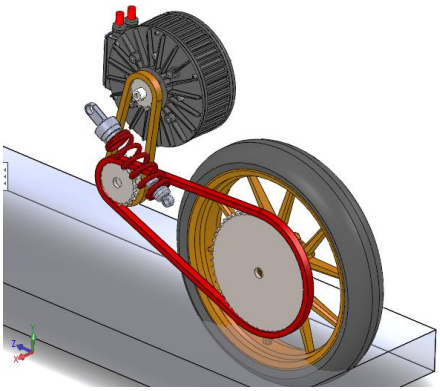

Figure 40 Perspective view of HE

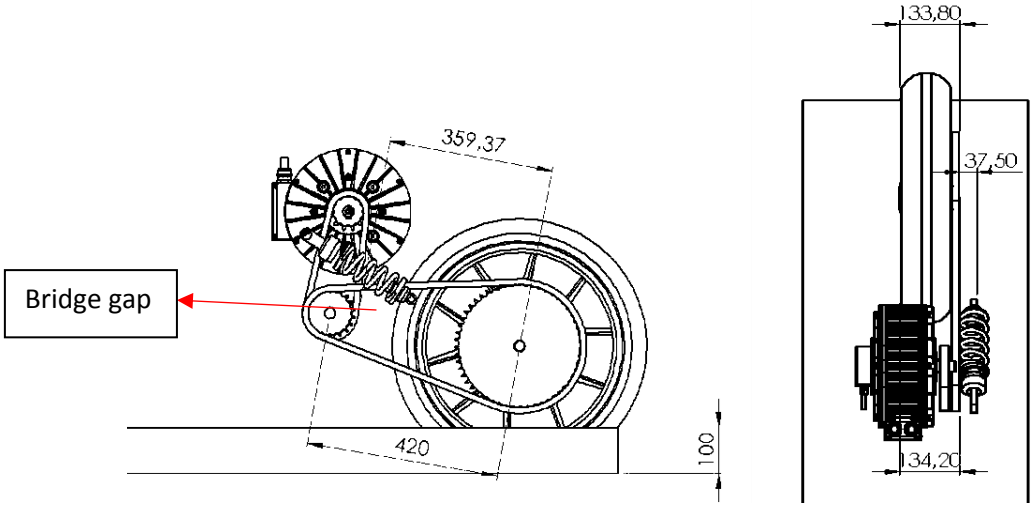

Figure 41 Main Dimensions and geometry limits of HE

The minimum ground clearance (100mm) is a common aspect between all design options, necessary to comply with, since it is one of MotoStudent rules [9]. This distance is represented in Figure 41, but as it is possible to see, it is not a particularly hindering limitation to any conventional swing arm.

The main geometric measures presented are the minimum swing arm length of 420 mm (measured from the swing arm pivot (point a) till the rear wheel axle (point b)). Also, the swing arm will inevitably have an H shape (Top view), Figure 42. This is a necessary geometry since clearance has to be created for both the rear wheel (point a) and all gearing and chain apparatus (point b). A total clearance, or two independent arms, would be a possible option, however the structural stiffness of such a structure would probably not comply with the inevitable torsional and lateral loads applied during normal use.

HE requires an asymmetrical rear suspension assembly. The electric motor is located as far as possible to the rear to permit a larger tolerance to a future battery box. Given the dual chain transmission system the motor is located right wise in relation to the centre trail of the motorcycle, thus only permitting a left wise suspension.

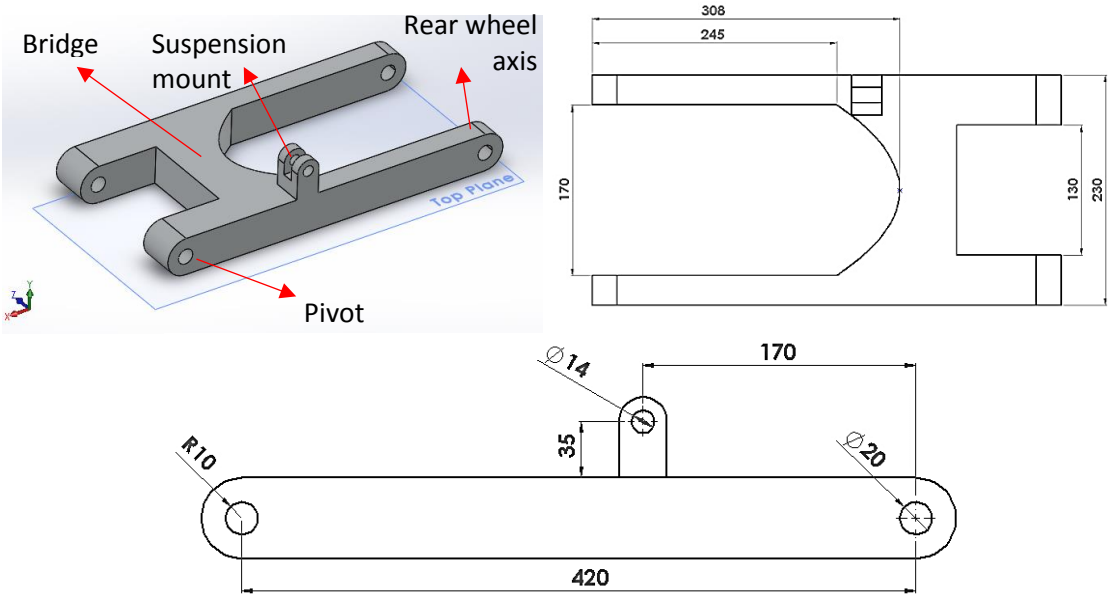

Figure 42 Main dimensions and geometry of HM1

The present model HM1 (High Motor – 1st iteration) complies with all geometric limitations. It was decided to install the rear suspension pivot, as near as possible to the structural bridge between arms, to decrease as much as possible asymmetrical displacement. A minimum clearance of 8 mm is allowed between rear tire and bridge.

HM1 has approximately a mass of 6,021 Kg.

After conducting all tests, initial results are as follows on Table 17 to Table 19:

Table 17 Lateral Loading Results (HM1)

Lateral Loading Test	**Force applied on right arm**	**Force applied on left arm**
Force	100 N	100 N
Lateral displacement of A	$9.61*10^{-3}$ mm	$9.62*10^{-3}$ mm
$K_{lateral}$	10,4 kN/mm	10,4 kN/mm

Table 18 Vertical Results (HM1)

Vertical Loading Test	**Force applied on C**
Force	100 N
Vertical displacement of A	$4,04*10^{-2}$ mm
$K_{vertical}$	2,48 kN/mm

Table 19 Torsional Results (HM1)

Torsional Loading Test	Torque applied counter clockwise	Torque applied clockwise
Torque	100 Nm	100 Nm
Vertical displacement of B	$6.82*10^{-2}$ mm	$6.82*10^{-2}$ mm
Vertical displacement of B'	$6.82*10^{-2}$ mm	$6.85*10^{-2}$ mm
$K_{torsional}$	2,94 kNm/°	2,94 kNm/°

HM1 proved to be extremely stiff under all loading conditions, showing how much potential there is to reduce mass. This model however can already demonstrate some of the expected characteristics of this design choice.

It was understood on chapter 3.2.3 that the most likely extreme situation to which this swing arm can be exposed to is front lifting (rear lifting is may also occur, but that situation will only stress the front wheel). To study that case, a vertical test according to Cossalter's approach was performed with an extreme vertical force, Figure 43.

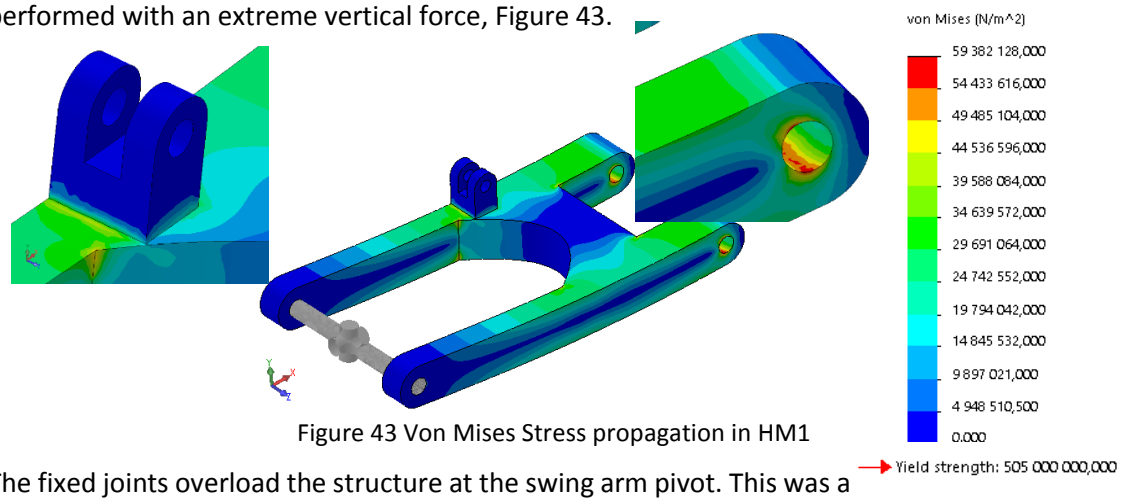

Figure 43 Von Mises Stress propagation in HM1

The fixed joints overload the structure at the swing arm pivot. This was a Cossalter's approach. The suspension support seems to be too close to the bridge, which with the sharp edges, generates an area of high stress at the base. Also, the lower corners at the base of the bridge need to be filleted, since these are all a source of high stress.

3.6 Model HMF

After an extensive iterative process, several differences are noticeable between Models HM1 and HEF (High Motor Final iteration), Figure 46. The main geometrical differences are as follows:

1. **Bridge** – Top and bottom trapezoidal holes are applied to reduce mass. Still, the centre is kept intact and a middle plate of 5 mm thickness ensures a continuous stress propagation.
2. **Rear suspension support –** moved -10 mm according to the *Z* axis. The aim is to increase distance from base of the bridge, avoiding local concentration of stress in sharp edges. Also, by increasing distance to the chain area of operation, a wider tolerance can be applied to suspension spring action and adjustment.
3. **Truss Strut –** Trusses are common solutions for structural load transfer. This way considerable amount of material can be taken from the swing arm with a minimum loss of mechanical properties.
4. Model 1.1 weights approximately 4.508 kg.

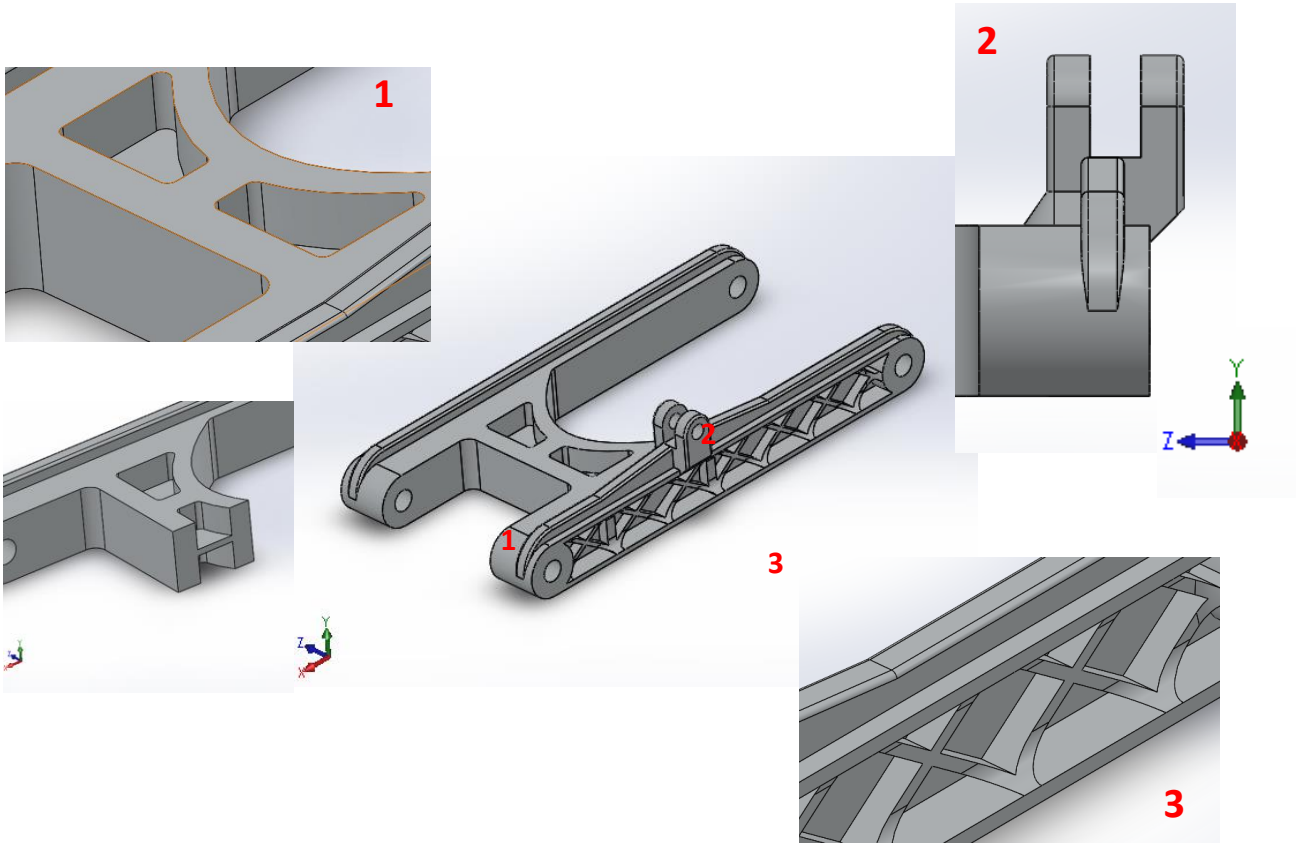

Figure 44 Design improvements on Model 1.1

The new main structural properties are presented on Table 20 to Table 22.

Table 20 Lateral Results (HMF)

Lateral Loading Test	**Force applied on right arm**	**Force applied on left arm**
Force	100 N	100 N
Lateral displacement of A	$1.95*10^{-2}$ mm	$1.95*10^{-2}$ mm
$\boldsymbol{K_{lateral}}$	5.12 kN/mm	5.13 kN/mm

Table 21 Vertical Results (HMF)

Vertical Loading Test	**Force applied on C**
Force	100 N
Vertical displacement of A	$4.38*10^{-2}$ mm
$\boldsymbol{K_{vertical}}$	2.28 kN/mm

Table 22 Torsional Results (HMF)

Torsional Loading Test	**Torque applied counter clockwise**	**Torque applied clockwise**
Torque	100 Nm	100 Nm
Vertical displacement of B	$1.45*10^{-1}$ mm	$1.44*10^{-1}$ mm
Vertical displacement of B'	$1.53*10^{-1}$ mm	$1.53*10^{-1}$ mm
$\boldsymbol{K_{torsional}}$	1,35 kNm/°	1,35 kNm/°

Table 23 Results Comparison (Models HM1 and HMF)

Parameter	**Model HM1**	**Model HMF**	**Relative Difference**
$\boldsymbol{K_{lateral}}$	10,4 kN/mm	5.13 kN/mm	50,77 %
$\boldsymbol{K_{vertical}}$	2,48 kN/mm	2.28 kN/mm	7,81 %
$\boldsymbol{K_{torsional}}$	**2,94 kNm/°**	**1,35 kNm/°**	**50,16 %**
Mass	6,021 kg	4,508 kg	25,13%

Model 1.1 has approximately less 25% of mass than HM1, which will improve considerably dynamic behaviour. However, it is admissibly less stiff in all regimes with an overall loss of 7.81%, 50.77% and 54.84% in $K_{vertical}$, $K_{lateral}$ and $K_{torsional}$. Yet, Model 1.1 is still very conservative

given the expected values provided by Cossalter of ($K_{lateral}$ = 0.8-1.6 kN/mm and $K_{torsional}$ = 1-2 kNm/°).

On an extreme situation where the front wheel lift off, the total load applied on the rear may reach 1968 N, which given the safety factor of 1.82, amounts for a testing force of approximately 3580 N. It is plausible to assume a total recoil of the rear suspension in such situation, meaning that the rear swing arm is completely restrained (there no rear absorption of energy). Cossalter's approach does not account for such situations. To study the behaviour of Model 1.1 under this conditions a vertical test simulation with 3580 N of force was conducted using fixture conditions presented on Figure 47.

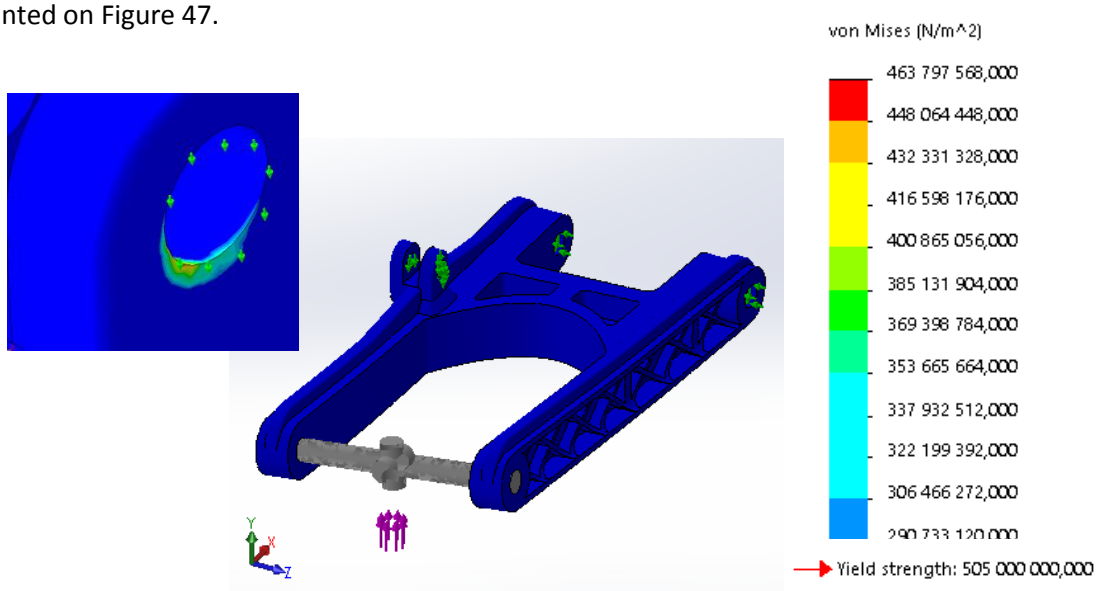

Figure 45 Local Stress concentration (rear suspension mount)

On Figure 50 it is clear a structural relieve of force transmission through the swing arm pivot. However, this happens because much of the vertical load is being absorbed by the suspension mount, to almost to the point of local structure failure (maximum von Mises stress 464 MPa). The loads in this test are over estimated, so the minimum safety factor still applies. This admittedly happens due to the sharp edges on the suspension mount, but mostly due to the asymmetrical assembly, which becomes clear once swing arm displacements are checked.

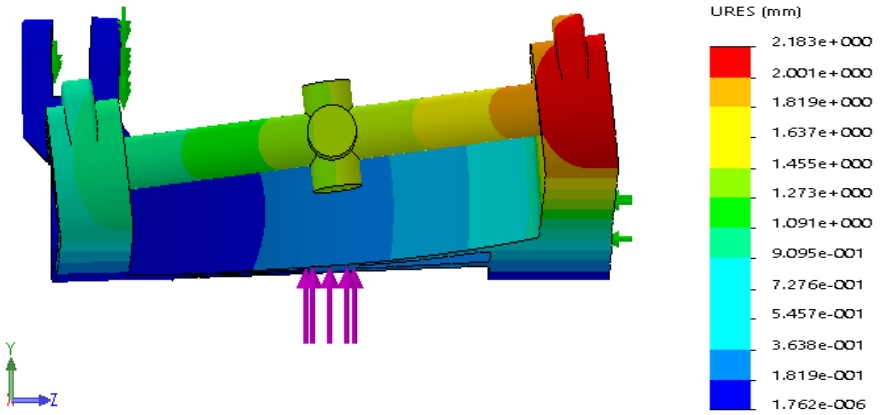

Figure 46 Deformed shape of HMF (Deformation scale 21.5)

Due to the asymmetrical property of the structure, the vertical force on the rear axle generates torsional loads and consequently twisting of the swing arm. The more restrained right arm will present lower displacement values, with maximum difference between both arms achieving approximately 1.2 mm. Considering the displacement achieved on point B (2.067 mm), $K_{vertical} = 1{,}73\ kN/mm$, which is approximately a 24.12% reduction than the value achieve according to Cossalter's approach.

Now that the main properties of these approach are understood, and before choosing a final swing arm model, the lower motor design approach will be studied.

3.7 Model LM1

LM (Lower Motor assembly) is characterized by the lower motor location, Figure 47. When compared to HM, geometrical limitations are, Figure 48:

- Bridge clearance is stays the same, since distance between swing arm pivot and rear tire remains constant.
- Rear suspension position changes from the right arm to the top centre of the bridge
- Interior width between arms remains, since no change are made to the rear wheel assembly.

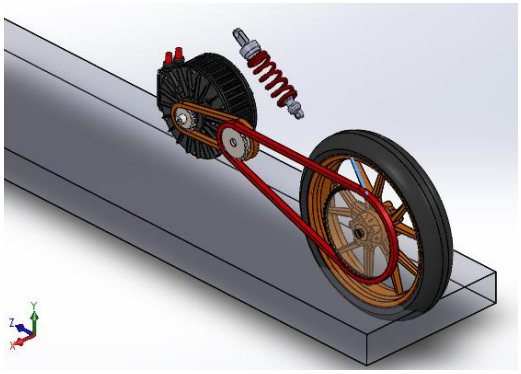

Figure 47 Perspective view of LM

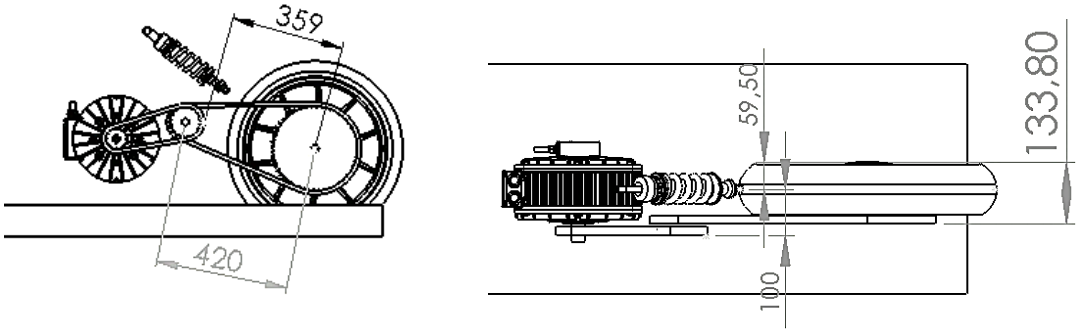

Figure 48 Main dimensions and geometry limits of LM

The central higher suspension mount should allow for a better stress distribution through the swing arm. Actually, the classic H shape model will be triangulated. Triangle arms should cope better with vertical loads, due to the increase first moment of inertia along the force direction.

To achieve a better mass balance, the motor is placed as central as possible according to the motorcycle trail. This is clear on Figure 48, however it will affect the swing arm final geometry (Figure 51). Faole experienced this while trying a similar dual chain assembly [11]. The pivotal swing arms require a wider distance between each other (166 mm), since chain 1 is in an outer position, when compared to HM.

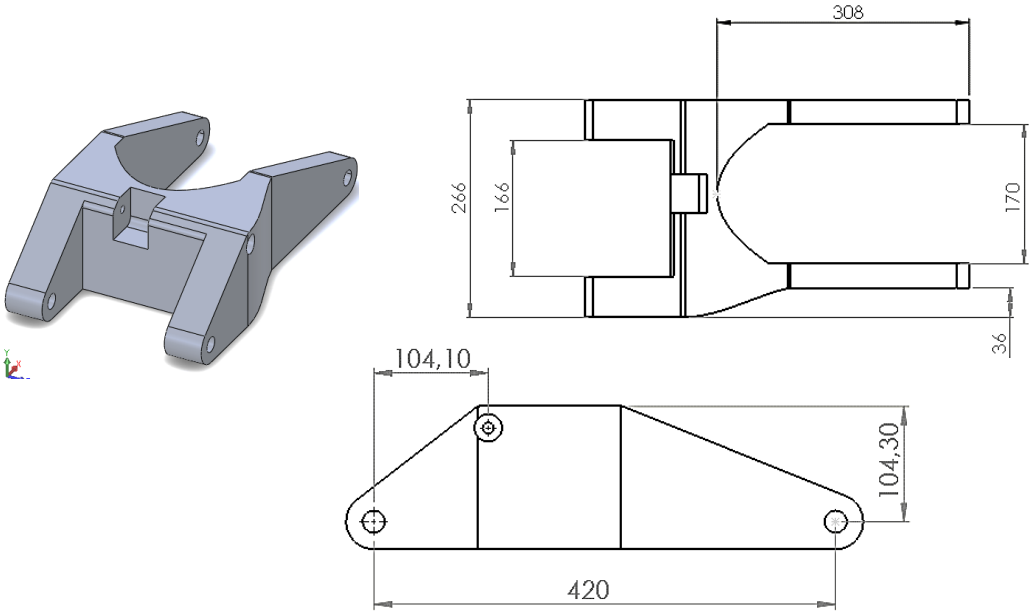

Figure 49 Main dimensions and geometry of LM1

The present LM1 complies with all geometric limitations. A minimum clearance of 8 mm is allowed between the rear tire and bridge.

HM1 has approximately 13.3 Kg.

After conducting all tests, initial results are as follows:

Table 24 Lateral Results (LM1)

Lateral Loading Test	**Force applied on right arm**	**Force applied on left arm**
Force	100 N	100 N
Lateral displacement of A	$4{,}99*10^{-3}$ mm	$4{,}98*10^{-3}$ mm
$\boldsymbol{K_{lateral}}$	20,10 kN/mm	20,10 kN/mm

Table 25 Torsional Results (LM1)

Torsional Loading Test	**Torque applied counter clockwise**	**Torque applied clockwise**
Torque	100 Nm	100 Nm
Vertical displacement of B	$2{,}43*10^{-2}$ mm	$2{,}43*10^{-2}$ mm
Vertical displacement of B'	$2{,}23*10^{-2}$ mm	$2{,}23*10^{-2}$ mm
$\boldsymbol{K_{torsional}}$	8,61 kNm/°	8,61 kNm/°

Table 26 Vertical Results (LM1)

Vertical Loading Test	**Force applied on C**
Force	100 N
Vertical displacement of A	$1{,}28*10^{-2}$ mm
$\boldsymbol{K_{vertical}}$	7,82 kN/mm

As expected, the increased arms thickness, as well as a more progressive propagation of stress through the swing arm, provide LM1 with initial mechanical properties, much more conservative than HM1. Also, due to trapezoidal lateral profile, it weights approximately 55% more than the initial HM1 with a classic H profile. This also means that the potential for improvement is probably higher than with the more conventional design, since possibilities for material removal while keeping structurally healthy loads paths is increased.

3.8 Model LMF

After an extensive iterative process, several differences are noticeable between LM1 and LMF, Figure 52. The main geometrical differences are as follows:

1. **Chain passage** – Given the increased frontal area of this design, it was necessary to create an opening though the bridge to permit for a chain to pass.
2. **Material reduction –** several holes are noticable on the lateral walls. These permit a local material reduction with a very reduced loss of mechanical properties, due to their circular profile and to the efficient load transfer thorugh inner wall truss struts.
3. **Truss Strut –** As previously, truss struts were used to reduce significantly material, ensuring a correct load transfer though the structure.
4. LMF weights approximately 4.52 kg.

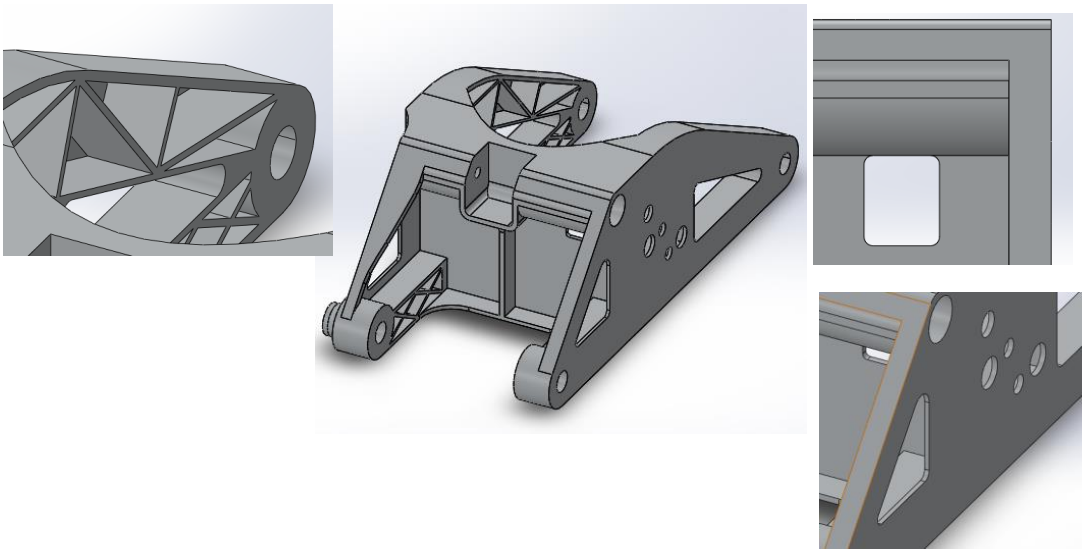

Figure 50 Design improvements on LMF

Table 27 Lateral Results (LMF)

Lateral Loading Test	Force applied on right arm	Force applied on left arm
Force	100 N	100 N
Lateral displacement of A	$2{,}73*10^{-2}$ mm	$2{,}72*10^{-2}$ mm
$K_{lateral}$	3,66 kN/mm	3,67 kN/mm

Table 28 Torsional Results (LMF)

Torsional Loading Test	**Torque applied counter clockwise**	**Torque applied clockwise**
Torque	100 Nm	100 Nm
Vertical displacement of B	$1{,}35*10^{-1}$mm	$1{,}35*10^{-1}$mm
Vertical displacement of B'	$1{,}13*10^{-1}$ mm	$1{,}13*10^{-1}$ mm
$\boldsymbol{K_{torsional}}$	1,62 kNm/°	1,62 kNm/°

Table 29 Vertical Results (LMF)

Vertical Loading Test	**Force applied on C**
Force	100 N
Vertical displacement of A	$4{,}80*10^{-2}$ mm
$\boldsymbol{K_{vertical}}$	2,08 kN/mm

Table 30 Results Comparison (LM1 and LMF)

Parameter	**Model HM1**	**Model HMF**	**Relative Difference**
$\boldsymbol{K_{lateral}}$	20,10 kN/mm	3,66 kN/mm	81,20 %
$\boldsymbol{K_{vertical}}$	7,82 kN/mm	2,08 kN/mm	73,35 %
$\boldsymbol{K_{torsional}}$	8,61 kNm/°	1,62 kNm/°	**81,20 %**
Mass	13,30 kg	4,52 kg	66,10 %

LMF has approximately 66.1% less mass than LM1, which improve dynamics considerable, 100%. However, like with the previous models, it is admissibly less stiff in all regimes with an overall loss of 73.4%, 81.8% and 81,7% in $K_{vertical}$, $K_{lateral}$ and $K_{torsional}$.

When models 1.1 and 2.1 are compared according to Cossalter's approach, it is noticeable that 1.1 presents and increased lateral and vertical stiffness by 28,5% and 8,8% effectively, while 2.1 shows a higher torsional stiffness by 16,8%. Mass is approximately the same, with 2.1 being only 8 g heavier.

Once again, before drawing further conclusions, LMF is tested under front wheel lift conditions, on a vertical test simulation with 3580 N of force.

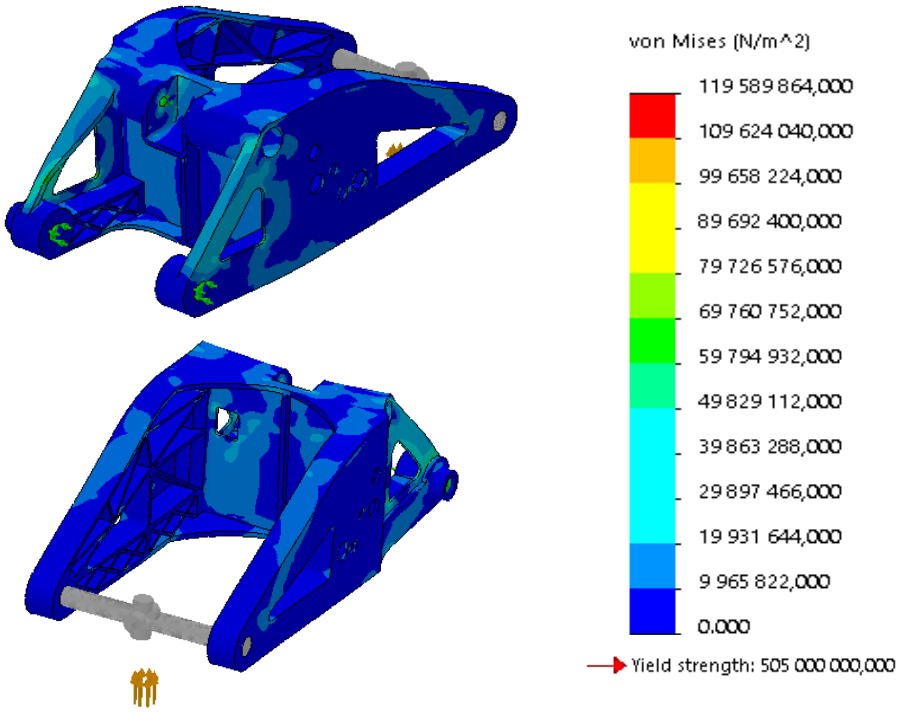

Figure 51 Von Mises Stress propagation in LMF

Opposite to Model 1.1, LMF does not overstress the suspension mount, distributing almost evenly loads through rear pivot and suspension mount. This denotes an obvious advantage, since although 2.1 does not show critical failure by locally exceeding maximum von Mises Stress of 505 MPa. The maximum value noted is still detected at the suspension mount, 119.6 MPa, which only amount for 23% of the limit stress (safety factor 4.24, over the minimum factor).

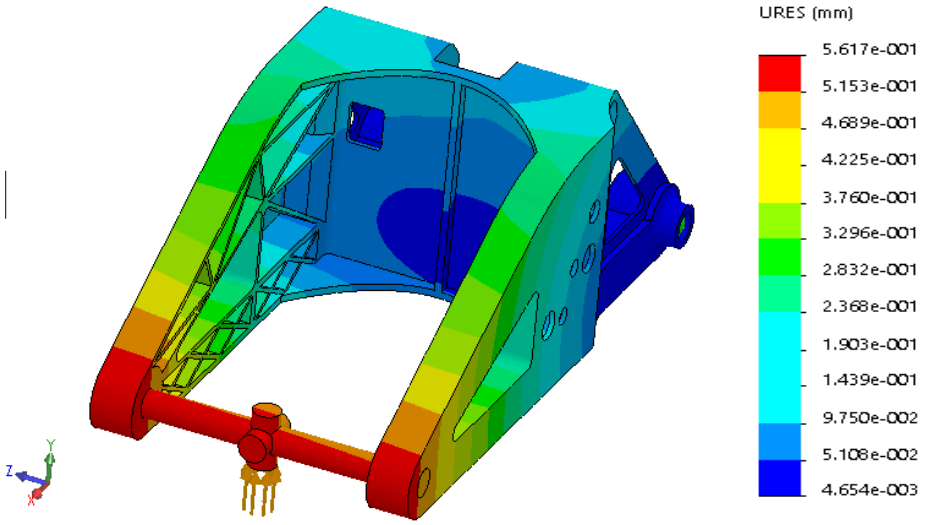

Figure 52 Deformed shape of LMF (Deformation scale 21.5

Furthermore, when analysing structural displacement, LMF shows an almost symmetrical shift of both arms (Figure 52), which correlates with a smooth load distribution. A local displacement

of 0.55 mm is observed at the rear axle, obtaining a new $K_{vertical} = 6.31\ kN/mm$, which is 3.65 times higher to model 1.1 under the same conditions.

3.9 Final Rear Swing Arm Model

As a result, from the previous iterations, it was concluded that both final models for approach HE and LE should perform under the safety boundaries defined for this project. However, LMF clearly proves to be more efficient under extreme situations. So, LMF was the base for the final swing arm model.

To conclude the design of the swing arm it is necessary to define the final attachment geometry for the rear wheel. These were not defined till now, for a matter of simplification of the testing iterative process. As in any commercial motorcycle, the swing arm should allow for rear wheel adjustment to some extent. Commonly, a slider system is used, where two parts, independent from the swing arm, are used to attach the rear wheel axle, as is shown on Figure 55.

The current geometry allows for an adjustment of up to 35 mm. The sliders may be manufactured in aluminium, or steel alloy. It is understood that this new geometrical feature may weaken the swing arm. To understand how much these changes affect the overall performance another run of simulations was performed. The worst situation where the rear wheel is assembled on the backward position was considered.

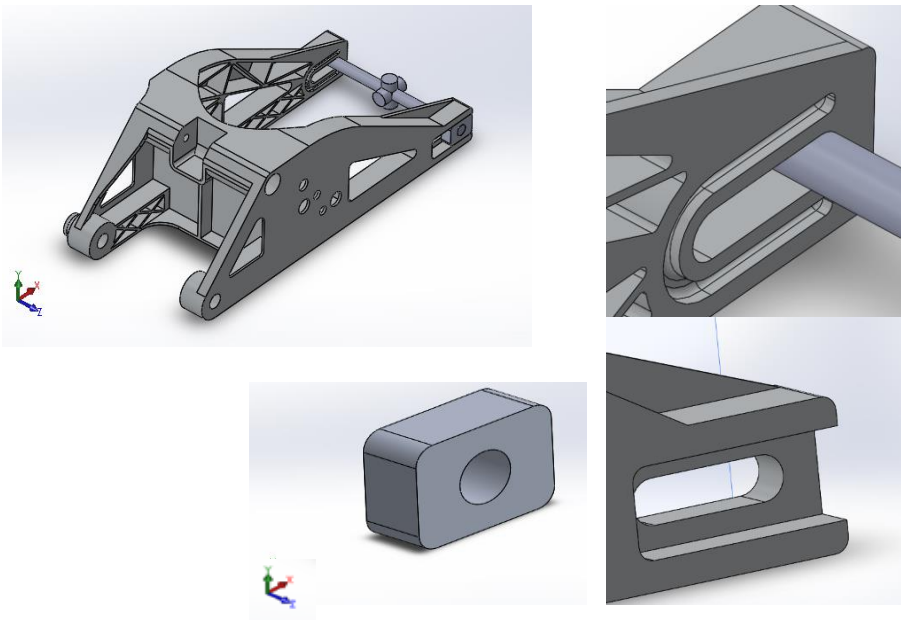

Figure 53 Final rear swing arm model

Table 31 Lateral Results (LMF)

Lateral Loading Test	Force applied on right arm	Force applied on left arm
Force	100 N	100 N
Lateral displacement of A	$3{,}74*10^{-2}$ mm	$3{,}80*10^{-2}$ mm
$K_{lateral}$	2,67 kN/mm	2,64 kN/mm

Table 32 Torsional Results (LMF)

Torsional Loading Test	Torque applied counter clockwise	Torque applied clockwise
Torque	100 Nm	100 Nm
Vertical displacement of B	$1{,}46*10^{-1}$mm	$1{,}46*10^{-1}$mm
Vertical displacement of B'	$1{,}70*10^{-1}$ mm	$1{,}69*10^{-1}$ mm
$K_{torsional}$	1,27 kNm/°	1,27 kNm/°

Table 33 Vertical Results (LMF)

Vertical Loading Test	Force applied on C
Force	100 N
Vertical displacement of A	$5{,}65*10^{-2}$ mm
$K_{vertical}$	1,77 kN/mm

As it is noticeable, according to Cossalter's approach, the swing arm still largely complies with safety limits defined for this project. Results for the extreme vertical situation are on Figure 58.

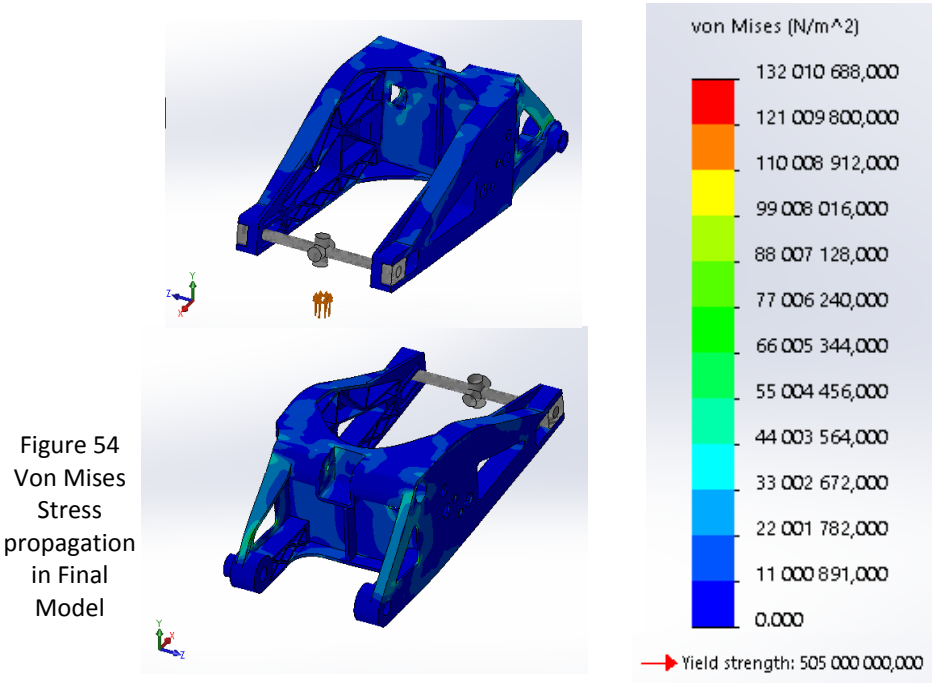

Figure 54 Von Mises Stress propagation in Final Model

The maximum value noted is still detected at the suspension mount, 132 MPa, which only amount for 26% of the stress limit.

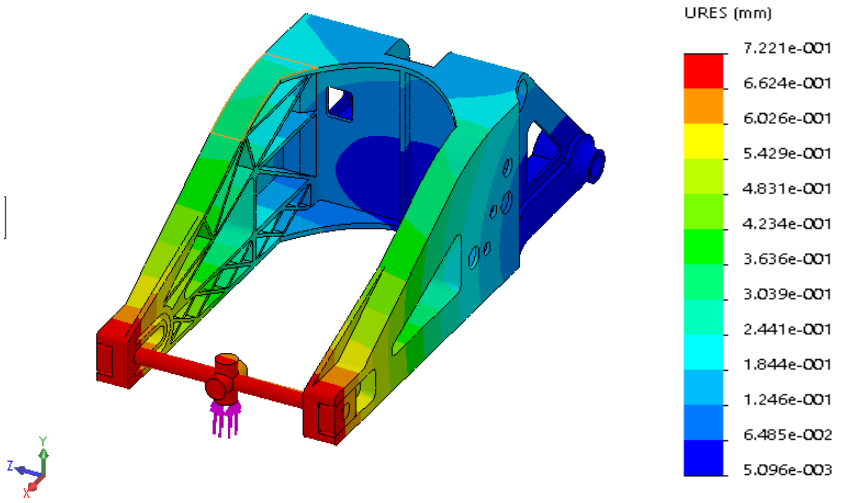

Figure 55 Deformed shape of Final Model (Deformation scale 21.5)

When analysing structural displacement (Figure 55), LMF keeps an almost symmetrical shift of both arms. A local displacement of 0.71mm is observed at the rear axle, obtaining a new $K_{vertical} = 5{,}05\ kN/mm$, which is 20% lower than model 2.1 under the same conditions.

3.9 Frontal Swing arm design

Frontal swing arms are not conventionally applied as solutions for the steering and frontal suspension systems on motorcycles. According to MotoStudent rule B.8.1.1 [9], any motorcycle should have minimum steering angle of 15^0 measured on both sides.

The concept behind frontal swing arm is much the same as for rear swing arms. They need to cope with any force transmitted through the front wheel, thus transmitting those loads efficiently through the suspension system and swing pivot, without any measurable structural displacement. Now difference resides on the fact that frontal system also need to cope with steering, limiting the amount of geometry solutions. According MotoStudent rule B.9.1.3, machining of rims provided by organization is strictly forbidden, meaning that any steering system will have to be located between swing arm and front wheel (not inside the wheel cube, as commonly applied on frontal swing arm systems [17]). This will be discussed further on.

Model FSS1 (front single suspension – first iteration) complies with these initial geometrical rules is presented on Figure 56. Like on the rear swing arm, width between arms at connection (pivot)

between arms is defined by the assumed width of a battery pack (Annex), while width at wheel is defined by minimum steering radius of 15^0.

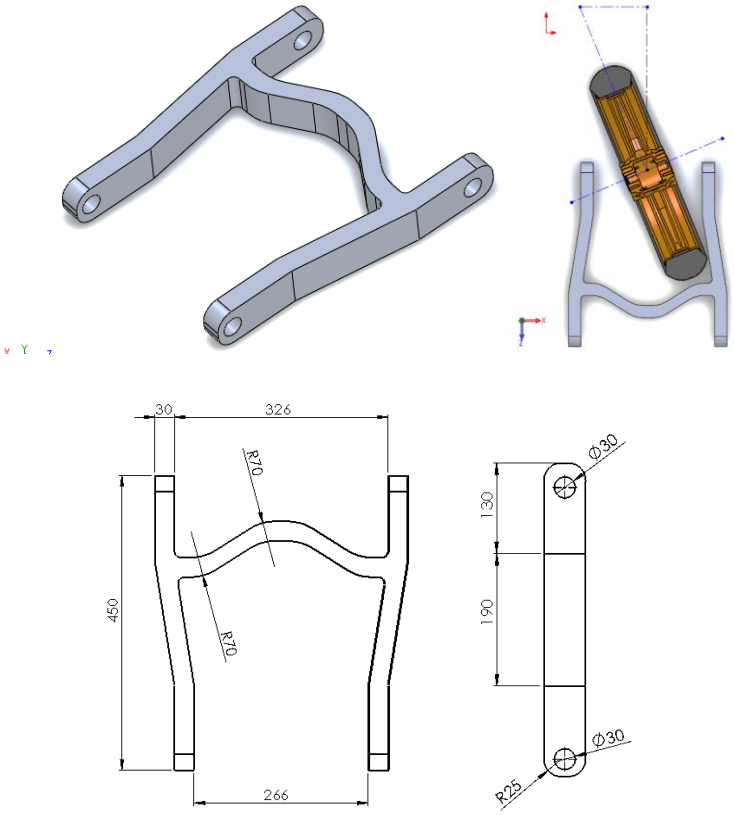

Figure 56 Main dimensions and geometry of FSS1

FSS1 has approximately 5.87 Kg.

Given the similarity of functionality and geometry, the frontal swing arm is also tested according to Cossalter's approach.

After conducting all tests, initial results are as follows:

Table 34 Lateral Results (FSS1)

Lateral Loading Test	**Force applied on right arm**	**Force applied on left arm**
Force	100 N	100 N
Lateral displacement of A	$1{,}16*10^{-2}$ mm	$1{,}16*10^{-2}$ mm
$\boldsymbol{K_{lateral}}$	8,60 kN/mm	8,60 kN/mm

Table 35 Torsional Results (FSS1)

Torsional Loading Test	**Torque applied counter clockwise**	**Torque applied clockwise**
Torque	100 Nm	100 Nm
Vertical displacement of B	$3{,}69*10^{-2}$mm	$3{,}74*10^{-2}$mm
Vertical displacement of B'	$3{,}74*10^{-2}$ mm	$3{,}74*10^{-2}$ mm
$K_{torsional}$	5,40 kNm/°	5,40 kNm/°

Table 36 Vertical Results (FSS1)

Vertical Loading Test	**Force applied on C**
Force	100 N
Vertical displacement of A	$2{,}58*10^{-2}$ mm
$K_{vertical}$	138,80 kN/mm

Although, FSS1 presents very conservative initial properties, it is already clear that the increased distance between both arms (when compared to rear swing arm design) dictates that the front swing arm is less stiff laterally. However, the analysis is still incomplete. FSS1 accounts for the minimum steering radius, but lacks a defined steering system and a suspension mounting.

3.11 Model FSS2

Due to the imposed limitations (MotoStudent rule B.9.1.3 in [9]) a unique steering system was idealized for this motorcycle, Figure 57.

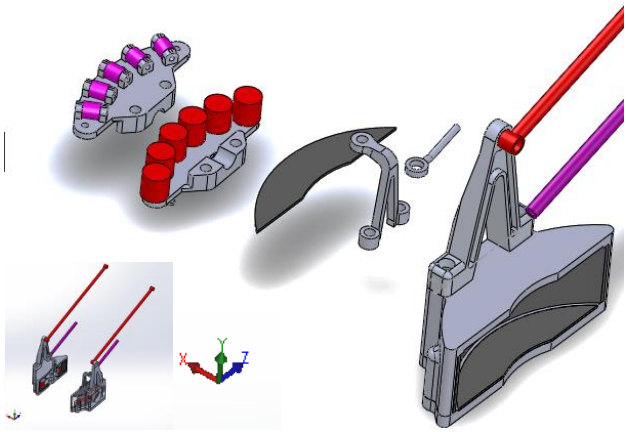

Figure 57 Proposed front wheel external steering system

This system is based on the existing hub-centre steering system, however all steering parts are external to the wheel. As it can be seen on Figure 57 the wheel would be attached between to roller sliders. The sliders would be composed by a series of top, lateral and bottom rollers. When both steering rods are actuated (purple rods), a torque would be generated around the wheel steering radius, thus transmitting a rotating moment to each slider system. The slider are in contact with a low friction surfaced (polish high carbon steel alloy, for example), contained inside an aluminium casing attached to the swing arm through (bearings on both ends of an axle). A couple of secondary swing rods (red rods) would keep a stable, but adjustable steering angle.

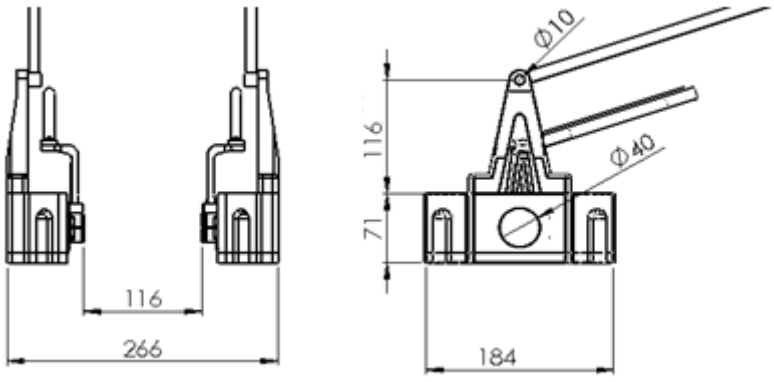

Figure 58 Main dimensions and geometry of steering system

Although this system could in theory provide the same advantages of a hub-centre steering solution, it has two main disadvantages:

- An approximate mass estimation for the assembly, considering steel alloy rollers and an aluminium casing, would result in an unsprang mass of 2.6 – 3.0 kg.
- The full a system requires a wide swing arm (266 mm minimum inside width), which as it was already acknowledge, affects lateral stiffness.

Due to a lack of optional solutions, FSS2 accounting this limitations is presented on Figure 59.

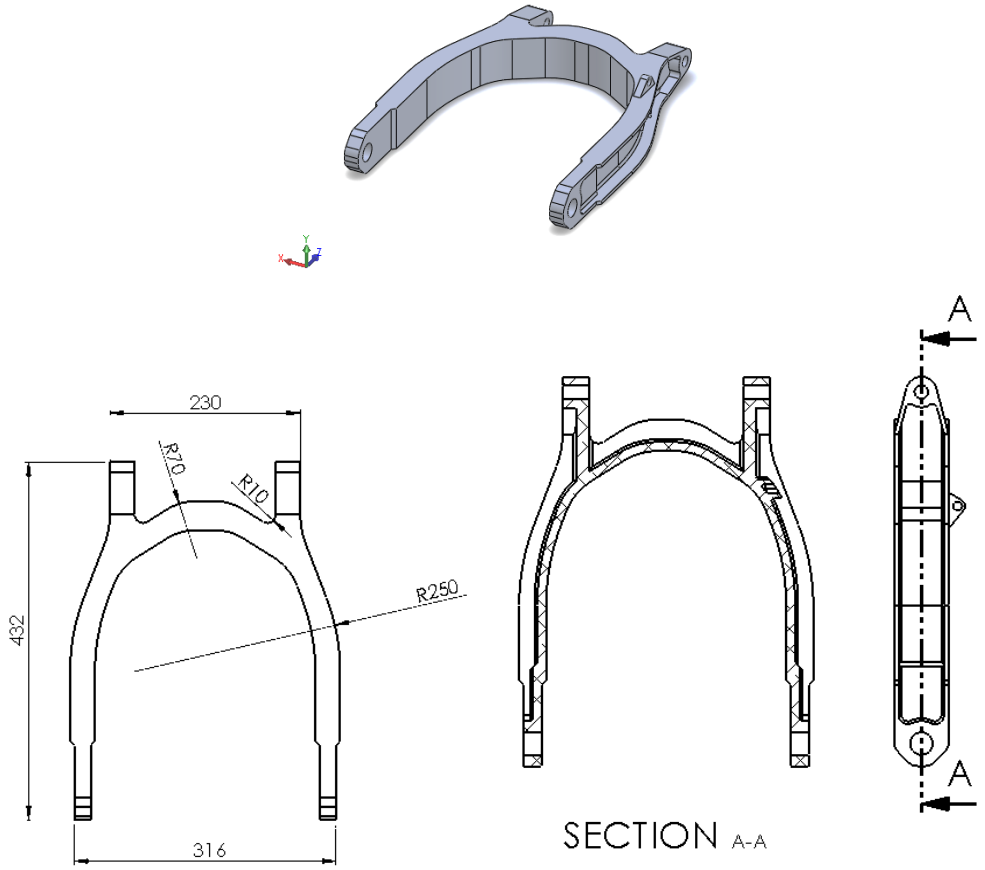

Figure 59 Main dimensions and geometry of FSS2

Main differences between FSS1 and FSS2:

1. **C section arms** – as in the rear swing arm, an open cross C section with truss struts to reinforce local stiffness was used. This option should keep good lateral and vertical stiffness values, while significantly reducing mass.
2. **Inner chassis swing arm pivot supports** – FSS1 presented an inner width of 326 mm. However this geometry would become too large in the case of an enlarged battery box, requiring an accordingly wide frame. To keep a compact and lightweight design, the

front swing can be mounted in forward frame mounts, becoming almost independent from battery box dimensioning.

3. **Single front suspension** – Again, single side suspension provides a more compact and light weight solution, than a dual telescopic fork.

After conducting all tests, initial results are as follows:

Table 37 Lateral Results (FSS2)

Lateral Loading Test	**Force applied on right arm**	**Force applied on left arm**
Force	100 N	100 N
Lateral displacement of A	$8{,}96*10^{-2}$ mm	$8{,}87*10^{-2}$ mm
$K_{lateral}$	1,12 kN/mm	1,13 kN/mm

Table 38 Torsional Results (FSS2)

Torsional Loading Test	**Torque applied counter clockwise**	**Torque applied Clockwise**
Torque	100 Nm	100 Nm
Vertical displacement of B	$1{,}67*10^{-1}$mm	$1{,}72*10^{-1}$mm
Vertical displacement of B'	$1{,}72*10^{-1}$ mm	$1{,}67*10^{-1}$ mm
$K_{torsional}$	1,18 kNm/°	1,18 kNm/°

Table 39 Vertical Results (FSS2)

Vertical Loading Test	**Force applied on C**
Force	100 N
Vertical displacement of A	$7{,}18*10^{-2}$ mm
$K_{vertical}$	49,85 kN/mm

Table 40 Results Comparison (FSS1 and FSS2).

Parameter	**Model HM1**	**Model HMF**	**Relative Difference**
$K_{lateral}$	8,60 kN/mm	1,13 kN/mm	81,20 %
$K_{vertical}$	138,80 kN/mm	49,85 kN/mm	73,35 %
$K_{torsional}$	**5,40 kNm/°**	**1,18 kNm/°**	**81,20 %**
Mass	5,87 kg	2,63 kg	66,10 %

This design excels in torsional and vertical stiffness, but it is noticeable that lateral properties are not so good. However, it respects the interval of values proposed by Cossalter (0.6 kN/mm to 1.6 kN/m) for swing arms, still exceeding the minimum limit by approximately 87%.

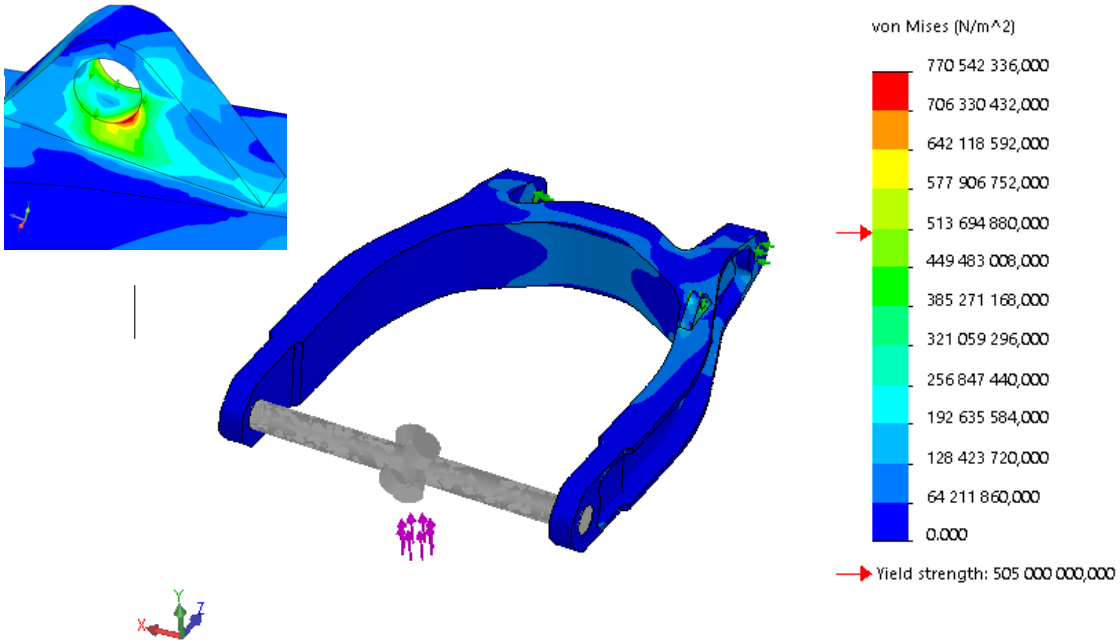

Figure 60 Von Mises Stress propagation in FSS2 with single side suspension

Also, after an extreme vertical load test, the swing arm fails at the suspension mount, Figure 64. To try to overcome this, a second version of this model was produced with two front suspensions mounts (Model FDS2 – Front Dual Suspension), Figure 61.

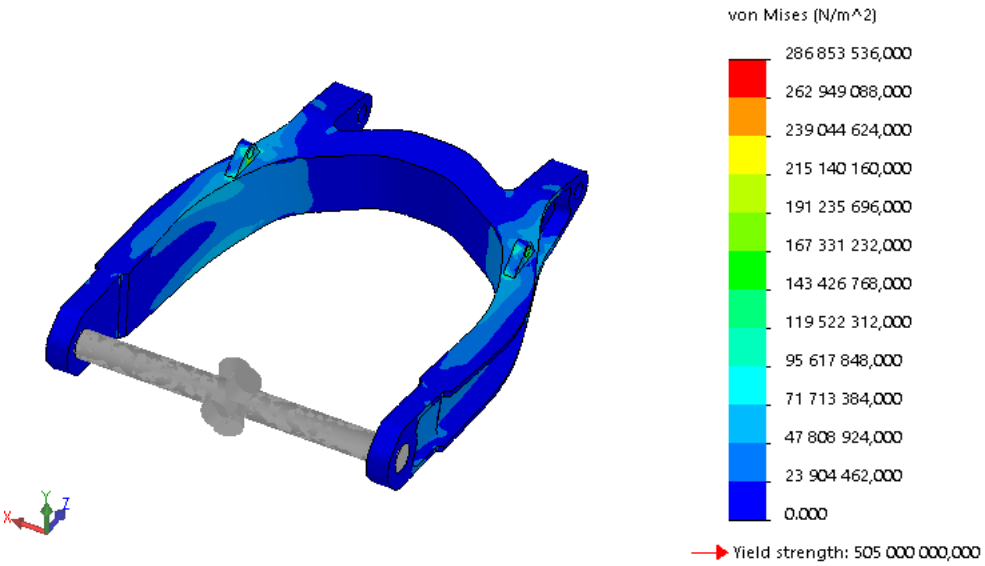

Figure 61 Von Mises Stress propagation in Final FDS2 with dual suspension

The use of two front suspensions becomes even more recommendable, when the derived vertical stiffness factors are compared for the current test conditions, Figure 62 and Figure 63.

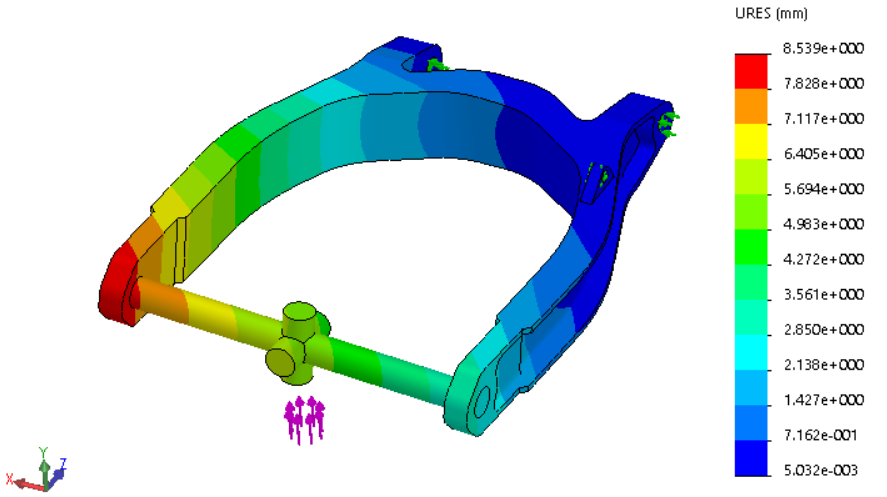

Figure 62 Deformed shape of FSS2 with single side suspension (Deformation scale 21.5)

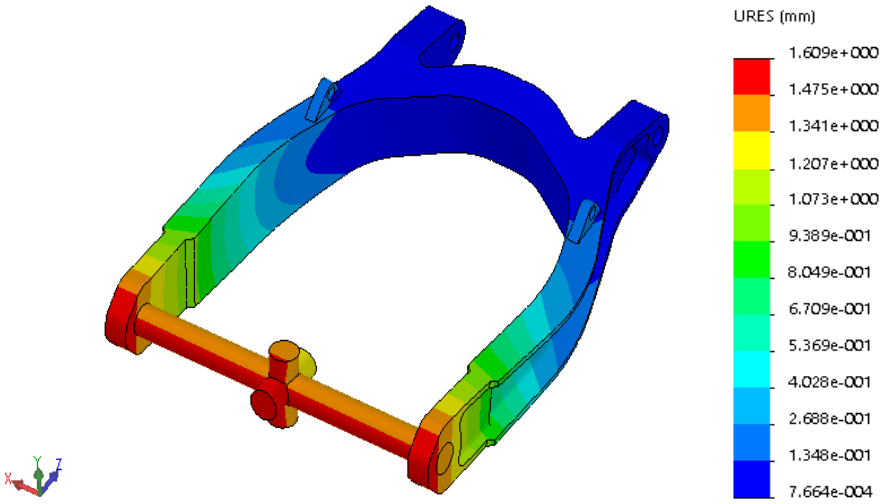

Figure 63 Deformed shape of FDS2 with dual suspension (Deformation scale 21.5)

FSS2 and FDS2 present $K_{vertical}$ results of 0.42 kN/mm and 2.56 kN/mm, respectively, which demonstrates a difference in performance of approximately 6.1 times, between the single and dual suspension scenarios.

4 Manufacturing

In this chapter, the main aspects involved on the manufacturing of these parts are discussed. Materials, machining and welding processes are assessed and

4.1 Designing to Manufacture

One of the requirements established prior to the design of these parts was that they would need to be manufacture using CNC machining (Section 1.3 Aims and Objectives).

CNC stands for Computerized Numerical Control and is an ever more common machining process used on a wide range of materials (metal alloys, plastic, wood, etc). Modern CNC systems contemplate to concept of end-to-end component design, which means the use of CAD (Computer Aided Design) and CAM (Computer Aided Manufacturing). A CAD model, after finalized, can be uploaded to machine processing system, where machining commands can be programed and automatized. In most modern CNC processes, no human intervention is needed during the machining process.

On current CNC machines, motion is controlled on multiple axis, generally at least two (x and y), while a tool spindle moves in depth (z axis). The position of the tool is driven by a direct-drive stepper motor. Close loop controls guaranty a high levels of precision, while controlling speed and position repeatedly. Nowadays, CNC machining is applied all, or has derivations on almost all processes that involve some kind of machining through cutting (laser cutting, welding, plasma cutting, drilling, etc).

For this project, a derivate of the end-milling process will be used. These is by far the most common and economically viable CNC process. Modern CNC mills are highly flexible, allowing from 3 to 6 rotational axis, however 4 is the common standard. These machines allow for face milling, tapping, and shoulder milling and drilling.

Due to the way most CNC mills operate (Endmill penetrates the initial material plate-block), there is a tendency to look for designs that involve as less material as possible. Aluminium alloys have become increasingly cheap and easy to recycle, however the same cannot be said regarding the machine tooling and man hours. Also, the machine might have a dimension limit for parts to machined, or even lack the necessary rotational degrees of freedom to machine the part as a

whole. Keeping this in mind, the following solutions are presented for both rear and front swing arms, Figure 64.

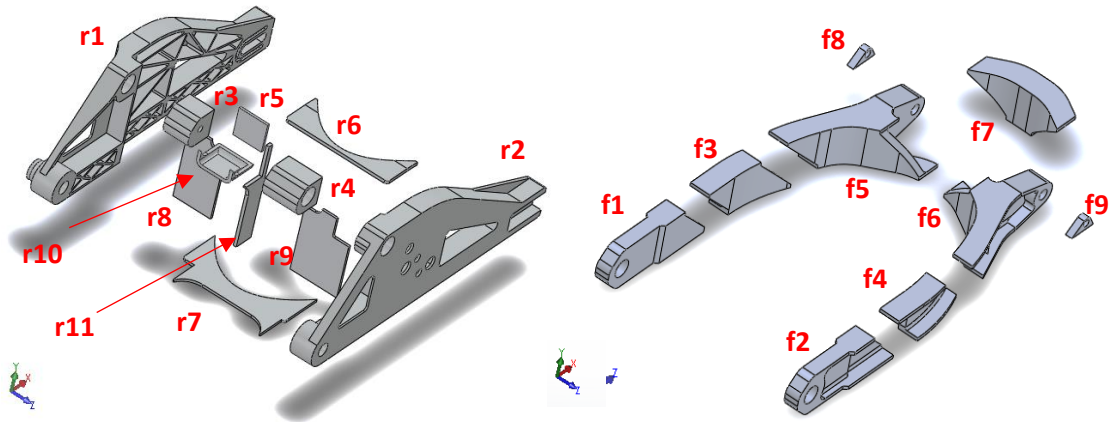

Figure 64 Rear (left) and Front (right) swing arms with respective composing parts

The priorities while defining these models were:

- **Reduction of welds complexity and length where possible** – Aluminium 7075 T6 is not an easy material to weld, requiring advanced weld edge processes as TIG [18]. This means that specialized work that can cost an average of 600+€/day. Also, this alloy can be sensitive to crack propagation, so, in order to minimise the risk of local crack sources due to weld edge defects, welds should be kept to a minimum.
- **Reduction of material consumption** – Considering that each part has to be machined from a either a solid block, or a plate, the minimum quantity of prime matter (Aluminium 7075 T6) required to manufacture part by part is:

Table 41 Raw material blocks and plates VS final machined part weight (Rear Swing arm)

Part	Initial material dimensions			Mass before machining (kg)	Mass after machining (kg)
	Length (mm)	Width (mm)	Height (mm)		
r1	505	50	165	11,707	1,954
r2	505	35	165	8,195	1,947
r3	50	45	42	0,265	0,188
r4	50	45	47	0.297	0,244
r5	5	47,5	45	0.024	0,024
r6	66	170	5	0,157	0,068
r7	117	170	5	0,280	0,099
r8	5	62,5	116	0.101	0,078
r9	5	77,5	116	0,126	0,089
r10	50	57	24	0,158	0,049
r11	42	5	156	0,092	0,054
Total	-	-	-	21.404	4,864

Table 42 Raw material blocks and plates VS final **machined** part weight (Front Swing arm)

Part	Initial material dimensions			Mass before machining (kg)	Mass after machining (kg)
	Length (mm)	**Width (mm)**	**Height (mm)**		
f1	**180**	**30**	**60**	**0,910**	**0,355**
f3	**142**	**52**	**60**	**1,244**	**0,210**
f5	**211**	**142**	**60**	**5,051**	**0,623**
f7	**47**	**140**	**60**	**1,416**	**0,220**
f8	**40**	**10**	**23**	**0,025**	**0,010**
Total	**-**	**-**	**-**	**17,292**	**2,836**

This an approximation, since careful planning could decrease the amount of material needed, through the utilization of a block for several parts. However, after analysing both tables 21 and 21, it can be assumed that approximately 40 kg of material at a precise of 300 € would be required.

- **Geometry to fit a small CNC machining table –** small size machines vary in dimension capacity, but a maximum dimension of 508mm length, 200 mm width and 200 mm height should be respected. [24]

4.2 Interior Corners

The next step is to understand the type of tooling necessary to machine inside corners.

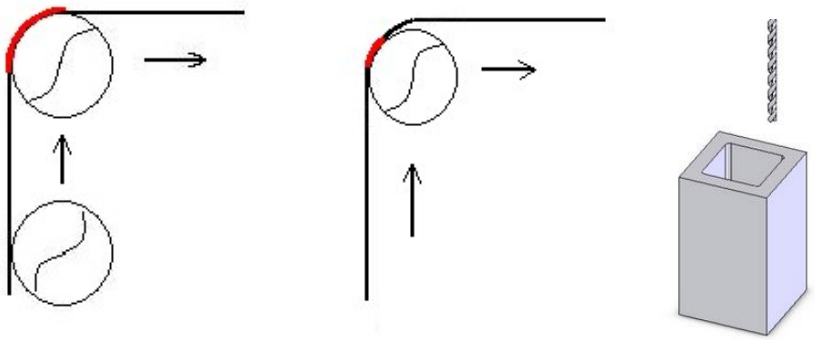

Figure 65 Interior corners and deep pockets machining

Sharp edges are very difficult to replicate using a drill. This happens due to the cylindrical are of contact of the endmill, as it can be seen on figure 75 a). Smaller diameter endmills can be used to minimise corner radius, however, this tools tend to be more fragile the wider ones, so it is advised to use these only when strictly necessary.

Endmills will perform better under rigid conditions. Deep pockets that require small diameter long endmills are the worst case scenario. According to Joe Osborn, in *Tips on Designing Cost Effective Machined Parts* [19], endmills should the best performance up to 4 times its diameter, but can cut as deep as 10-15 times their diameter, with progressive cost of material and machining time.

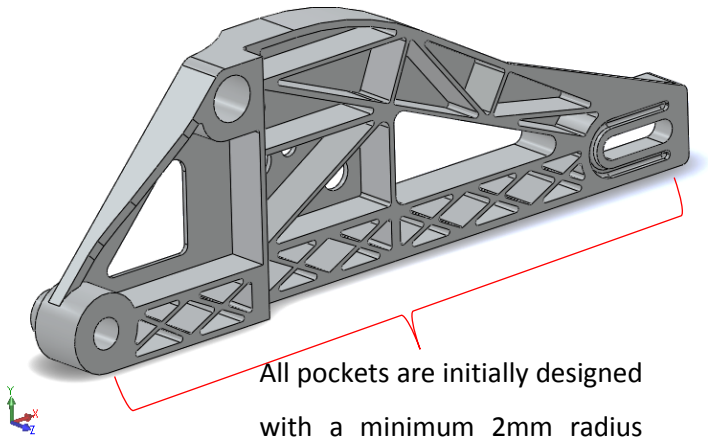

Figure 66 Rear Swing Arm interior pockets

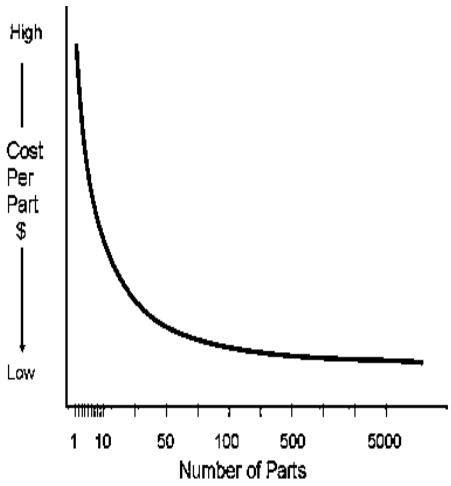

Graph 8 Machining cost distribution

Pockets with a minimum 2 mm radius should be machine with a standard tool with a maximum cutting diameter of 3 mm. Such tools can be found in the market for approximately 17,5 €. The pockets average depth is 30 mm which stay within the 15-10 times length/diameter rule suggested previously. However, widening the corners is an option possible to explore to make the machining of this part more cost effective.

Both swing arms won't be part of a mass produced vehicle, which, after analysing graph 16, clearly demonstrates that a cost/efficient design can critically affect final price. Given the total number of interior corners (102), these are likely to weight on the final machine and tooling expenses. Thus, the following options are presented on table

Table 43 Increase in weight VS increase in interior corner radius

Part	Interior corner minimum radius (mm)	Maximum Endmill diameter (mm) *1	Endmill overall length (mm) *1	Mass after machining (kg)
r1	**2**	**3**	**38**	**1,954**
	2,5	**4**	**50**	**1,978**
	3	**5**	**50**	**2,007**
	3,5	**6**	**50**	**2,041**
	4	**7**	**63**	**2,083**

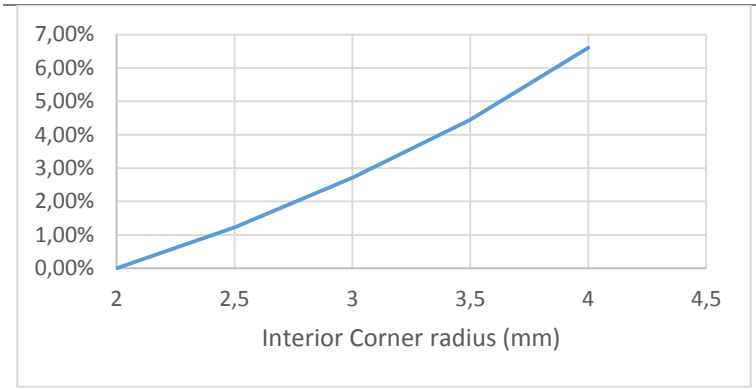

*1 – Endmill standard dimensions provided by DeArmond Tool [19]

A final increase in mass of 1,23% might be acceptable, given that interior corners of 2,5 mm can be machined by a 4 mm endmill with an increased overall length of 50 mm. A better fixture area is permitted, while maintaining an inferior diameter to the interior corner, thus decreasing the probability of chatter and tool erosion.

4.3 Weld location and sizing

Several edge welds will be required to assemble and connect all parts after machining. Once again, since these are not a mass produced parts, automatizing the welding process is not an option, meaning that average price for working man hours (Section 4.1) stands. Two specific type of weld edges will be required:

- **Groove welds** - weld applied in a performed opening or groove between two metal parts
- **Fillet welds -** triangular weld that joins two metal parts at a 90º angle.

SolidWorks 2014 permits the study and dimensioning of edge welds, through the ***Edge Weld Connector*** tool. The theoretical process behind this tool, can be explained by Figure 77.

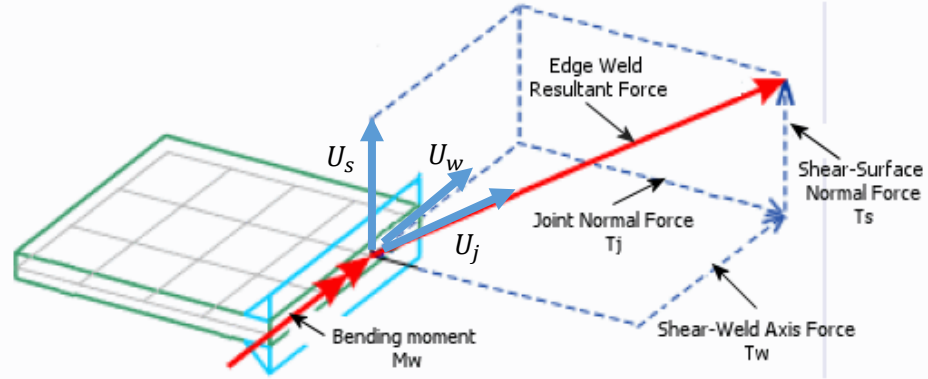

Figure 67 Edged weld formulation (SolidWorks 2014)

- **Joint Normal Force [N/m]** - T_j (joint normal force) acts normal to the intersecting shell edge of the terminated part along the weld joint normal axis, U_j
- **Shear Weld Axis Force [N/m] -** T_w (parallel seam force) collinear with the local weld axis, U_w
- **Shear Surface Normal Force [N/m] -** T_s (surface normal force) acts along the local surface normal, U_s
- **Bending Moment [Nm/m] -** M_w (Seam moment) acts along the local weld axis, U_w

Given the geometry of both swing arms, edge welds on different locations will be necessarily exposed to different local loads. For the purpose of this project, it is important to know what this locations and what is the minimum weld size necessary to overcome those loads, still complying with the project safety factor.

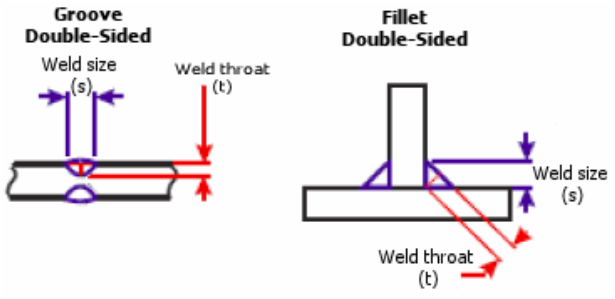

Figure 68 Edge weld main dimensions

Aluminium 7075-T6 requires 5154 Rod (Tensile Strength – 241 MPa) to be used as filler material.

Weld estimation simulations are computationally heavy. To simplify this analysis, both swing arms were considered approximately symmetric. This assumption permits the test of only half

of the swing arms per turn, given that the right fixtures are applied. Also, weld edge simulation only permit the connection between shell-solid, or shell-shell elements FE. This brings some obstacles to the correct simulation using the current models.

The first and easiest to simulate was the front swing arm.

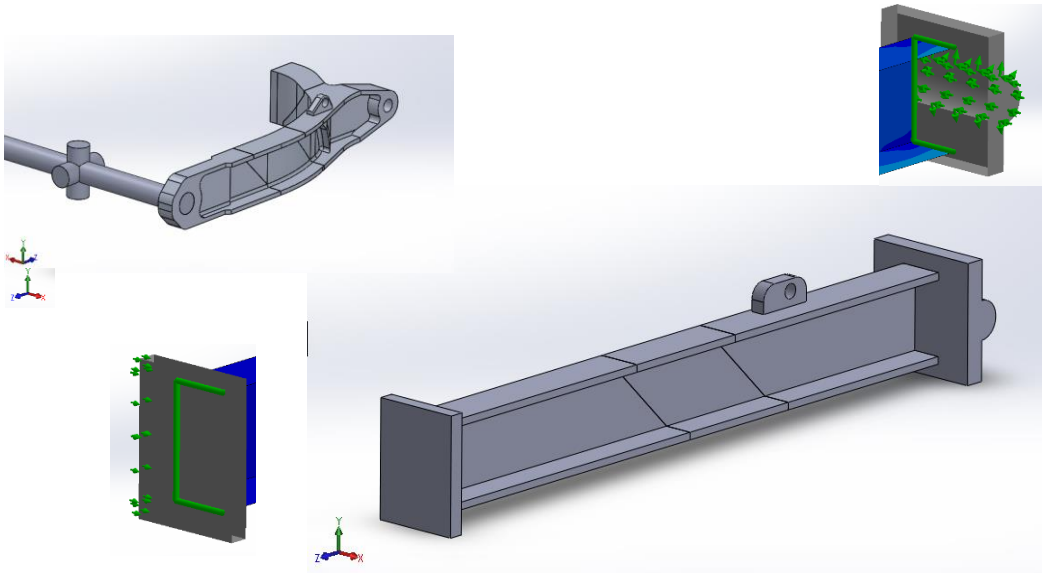

Figure 69 Simplification of half of frontal swing arm

SDS2 is a simplified shell element version of the frontal swing arm. Given that weld edges are the main subject of analysis at this stage, such a simplification is plausible, knowing that the structure keeps performing under its design properties. Again, the vertical extreme scenario was considered, with half of the vertical load (1790 N). The weld lines of interest in this case are the ones located along the length of the arm, with an angle of 45°, since these will be exposed to bending conditions.

Type	Min	Max	Mean
Weld size (mm.)	0.019097	3.738	0.3159
Weld throat size (mm.)	0.019097	3.738	0.3159
Joint normal force (N/m)	-1.1147E+006	3.6892E+005	-21601
Shear-Weld axis force (N/m)	-2.6829E+005	2.6289E+005	328.38
Shear-Surface normal force (N/m)	0	0	0
Bending moment (N.m/m)	-1081	298.38	-44.641

Table 44 SolidWorks general weld sizing prediction under vertical loading of 1790 N

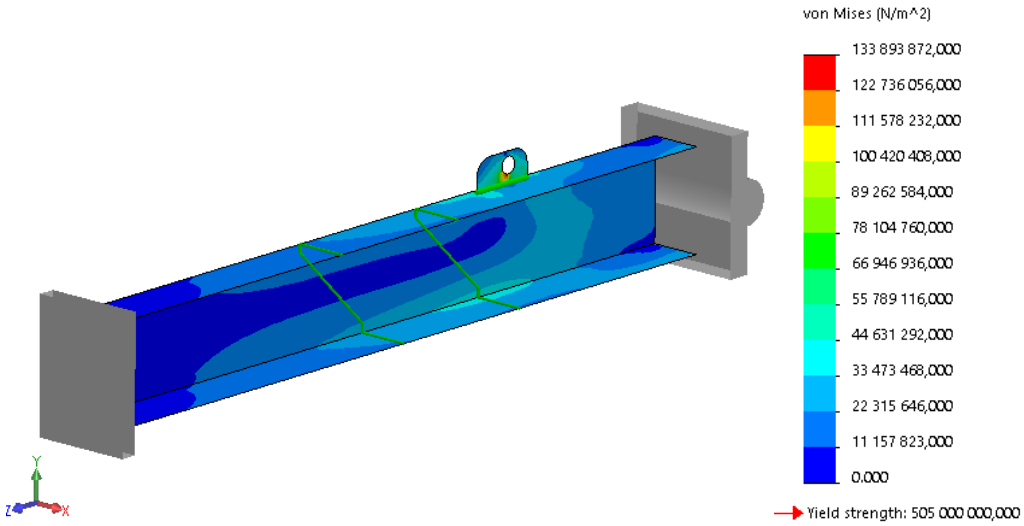

Figure 70 Von Mises Stress propagation in simplified model

SolidWorks Edge Weld Creator estimated a mean throat and weld size of 0,3159 mm. These dimensions results are arguable, given the minimum thickness of 5 mm measured on the swing arm top and bottom walls.

The same process was attempted with the rear swing arm. Unfortunately, no stable model was achieved. Still, 45^0 welds across the arm should be used. Since the entire arm needs to me divided in several parts to be machined, welds with an angle should help the final parts cope with future cutting stresses due to vertical loading.

5 Conclusions and future developments

5.1 Conclusions

It was intended with this project to develop a study on the structural design of the swing arms of a racing electric motorcycle in accordance with the rules set by MotoStudent Competition. For this an initial research was conducted on the basis of nowadays motorcycle design and what are the current challenges faced by EV. Several solutions were explorer for the main components present on these vehicles: battery box, electronic controls, frame and finally swing arms.

To begin with the theoretical implementation of this study, an Aluminium 7075-T6 was chosen for the main structural applications (swing arms models). Also, the main criteria of swing arm performance evaluation, Cossalter's Approach [14]. The next step, was the determination of a safety factor for the project, characterized by material quality, manufacturing process and accuracy of initial modelling ($n_{proj} = 1.82$).

The simplified motion of a motorcycle was studied, since understanding the main limits to be applied to the system rider + motorcycle is crucial before structural designs. The successful racing example of the Aprilia RS250 was used as benchmark. Also, some considerations were taken about Squat and Dive behaviour, and how the final swing arms could affect these.

The structural analysis started with a brief introduction and study about FEA. A rear suspension rocker was designed to test and define main mesh properties to be used (adaptative [5;1] mm).

Two specific scenarios were considered for the design of the rear swing arm, HE (high motor assembly) and LE (low motor assembly). Both solutions were explored through models 1.1 and 1.2. On both models it was verified that a truss type design is the most efficient way to reduce total mass, while keeping satisfactory mechanical properties (a reduction of up to 66.1% was achieved between first and last iterations). A final version, derived from the HE scenario was chosen due to its superior load transfer capabilities, with a final safety factor of 3.8.

The front swing arm design process started with the definition of a structure that would comply with MotoStudent's minimum steering radius rule (15º at the handlebar). However, it became clear that this approach was too simplistic in the absence of a steering system. Such a system was designed for dimensional purposes, but not tested.

Two scenarios where considered, single and dual front suspension, with the las being the chosen one due to being thanks to outstanding vertical stiffness (approximately 6.1 times larger than single suspension model).

CNC manufacturing was the machining process defined for this project. It was concluded that this is a very flexible process, permitting a great variety of interior details. However, due to the dimension and complexity of the final models, it became clear that the tooling, man power and welding needed to achieve them would greatly undermine the cost efficiency of this project. Furthermore, some questions remain related to the proper simulation and dimension of weld edges in structures so complex as this one.

It is finally advised that, although CNC machining is a plausible and common process nowadays, it should be used on smaller, less detailed parts, decreasing material waste and high costs. Other more conventional processes, less expensive and easier to work on materials to use and weld should be in the core design for low budget student teams.

5.2 Future Developments

Steering system

The steering system presented in Section 3.10 could become the basis for a new type of mechanism. The only existing successful front swing arm system in existence is the centre cube steering, so, if a cheaper and easier to manufacture solution that does not require for specific front wheel design, could be found, market and competition applications would be possible.

Battery Box

After the brief study on the topic of battery packs for Electric motorcycles, a study on this topic is suggested. Motorcycles have specific requirements and structural dynamics that are greatly affected by the final battery box pack.

Suspension Influence

After completing the swing arms design, the next study in line would clearly be suspension assembly options and how this could affect the overall dynamics of the system.

References

[1] Team, G. (2016). *1894 Hildebrand & Wolfmuller - world's first production motorcycle sells for GBP86,200*. [online] Gizmag.com. Available at: http://www.gizmag.com/1894-hildebrand-wolfmuller-auction-result-gbp86200/14913/

[2] MotoGP. (2016). *History of Motorcycle Racing - MotoGP*. [online] Available at: http://motogp.hondaracingcorporation.com/history/

[3] Bielaczyc, P., Woodburn, J. and Szczotka, A. (2014). An assessment of regulated emissions and CO2 emissions from a European light-duty CNG-fueled vehicle in the context of Euro 6 emissions regulations. *Applied Energy*, 117, pp.134-141.

[4] Vogel, C. (2009). *Build your own electric motorcycle*. "Chapter 1: Why you need to get an electric motorcycle today", New York: McGraw-Hill.

[5] James, (2005). *Alternative Fuel Cars: Plug-In Hybrids and Electric Cars*. Available at: www.alt-e.blogspot.com/2005/01/alternative-fuelcars-plug-in-hybrids.html

[6] Drivingthefuture.com. (2016). *Nissan LEAF, EV1, RAV4-EV, HondaEV, VOLT-hoax, Plug-in Electric cars and Solar Photo-Voltaic rooftop power are Driving the Future*. [online] Available at: http://drivingthefuture.com/

[7] Robinson, A. and Janek, J. (2014). Solid-state batteries enter EV fray. *MRS Bull.*, 39(12), pp.1046-1047.

[8] Iomtt.com. (2016). *Isle of Man TT Official Website*. [online] Available at: http://www.iomtt.com/

[9] Rules & Regulations MotoStudent 2015 - 2016. (2016). 1st ed.

[10] T. U. Daim, X. Li, J. Kim, and S. Simms, (May 2012) "Evaluation of energy storage technologies for integration with renewable electricity: Quantifying expert opinions," *Environmental Innovation and Societal Transitions*, vol. 3, pp. 29-49

[11] Foale, T. (2002). "Motorcycle Handling and Chassis Design", Chapter 10: Structural Considerations, Tony Foale Designs.

[12] Rechena, D. (2014), Motorcycle Chassis Analysis, Mechanical Engineering, Lisboa, Instituto Superior Técnico.

[13] Bradley, J. (1996), "The Racing Motorcycle: A technical guide for constructors", Section 3: General Layout, Volume 1, The Ebor Press, York, England

[14] Cossalter, V. (2006). *Motorcycle dynamics*. Chapter 6: Motorcycle Trim, Germany, Amazon Distribution.

[15] Motorcycle Chain Specification. (2016). 1st ed. [ebook] YBN. Available at: http://www.yaban.com/upload/en/85/14_file_1.pdf.

[16] Schmidt, S. R., B. J. Hamrock and B. O. Jacobson (2013). Fundamentals of Machine Elements, McGraw-Hill.

[17] Blain, L. (2016). *Single-sided front swingarm could steer the way to better motorcycle handling*. [online] Gizmag.com. Available at: http://www.gizmag.com/single-sided-front-swingarm-could-point-the-way-to-better-motorcycle-handling/10484/.

[18] Zhang, Y., Huang, J., Cheng, Z., Ye, Z., Chi, H., Peng, L. and Chen, S. (2016). Study on MIG-TIG double-sided arc welding-brazing of aluminum and stainless steel. *Materials Letters*, 172, pp.146-148.

[19] Osborn, J. (2016). *Designing machined parts, How to design machined parts, CAD design*. [online] Omwcorp.com. Available at: http://www.omwcorp.com/how-to-design-machined-parts.html

[20] Macrotrends.net. (2016). *Crude Oil Prices - 70 Year Historical Chart*. [online] Available at: http://www.macrotrends.net/1369/crude-oil-price-history-chart

[21] L. P. Rodgers, (Jun 2013) “Electric Vehicle Design, Racing and Distance to Empty Algorithms” *Massachusetts Institute of Technology*, USA.

[22] Cossalter, V. (2006). *Motorcycle dynamics*. Chapter 8.10.3: Structural Stiffness of the Swing arm, Germany, Amazon Distribution.

[23] Hosford, W. F. (2005). *Mechanical Behaviour of Materials*. New York

[24] Haas Automation, I. (2016). *Haas DM-1 | Haas Automation®, Inc. | CNC Machine Tools*. [online] Haascnc.com. Available at: http://www.haascnc.com

Annex 1

Why Electric? [4]

- Electric motorcycles are the environmentally viable option due to zero emissions during usage. The energy generated to power an EV can be up to 97% cleaner in terms of human and nature harmful gases [4].
- Electric motors can provide high torque at almost any operating speed.
- When analysing general gasoline based combustion reactions, only 20% of the chemical energy is converted into useful work (kinetic energy) at the wheels of the vehicle, while 75% or more battery based energy reaches the wheels of an EV. [4]
- One plausible argument presented to EV market expansion by automobile companies is related to Life Cycle Assessment (LCA) of EVs. Although electrical motors produce no emissions, the same can't be said to electricity sources. Coal, petroleum and gas power plants are still common in most countries and will probably stay that way for decades to come. However, when carefully analysed, this argument is only proven right for very rare situations. Three reasons are pointed:
    - Taking the example of the USA, only 2% of electricity is generated through the burning of oil, which means that using electricity as a transportation fuel would significantly reduce requirement of imported petrol [5].
    - Assuming the worst case scenario. Considering the same amount of energy production per carbon emission, 100% of electricity produced by a coal power plant is still considerably cleaner to use to power an EV, than gasoline produced from oil refinement [6].

Annex 2

MIT Electric Race BMW Motorcycle [21]

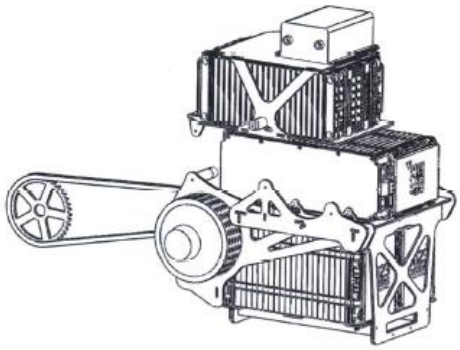

Figure 71: Final design of the battery and motor structural frame.

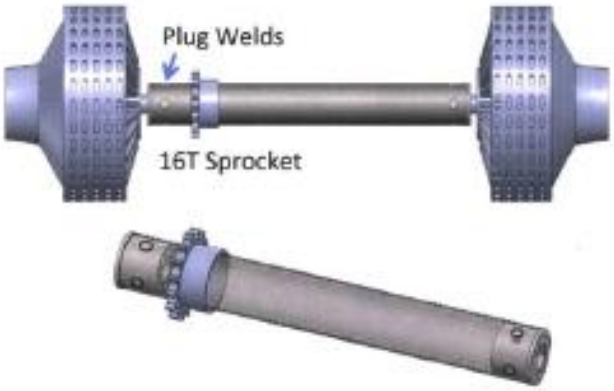

Figure 72: Two DC electric motors connected by a steel shaft with a 16T sprocket

(a) (b)

Figure 73 (a) battery module assembly; (b) frame fabricated using waterjet

Annex 3

Motor options

Electric Motor Types	
DC	**AC**
• Series • Shunt • Compound • Permanent magnet • Brushless • Universal	• Single-Phase Induction Motor • Synchronous Motor • Three-Phase induction motor

Table 5: Electric motor types

All these types of motors can be used to power an EV. This means that, differing from combustion enginess, EM builders need to weight down on a different set of knowledge, tools and vehicle requirements. Some basic considerations might be suggested when choosing these:

- Power and torque
- Cost
- Voltage
- Current
- Size
- Efficiency
- Shaft size
- Controllers compatibility

The suggested considerations are however basic. Much more complex analogies can and should be taken by professional engineering teams when choosing a particular motor for a race prototype. Nevertheless, that is not the aim of this document and in fact, MotoStudent details that all participating teams must use the same electric motor model [9].

As part of the Competition rules, all teams need to use the same motor model. For 2015/2016 Edition, the electric motor is a Heizmann PMS 150 Air-Cooled. The main technical specs for this motor are as follows:

Type	AFPM Motor
Rated Power	13 KW
Cooling	Air (External ventilation)
Max Speed	6000 rpm (without field weakening)
Rated Voltage	96 VDC
Rated Current	153 A
Peak Stall Current	550 A
Rated Torque	20.7 Nm
Peak Stall Torque	71 Nm
Motor Constant	0.0087 V/rpm
Weight	22.3 kg

Table 6 Heizmann PMS 150 Air-Cooled Specs

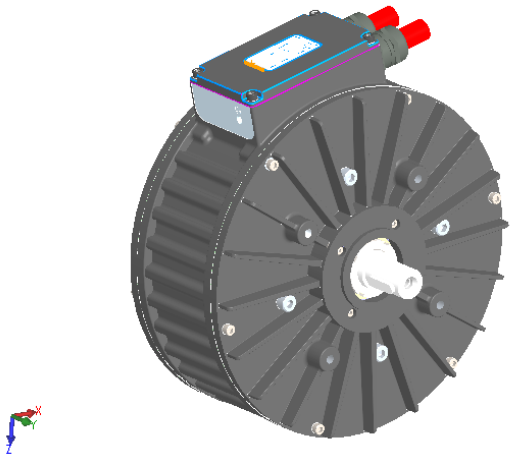

Heizmann PMS 150 Air-Cooled CAD model

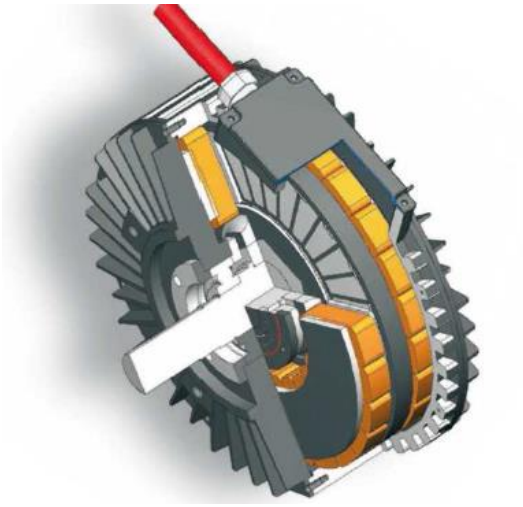

Heizmann PMS 150 Air-Cooled cut view

Annex 4

Motor Controller

The controller unit is not necessarily critical to an EM structure. However, it is essential to the electric and electronic systems of the motorcycle. Most motor controllers used nowadays in EM are what is called Solid-State that, more specifically, after late 1970s, became pulse-width modulated (PWM).

Controller's most basic function is to regulate speed and power of electric motors. Yet, modern models can go much beyond those functions, incorporating heating regulation, battery monitoring, safety, traction, backing and recharge control. It is then clear that although not important as a load carrying component, EMs need to be designed keeping in mind the volume and weight of such controllers and how to keep them easily accessible. An example is shown on **Error! Reference source not found.**.

Figure 74 Example of Altrax PWM Controller 24-48V 300A

Batteries and Battery Box

Initial battery design and sizing could can become extremely complex. However, as assumptions need to be made to simply and speed up the design process till test phase. The following assumptions were taken:

- It was briefly analysed that Li-ion batteries and similar exemplars are the most common choice for competition Ems. With this in mind, the next step was to do a market search on this battery type.
- Since “racing day” conditions depend on a number of factors: temperature, wind direction and speed, track inclination, pilot experience and driving behaviour, total weight of pilot and motorcycle. This implies that a full throttle analysis should be taken (worst case scenario, where full power is constantly being solicited to the power unit), which given the low power of the electric motor (13kW), it is in fact close to reality.

  This assumption has deep implications to the battery pack design. It is known the race lasts for approximately 25 minutes. This means 25 minutes with a full power output of 13kW. Using simple calculations it is possible to derive the minimum Wh capacity necessary for the total battery pack.

$$P\,[Wh] = Power[W] * RaceTime[hours] \tag{4.1}$$

$$P\,[Wh] = 13000W * \frac{25}{60}h = 5416{,}67Wh$$

Battery capacity of discharge is not considered for this pre-testing stage. The reason is related to the non-linear, highly unpredictable behaviour of batteries under stress.

Battery
1.
2.
3.
4.
Battery models :
1. 4.2 V
196

Unit Price	Number of Units	Total Price	Voltage [V]	Ampere hour [Ah]	Volume total	Weight per Unit	Total Weight	Energetic Density	Energetic Density	Capacity [C]
1,3	215	279,5	4,2	6	17725,91	0,044	9,46	572,73	25,2	1
5,25	188	987	3,7	7,8	32397,67	0,080	15,13	358,67	28,86	1
13,745	293	4027,29	3,7	5	36930,32	0,096	28,16	192,51	18,5	1
8	325	2600	3,7	4,5	519,75	0,090	29,19	185,41	16,65	35

Batteries properties comparison

A number of Li-PO, LiFePO4 and LiNiMnCo on the market were also checked, but as expected after the initial comparison between models, these options are in general

more expensive. However, it is understood that performance would likely be superior due to higher discharging capacity, but once again, this is effect would be intrinsically non-linear and difficult to predict with an acceptable precision. It is preferable to start the designing process with a nominal conservative structure and start improvements during test phase.

The batteries comparison table gives a good initial impression of how Li-ion batteries should perform. It is mainly interesting to assess energy density between options. From this point of view, options 1 would be the most suitable candidate. Unfortunately, after a further market search on this particular models, and simple in-house testing (voltage measurement), it was clear that the advertised 4,2V voltage is wrong, since all units bought showed a nominal voltage inferior to 3,7V. Model 2 is then the most suitable candidate, since these models performed in average as it is advertised. Energetic density is an important property of batteries, but another initial aspect should be commented on, Ampere hour properties.

The initial total number of batteries per model provided on table [] is too simplistic. This happens because, in reality, batteries need to be assembled in series packs and, consequently, packs need to be linked in parallel to achieve nominal Amperage and Voltage required by the motor, respectively. To calculate the real number of necessary batteries it is possible to use basic circuit's theory:

Series Circuits

$$I_{total} = I_1 = I_2 = I_n \quad (1)$$

$$V_{total} = \sum_{i=1}^{i=n} V_n \quad (2)$$

Parallel Circuits

$$V_{total} = V_1 = V_2 = V_n \quad (3)$$

$$I_{total} = \sum_{i=1}^{i=n} I_n \quad (4)$$

Battery Assembly	Model 2	
Nº batteries in series (pack)	**Volt pack**	**Amp pack**
20	96	4,5
Nº packs in parallel	**Volt total**	**Amp pack**
34	96	153
Total number of batteries	**Total Weight [kg]**	**Price [€]**
680	66,64	3570

Battery Calculations (Model 2)

Battery Assembly

Now that a battery model is chosen, the next step is to define the general dimensions of a battery box can be defined. For that matter, the standard CAD model of an 18650 demonstrated on Figure 34a was used.

Knowing that each pack has to be grouped in series of 20 batteries, the pack showed on **a** was created.

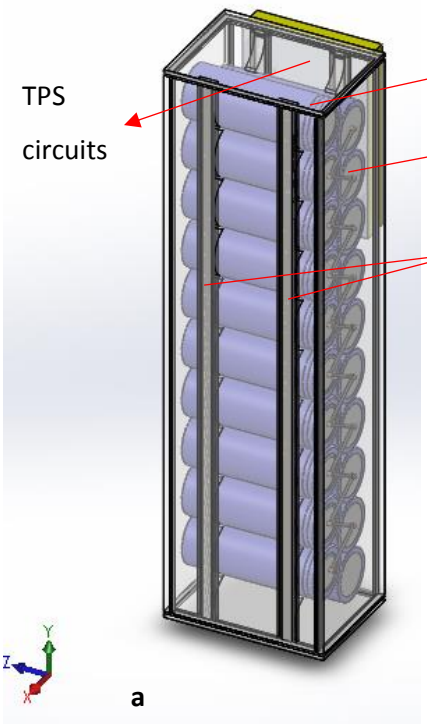

Main Dimensions	
Mass	2,0 kg (approx.)
Length (x)	71,5 mm
Width (z)	78 mm
Height (y)	278,2 mm

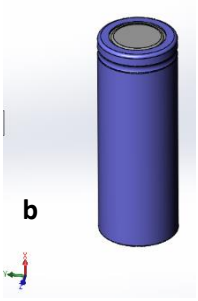

a Complete pack of 20 batteries;
b single battery unit.

The following design aspects were taken into consideration:

1. The battery pack needs to be partially waterproof.
2. All batteries must be easily removable.

3. All batteries need to be properly restrained during working conditions.
4. All batteries need to have an independent control of temperature during working conditions.
5. The battery pack should be contain within an isolated package.
6. An additional 15% - 20% capacity should be considered to avoid battery system stress.

Point 1. and 5. are directly related to two characteristics of this project. First, rain is a possibility during competition. Secondly, one of the scoring aspects of this competition is the possibility of turning this prototype into a mass production vehicle, implying that environment must affect as little as possible to performance and safety of the vehicle. This point was addressed by placing the batteries into a rigid acrylic package. Acrylic Polymers are cheap, easy to machine and, as most polymers, weak electricity conductors.

Point 2. Defines that in case of maintenance, or even critical failure in one of the battery packs, all units should be easily removable and replaced. This design aspect can be fulfilled by incorporating a rail on each pack internal wall, permitting a “slide in and out” action.

Point 3. Can be achieved by machining semi-circular individual supports on the acrylic rails. Batteries remain properly restrained during working conditions.

Point 4. Is related to rule D.3.5.5 [], when batteries go through internal chemical collapse, conductivity and discharge properties are affected. This phenomenon can be detected in real time by individual temperature measurement of each unit. This aspect becomes increasingly important, since faulty batteries can propagate failure through the entire pack, since linked units become overloaded. A standard TPS (Temperature Processing System) was considered for this scenario.

Point 6. Is linked to the fact that although batteries are assembled and controlled by a strict number of quality standards, this type of project involves deep “in-house” manufacturing and manipulation. Batteries may perform differently under such conditions, by which an initial design should contemplate a safety factor to a certain extend. Given the volume, weight and type of batteries chosen 15%-20% extra capacity discharge is an excepted safety design assumption.

The initial total battery package was then modelled.

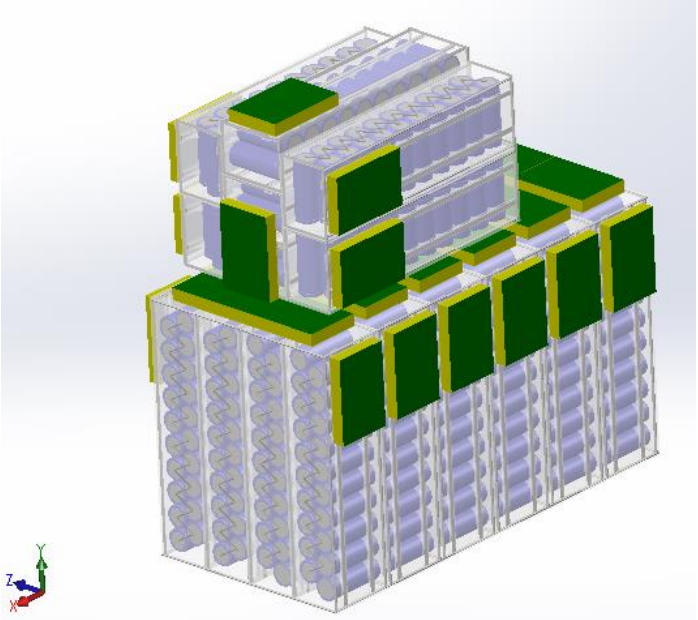

Final Battery Assembly

Main Dimensions	
Mass	83,9 kg (approx.)
Length (x)	464 mm
Width (z)	252 mm
Height (y)	481 mm

Annex 5

Resistance forces and Maximum Performance

There are two main resistance forces to the movement of the motorcycle: Aerodynamic and rolling resistance.

Aerodynamic resistance, or drag, is the most influential of these forces. Drag is the force that a surrounding fluid exerts on a moving object. This force is function of:

- Speed, V
- Fluid density, ρ
- Frontal area of the object, A
- Drag coefficient, C_D

$$F_D = \frac{1}{2}\rho C_D A V^2 \quad [13] \qquad (4.6)$$

Although the aerodynamic study of the motorcycle falls under responsibility of the fluid dynamics department, this does not mean that limit conditions cannot influence the design of other structural parts. It is important to define in the beginning of a project, what should be the limits of motorcycle + rider, **Error! Reference source not found.**.

Figure 75 General Cd distribution for different vehicles

Rolling is best described as the force contrary to the forward movement due to tire contact with the road. It is given by the product of vertical load and a rolling resistance coefficient f_w.

Kevin Cooper (J. Bradley, 1996, [13]) proposed an empirical approximation to derive f_w, taking into consideration inflation pressure and forward velocity (tire pressure properties change with speed).

$$f_w = 0{,}0085 + \frac{0{,}018}{p} + \frac{1{,}59 * 10^{-6}}{p} V^2, \quad (4.7)$$
$$for\ velocities\ below\ 165\ km/h$$

A second empirical approximation is also presented for energy dissipation, P.

$$P[kW] = \left(2{,}36 * 10^{-6} V + \frac{4{,}88 * 10^{-6}}{p} V + \frac{4{,}41 * 10^{-10}}{p} V^3\right) F_t, \quad (4.8)$$
$$for\ velocities\ below\ 165\ km/h$$

Where F_t represents the load on the wheel (rear wheel) and V in km/h.

For initial limit conditions, **Error! Reference source not found.** applies

Wheels radius (with tire) [mm]	**300**
Assumed total weight [kg]	200
Rear wheel load Ft [N]	885,53
Tire Pressure [kgf/cm^2]	2,1
Drag Coefficient, CdA	0,32

Table 7 Initial limit conditions

Purely electric motorcycles do not require a classic gear box of several different relations. This happens due to the behaviour of electric motors in general – high torque response from start to limit rotational motor speeds. What is indeed required, depending on electric motor option, is a differential box, since it is common for certain brushless designs to achieve as high as 20000 rpm. However, the a Heizmann PMS 150 motor will only achieve 6000 rpm as a max speed, before field weakening. In this case, a differential box is not necessary, since the dual chain system allows for the necessary speed and torque transformation between motor and rear wheel.

First, the resultant of resistant forces had to be calculated. For that matter, equations 4.6 and 4.7 were used in a scenario of increasing forward speed.

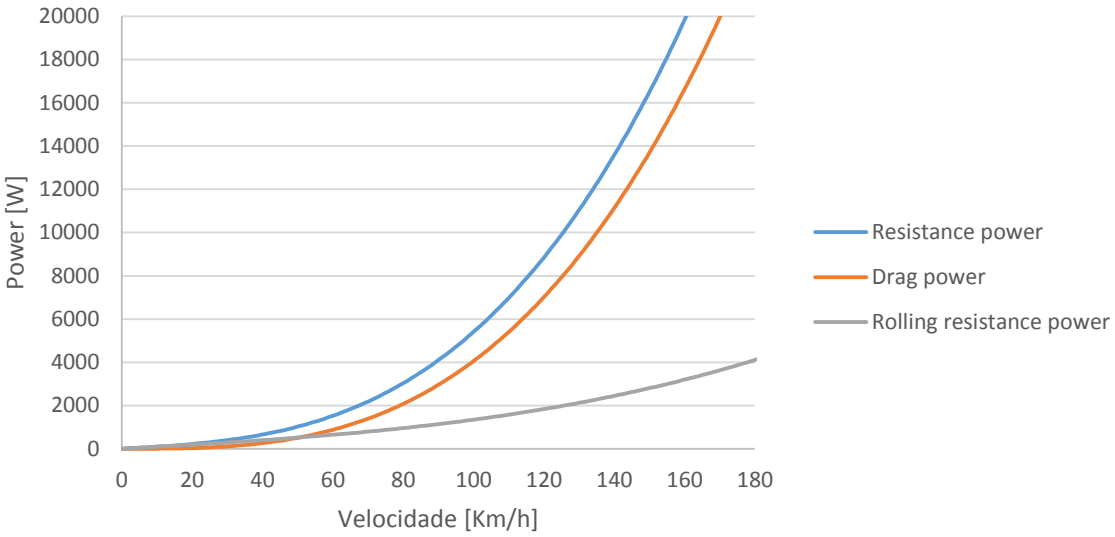

Graph 9 Resistance Power

Graph 9 shows that the resistance power applied to the motorcycle and driver system will equalise 13 kW at an approximate speed of 140,8 Km/h. This is a simple calculation, but it defines a clear limit on the design. In perfect conditions, that should be approximately the speed achievable, however, it necessary to calculate the right transmission relation between motor and rear wheel.

Torque and Power relations can be used for the following calculations.

$$P[W] = T[Nm] * \omega[rad/s] \qquad (4.9)$$

This relation is ultimately defined by the number of teeth on motor and rear wheel sprockets. After a number of iterations, it was understood that if max speed is to be achieved, the most advantageous relation would be 11/53.

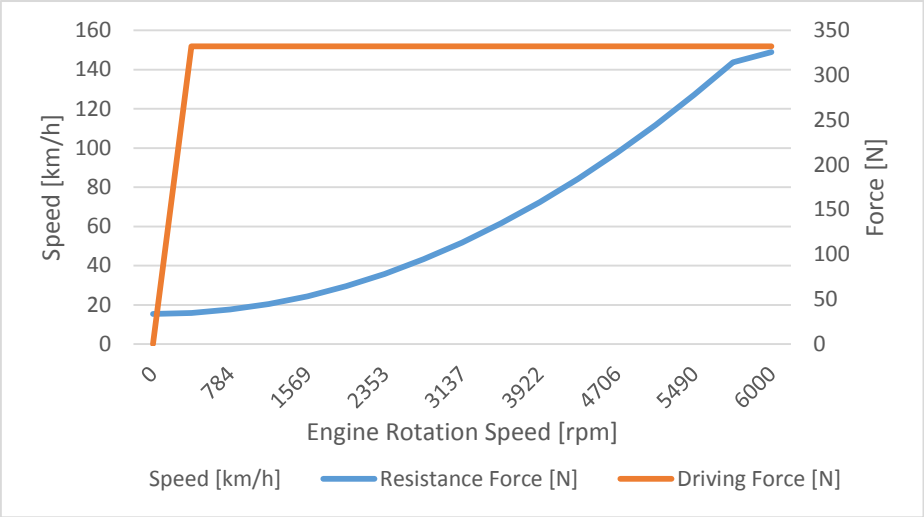

Graph 10 Driving and Resistance Forces

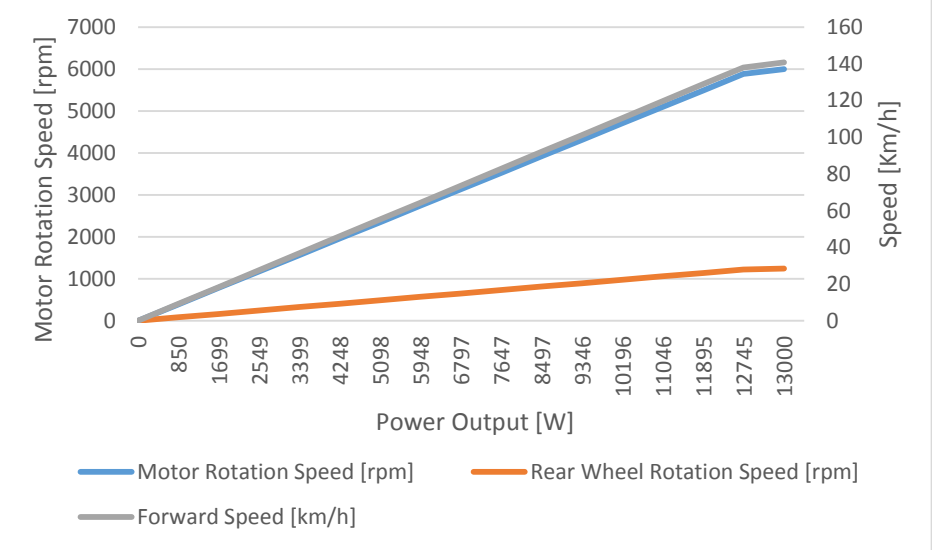

Graph 11 Relation of Rotation Speeds between Rear wheel and Motor

Graph 11 shows that when achieving limit motor rotation speeds the driving force (calculated at the rear wheel) is balanced by the resisting force.

If the relation was higher, for example 11/50, the torque at the rear wheel would be consequently decreased, resulting in a lower driving force that would be equalised by the resisting force at lower speeds. This scenario would only make sense, if it was decided to input a mechanic limitation (through transmission) on motor regime usage.

The opposite also applies, lower relations, for example 11/56, would achieve a higher torque at the rear wheel and consequently a higher driving force. However, the motor would achieve its limit rotation speed, before driving force could be equalised by resisting force. This scenario may become relevant in competition conditions, if teams are allowed to explore motor performance regimes above manufacturer advice.

To conclude, it is understood that 11/53 is approximately equivalent to other relations, 10/48 and 12/58. These may become plausible options to test, as this project moves forward. Ultimately, given the standard character of these parts, it might be preferable to opt for parts already available in the market.

Chain

Chains as means for power transmission are a commonly applied throughout all industry. Standards for motorcycle application are well known [15] and several manufacturers worldwide provide products according to these, **Error! Reference source not found.**. It is important to define chain dimensions, since it will interfere directly with swing arm design, **Error! Reference source not found.**.

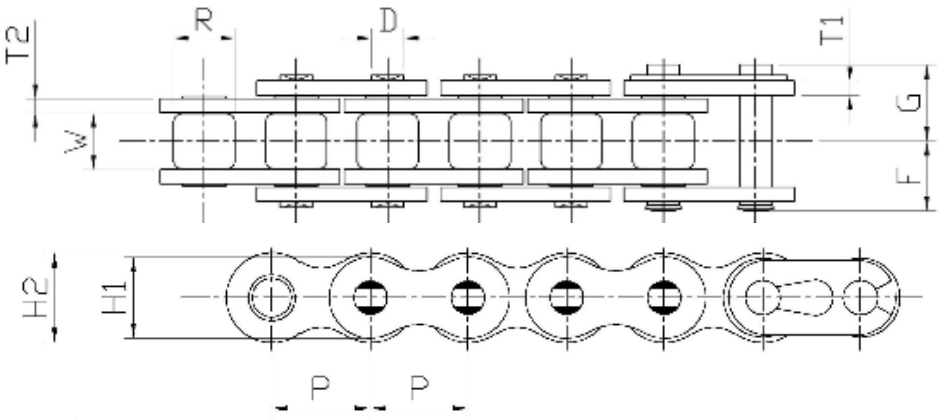

Figure 76 Chain Standard dimensioning

YBN Chain No.	Pitch xWidth P x W inch	m/m	Roller Dia R	Links Height H1	H2	Thickness T1	T2	Pin Dia D	Lengths F	G	Average Strength	Cylinder cc (max)
Regular												
25	1/4"x1/8"	6.35x3.18	3.30	5.00	5.80	0.75	0.75	2.30	3.30	4.50	400	
415E	1/2"x3/16"	12.70x4.76	7.77	10.20	10.20	1.00	1.50	3.96	6.15	7.30	1650	50cc
420	1/2"x1/4"	12.70x6.35	7.77	10.20	11.80	1.50	1.50	3.96	7.50	8.40	1750	90cc
425	1/2"x5/16"	12.70x7.94	7.77	10.20	11.80	1.50	1.50	3.96	8.55	9.70	1800	100cc
428	1/2"x5/16"	12.70x7.94	8.50	10.20	11.90	1.50	1.50	4.44	8.55	9.70	1850	125cc
428S	1/2"x5.2	12.70x5.2	8.50	10.20	11.90	1.50	1.50	4.44	7.00	8.40	1850	125cc
520	5/8"x1/4"	15.875x6.35	10.16	13.00	14.80	2.00	2.00	5.06	8.50	10.10	3100	250cc
525	5/8"x5/16"	15.875x7.94	10.16	13.00	14.80	2.00	2.00	5.06	9.30	10.90	3100	400cc
530	5/8"x3/8"	15.875x9.53	10.16	13.00	14.80	2.00	2.00	5.06	10.10	11.60	3100	500cc

Table 45 Chain Standards and Motor size

The power delivered by the electric motor clearly places this motorcycle on the 250cm^3 range.